Lightweight Vehicle Structures that Absorb and Direct Destructive Energy Away from the Occupants

by

Weiran Jiang

A dissertation submitted in partial fulfillment
of the requirements for the degree of
Doctor of Philosophy
(Naval Architecture and Marine Engineering)
in The University of Michigan
2016

Doctoral Committee:

Professor Nickolas Vlahopoulos, Chair
Matthew P. Castanier, U.S. Army TARDEC
Professor Pingsha Dong
Professor Bogdan Epureanu

To my dear grandpa

ACKNOWLEDGMENTS

My story in Ann Arbor started six years ago when I left home and came to the United States as a twenty-one years old boy. I learnt, grew, and spent most of my twenties in this lovely city, where I was embraced by support and love, and fulfilled myself with passion and peace. I will not try to collect names and create a long list in this acknowledgement, but I thank and will never forget every one of you who has helped and accompanied me along the way of being a better man. The great journey at University of Michigan turns every moment in the past six years into a beautiful memory that I will treasure for a lifetime.

First and foremost, I want to express my deepest appreciation and sincerest gratitude to my advisor, Prof. Nickolas Vlahopoulos, who changed my life three and a half years ago by offering me the opportunity to continue my graduate study as a Ph.D. student, which was something I never thought I could be capable of. Prof. Nick, you trusted me with understanding, mentored me with patience, encouraged me with respect, and most of all, you always made me feel inspired and fully self-motivated with an inexplicable power. You placed me in challenging positions within my reach, and in doing so accelerated my growth, expanded my capability, and showed the direction of discovering my own potential. Now, standing at the destination of this long journey and looking back, I feel so fortune that I can be one of your students, and I could have never possibly completed my Ph.D. studies so smoothly without your guidance. By the way, I totally agree with Hong Yoon about the fact that your wife is so much better looking than you

are. I am glad I am doing the same. This is definitely also one of the invaluable lessons I learnt from you. Thank you Prof. Nick!

I would also like to extend my thanks to Dr. Matthew Castanier, Prof. Bogdan Epureanu, and Prof. Pingsha Dong for being my Ph.D. committee members and providing instructive advice. This research was initiated by the U.S. Army Tank Automotive Research, Development and Engineering Center, and the Automotive Research Center, a U.S. Army Center of Excellence for high fidelity modeling and simulation of ground vehicles led by the University of Michigan. I appreciate their generous financial support during my Ph.D. studies. I also thank the department of mechanical engineering for covering the tuition and expenses in my last semester.

Most importantly, I would not be able to achieve this doctoral degree without the sacrifices from my family. Mom and Dad, words cannot express how grateful I am for everything you have done for me. You have always been trusting me on each and every of my decision regardless of success or failure. It was your understanding that supported me to cross one hurdle after another, and it was your love that fueled me to keep pushing the limit and placed me in the position to succeed. I would never have been able to learn so much and become a doctor had I not learned certain lessons from you. Thank you Mom and Dad, without you none of this achievement would have been possible. Also, to my closest friend and beloved Yan, who has been extraordinarily brave and considerate in our four years long-distance relationship between the United States and Germany. Your love and determination have carried me through the low and difficult times, and turned such a tough march into a bright and enjoyable journey. Thank you for your persistence, encouragement, and trust throughout the years.

Lastly, I want to say thank you to that young boy, for always following his heart, steadfastly fighting for his dream, and never giving up.

TABLE OF CONTENTS

CHAPTER 6

LIST OF FIGURES

LIST OF TABLES

ABSTRACT

Lightweight Vehicle Structures that Absorb and Direct Destructive Energy
Away from the Occupants
by
Weiran Jiang

Chair: Prof. Nickolas Vlahopoulos

One of the main thrusts in current automotive industry is the development of occupant-centric vehicle structures that make the vehicle safe for the occupants. A design philosophy that improves vehicle survivability by absorbing and redirecting destructive energy in underbody blast events should be developed and demonstrated. On the other hand, the size and weight of vehicles are also paramount design factors for the purpose of providing faster transportation, great fuel conservation, higher payload, and higher mobility. Therefore, developing a light weight vehicle structure that provides a balance between survivability and mobility technologies for both vehicle and its occupants becomes a design challenge in this research.

One of the new concepts of absorbing blast energy is to utilize the properties of "softer" structural materials in combination with a damping mechanism for absorbing the destructive energy through deformation. These "softer" materials are able to reduce the shock loads by absorbing energy through higher deformation than that of characteristic of normal high strength

materials. A generic V-hull structure with five bulkheads developed by the TARDEC is used in the study as the baseline numerical model for investigating this concept.

Another new concept is to utilize anisotropic material properties to guide and redirect the destructive energy away from the occupants along pre-designated energy paths. The dynamic performance of multilayer structures is of great interest because they act as a mechanism to absorb and spread the energy from a blast load in the lateral direction instead of permitting it to enter occupant space. A reduced-order modeling (ROM) approach is developed and applied in the preliminary design for studying the dynamic characterization of multilayer structures. The reliability of the ROM is validated by a spectral finite element analysis (SFEA) and a classic finite element analysis by using the commercial code Nastran.

A design optimization framework for the multilayer plate is also developed and used to minimize the injury probability, along with a maximum structural weight reduction. Therefore, the goal of designing a lightweight vehicle structure that has high levels of protection in underbody blast events can be achieved in an efficient way.

CHAPTER 1

Introduction

1.1 Research Overview

One of the primary functions of vehicle structures is to protect the occupants in extreme crash situations, which can be categorized into five major groups: front crash, rear crash, side impact, roof crush and roll-over. The structural topology and material selection play an important role in the design of crashworthiness. A variety of design strategies have been extensively studied by many researchers and applied to increase the levels of safety of the vehicle structures to protect the occupants from severe injury in crash events. Government standards have also been well established in many countries to ensure that vehicles meet a minimum performance level in those dangerous events.

However, in the last few decades, the appearance of regional militarization and worldwide terrorism has made blast events, especially underbody explosive events caused by IEDs and mines, a rising threat to the occupants in vehicles that may be exposed to them. Despite the potential for severe injuries and even massive casualties, limited design strategies have been considered, and few standards have been established for the design of vehicle structures facing these dangerous situations. Therefore, one of the new important designs thrust in automotive

industry is developing occupant-centric vehicle structures that provide a high level of survivability from underbody explosive threats while at the same time making the operation of the vehicle comfortable and safe for the occupants.

Alternatively, the size and weight of vehicles are also paramount design factors for the purpose of providing faster transportation, great fuel conservation, higher payload, and higher mobility. The intuitive strategies to improve the levels of protection, i.e. employing additional materials or protective armors, are a mutually exclusive with reducing weight and this poses a challenge in vehicle structure design. Therefore, developing a light weight vehicle structure that provides a balance between survivability and mobility technologies for both vehicle and its occupants becomes a design challenge in this research.

The design philosophy of energy absorption and re-direction is applied in vehicle structure designs for improving vehicle survivability and increasing occupant safety. For a certain amount of destructive energy, if more of the energy can be absorbed or redirected by the vehicle structures, less of the energy will get to the occupants and cause injuries. For example, a network of connected structural elements is widely used in the design of crashworthiness to distribute the crash energy more evenly throughout the front of the vehicle at a reduced structural weight. But due to space and packaging constraints, utilizing these traditional connected elements is often infeasible for chassis structures of the vehicle subjected to underbody blast loads. Hence, new non-traditional design concepts must be developed, to deliver the simultaneous goals of destructive energy management and structural weight reduction.

One of the new concepts of absorbing energy is to utilize the properties of “softer” structural materials in combination with a damping mechanism that can be used for absorbing the destructive energy through deformation. These “softer” materials are able to reduce the shock

loads that are transferred in the interior of the vehicle by absorbing energy through higher deformation than that of characteristic of normal high strength materials. Through the tuning of material properties, the structural components made of the "softer" materials can be utilized to their full advantage as an energy absorber and isolator to enhance the survivability of the vehicle in blast events. A generic V-hull structure developed by the US Army TARDEC is used in the study as the baseline numerical model for investigating this concept.

In underbody blast events, lumbar and spinal injury would be the most likely threats to occupants. But in the absence of an anthropomorphic test device in numerical models to measure lumbar loads, which is highly non-linear and highly dynamic in reality, the dynamic response index (DRI) is selected as an alternative linear indicator of lumbar injury assessment. The DRI is a dimensionless parameter proportional to the maximum spinal-lumbar compression, and it is often employed as a standard occupant injury metric for underbody blast simulation and testing. In this research, the value DRI is used as an evaluation of structural performance with respect to survivability.

Another new concept is to utilize anisotropic material properties to guide and re-direct the destructive energy away from the occupants along pre-designated energy paths. However, few monolithic materials and structures appear likely to be able to meet the above expectations and handle the conflicting demands of greater survivability and lighter structural weight. Thus, innovative functional-graded materials and multilayer structures have been proposed and developed. The dynamic performance of multilayer structures is of great interest because they act as a mechanism to absorb and spread the energy from a blast load in the lateral direction instead of permitting it to enter occupant space. This concept is promising but it is also extremely costly in modeling and computing if we use the general finite element analysis (FEA) in parametric

study and design optimization for a large number of alternative design configurations. However, no good alternative to FEA has been available.

To reduce the expensive modeling and computational cost resulting from the use of finite element analysis, a reduced-order modeling approach is developed and applied in the preliminary design for studying the dynamic characterization of multilayer structures. This reduced-order model (ROM), based on the reverberation matrix method and generalized ray theory from the perspective of wave propagation in solids, is able to rapidly generate information for identifying the preferred spreading directions and amounts of energy transfer. In combination with a DRI-based screening metric, the reduced-order model can be modified and used as an efficient tool to evaluate the performance of thousands of candidate multilayer plates. In this study, the reduced-order model is implemented, and three representative numerical examples of a three-layer plate configuration are examined.

The reliability of the reduced-order model is validated by a spectral finite element analysis (SFEA) and a classic finite element analysis using the commercial code Nastran in the preceding numerical example of a three-layer plate. The free response results, i.e. the eigenvalues, obtained by the ROM have good agreement with those obtained by the SFEA. Then, the forced response results, i.e. the screening metric, obtained by the ROM are evaluated and ranked for different multilayer plate design configurations. These response results are also validated successfully by comparison to the ranking obtained through much more computationally expensive finite element analysis results by using the solver in Nastran.

Based on the significant computational time saving by using the ROM, a design optimization algorithm for the multilayer plate is implemented and used to minimize the screening metric, along with a structural weight reduction. The optimization is applied on a set of

four case studies in which the number of sublayers varies from three to six. A material is selected from among several candidates for each sublayer and convergence studies are performed for each case study. The results of the optimal configurations show similar rankings to those obtained by using the FEA solver in Nastran, which indicates that the ROM shows promise for future use in parametric studies. Using the information generated by the ROM, a higher-fidelity structural analysis can be performed using a finite element code for relatively few configurations within the subset of the design space. Therefore, the goal of designing a lightweight vehicle structure that has high levels of protection when subjected to underbody blast events can be achieved in an efficient way.

1.2 Literature Reviews

In the last few decades, many researchers have been interested in the question of how light weight vehicle structures can be designed to improve vehicle survivability and levels of force protection by mitigating injury probability of occupants in blast events. In general, designers have used thin-walled tube structures as weight efficient kinetic energy absorbers in protective cabin designs, because they can dissipate a substantial amount of destructive energy through plastic deformation and fracture at the time of impact and blast occurrence. It's also crucial to develop a mechanism for redirecting destructive energy away from occupants other than merely absorbing the energy. This mechanism has been employed in vehicle design of recent years and it will guide the blast energy towards sacrificial parts of the vehicle structure that made of energy absorbing materials, instead of entering occupant compartment that enables the occupants to have a serious injury. The architecture of occupant-vehicle interfaces, which

combine the energy absorbing materials and the energy redirecting mechanism, needs to be carefully designed to maximize the isolation between vehicle surfaces and the occupants in the case of an explosion.

However, due to space restrictions, it is challenging to design an effective structure to protect occupants from underbody explosive events, and only a handful of researchers have been interested in studying this topic. Tabiei and Nilakantan (2007) studied reduction of acceleration-induced injuries from mine blasts under vehicles. Cherkaev and Leelavanichkul (2009) discussed principles of various designs of optimal structures that are capable of sustaining blast loads and keeping the structural integrity. A set of end-to-end full system level tools were developed by Thyagarajan (2010) to model the performance of vehicles subjected to underbody blasts, and numerous advanced modeling and simulation methodologies for improving occupant survivability and reducing structural weight of vehicles were studied and implemented by Vlahopoulos, Sun, and Zhang (2006-2011).

Based on their research, the concepts of absorbing and redirecting underbody blast energy through a lightweight ground vehicle structure have been proposed and shown to be critical, and the need for a non-traditional design philosophy as well as new simulation algorithms has become apparent to overcome the design challenge from the space restriction.

1.2.1 *Energy absorbing materials and structures*

Despite the promise of utilizing plastic deformation and fracture of the thin-wall tube structures, various non-traditional approaches have also been investigated to absorb energy

without high demands of space. Such approaches employ the properties of certain materials and structures as an energy absorbing mechanism in the design of protective structures.

One of the non-traditional approaches is utilizing properties of shear thickening fluid, which has large capacity for energy absorption. Shear thickening fluid is a specific type of non-Newtonian fluid whose viscosity dependents on the strain rate. It acts like a solid when experiencing a large shear load, such as an impulse of high pressure but of short duration from a blast, and returns to liquid form when the load is removed. Ahn and Osaki (1994) investigated the rheological characteristics of shear thickening fluid by a network model. Lee, Wetzel and Wagner (2003) studied the ballistic impact characteristics of Kevlar woven fabrics impregnated with a colloidal shear thickening fluid to design lightweight energy-absorbing body armor. By utilizing the rheological properties of shear thickening fluid, Zhang, Li and Gong (2008) developed a shear thickening fluid-filled damper, and a mathematical model was created on the basis of their experiments. An impact testing experiment was also conducted by Price (2012) to measure the energy absorption capacity of shear thickening fluid. While these applications show promise, the shear thickening fluid is still not suitable for vehicle structure designs in the current state because its non-controllable shape makes it too risky for vehicle structure components which require a high level of rigidity not only under blast shock loadings but also under normal circumstances as well.

Another non-traditional approach is utilizing the energy absorption and dissipation in failure phenomena of fiber reinforced composites. The failure mechanism of unidirectional fiber-reinforced composites of delamination, fiber-matrix deboning, matrix cracking, and fiber breakage can be considered for creating blast mitigation configurations. In the 90s of last century, the rising of composite material and its extensive application attracted many researchers in

multidisciplinary engineering fields, including aerospace engineering, naval engineering and biomechanical engineering. Great books of engineering mechanics of composite were published by Agarwal and Broutman (1990), Daniel and Ishai (1994), Herakovich (1998), and Jones (1999). As a consequence, numerous studies of how impact and blast energy can be dissipated by damage and failure in composites appeared at that time. Kyriakides, Arseculeratne, Perry, and Liechti (1995) systematically studied the compressive failure of fiber reinforced composites. Mouritz (1995, 1996) performed extensive research on the damage and failure behavior of glass-reinforced plastic (GRP) composites subjected to underwater explosion shock loadings. The dynamic response of strucutres subjected to blast load was explored by Türkmen and Mecitolu (1999) for stiffened composite laminates and by Comtois, Edwards and Oakes (1999) for polymer matrix laminates. In the 21st century, booming development of advanced composite materials and increasing threats of explosives directed towards vulnerable structures make research of blast resistance composite structures very necessary. Batra and Hassan (2006, 2007) studied the blast resistance of fiber reinforced composites subjected to air blast and underwater blast. Buchan and Chen (2007) studied and reviewed the blast resistance of polymer strengthened concrete and masonry structures. Yungwirtha, Radforda, Aronsona, and Wadleya (2007) conducted experiments to assess the blast resistance of composite pyramidal lattice truss structures. Currently, the extremely high cost of manufacturing the advanced composites and their low cost-performance ratio make utilizing the failure mechanism of composites to absorb energy not a good choice for the automotive industry. Nonetheless, the failure mechanism of composites is not directly applicable, and the concept of using multilayer composite materials instead of monolithic materials remains a promising approach for future research. In fact, Qiao, Yang, and Bobaru (2008) have already analyzed impact mechanics of multilayer materials with

high-energy absorbing layers. Mullin and O'Toole (2011) have also successfully simulated the multilayer energy absorbing materials in blast loaded structures with LS-DYNA.

The work of these researcher demonstrated that most of the energy absorbing mechanisms are implicitly associated with either large structural deformation or high engineering viscosity. A "softer" material with appropriate damping properties will be an ideal model with those two properties. Viscoelastic material, which works as a spring-damper system with moderate stiffness and damping properties, is such a model, and it has been considered as another suitable candidate for energy absorption. Carcione and Kosloff (1988) simulated wave propagation in a linear viscoelastic medium, and Roylance (2001) outlined mechanical properties and dynamic characteristics of linear engineering viscoelastic materials. Bartoli, Marzani, Matt, Scalea, and Viola (2006) extended the semi-analytical finite element method for modeling guided wave propagation in linear viscoelastic materials. Recently, viscoelastic material has been becoming prominent rapidly and has been applied widely in many research and engineering designs, in which performed as great energy absorbers. Behnke and Kaliske (2013) studied energy dissipation rate of generalized viscoelastic material models in a large scale application of steady state rolling tire structure. Hanyga (2013) studied wave propagation in linear viscoelastic media with completely monotonic relaxation moduli and its potential for energy absorption. Panchenko (2014) developed a numerical model of viscoelastic material using finite element method and compared the numerical results with experimental data. Because of its controllable shape, low cost, easy manufacturing, and considerable energy absorbing capacity, viscoelastic material shows great promise for the development of an effective energy absorbing vehicle structure that will protect the occupants from serious underbody explosive injuries.

1.2.2 *Anisotropic material properties and energy redirection*

The general approach to redirect energy is utilizing anisotropic material properties. The energy is usually carried by propagating stress waves and prefers to flow along directions with high group wave velocity, which depends on the ratio of local modulus of elasticity and local mass density. Therefore, microstructures of a material with anisotropic material properties, i.e. an elasticity tensor and a mass density tensor which vary smoothly with position, can be designed to build a stress wave path that is able to control and redirect the energy propagation.

Dewey, Adler, King and Cook (1977) measured the anisotropic elastic constant of Type 308 stainless-steel to build preferred local energy propagating orientations. Norris (1987) described how a pulse wave propagated in anisotropic elastic solids and developed a theory to explain that phenomenon. Carcione (1990) developed a theory and numerically simulated wavefields of wave propagation in anisotropic linear viscoelastic media. Fellinger, Marklein, Langenbergy, and Klaholz (1995) numerically modeled elastic wave propagation and scattering for three-dimensional anisotropic inhomogeneous media by using elastodynamic finite element integration technique. Norris and Wickham (2001) studied wave motion and energy transfer in inhomogeneously orientated isotropic materials. Ebrahimi, Abyazi, and Abbasi (2008) measured anisotropic mechanical properties in microalloyed S355N steel and studied effects of its microstructural anisotropy in a tensile test. Alireaza, Amirkhizi, Tehranian, and Nemat-Nasser (2010) summarized methods for managing stress-wave energy through the material anisotropy, and performed both numerical analysis and experiments to study the capability of energy redirection by smoothly changing material properties in various configurations.

In microstructure scope of a material, the stress waves travel spatially among lattices whose arrangement has a significant effect on the wave propagation direction. The mass density tensor consists of the mass of each particle, and the elasticity tensor consists of the bonds between any two particles, which can be treated as a net of massless springs. Numerous studies treating wave beaming, wave localization, and wave direction control, have been appeared in the last decade for the purpose of energy redirection. Phani, Woodhouse, and Fleck (2006) studied wave propagation in two-dimensional periodic lattices and investigated bandgap and wave directionality in hexagonal square and triangular honeycombs. Gonella and Ruzzene (2008) characterized the wave properties in terms of frequency and wavenumber relations, which is the dispersion relation of the lattice, and studied their dependence on direction of wave propagation. Kohrs and Peterson (2008) investigated the wave beaming and wave propagation in light weight plates with one-dimensional periodic truss-like cores and studied the dispersion characteristics theoretically and experimentally. Colquitt, Jones, and Movchan (2011) developed a mathematic model of elastic waves within a microstructural lattice system to study the dispersion relation and wave localization, and they also numerically validated the model. Osharovich and Ayzenberg-Stepanenko (2011) studied the steady state and transient anti-plane dynamic problems for wave localization in periodic stratified square-cell lattices and investigated how the anisotropy traps source energy within the stratified material. Charlotte and Truskinovsky (2012) developed a novel continuum model that could be used to build continuum approximations for lattice dynamics and served as a seamless interface between discrete and continuum elasticity theories. Casadei and Rimoli (2013) investigated two-dimensional periodic lattices as a means to induce strongly directional stress wave propagation in solids in a low-frequency broadband regime, and simulated the wave propagation under both harmonic excitations and impulsive loads. It is

found that, in general, redirecting energy not only requires the material anisotropy, but also requires a sufficient space for laying the "anisotropic energy path" within a material. Moreover, the stress waves usually have higher group velocities when they are travelling in elastic solids than any other medium, and as a result, enough space is more necessary for redirecting the blast energy in a short time period. Therefore, the constrained design space for underbody vehicle structures makes it extremely challenging to redirect the blast energy by utilizing material anisotropy smoothly in space, if not impossible.

Another category of applications that uses material anisotropy to change the direction of energy flow is functionally graded materials (FGM). The functional graded materials are characterized by the continuous variation in composition and structure gradually over volume, resulting in corresponding changes in the properties of the materials. Bertolino, Monagheddu, Tacca, Giuliani, and Zanotti (2003) studied functionally graded materials as thermal protection systems and tested their thermal insulating capability. Sioh (2010) studied functional graded materials made of metal and ceramic with nano-structured coating for protection, and performed experiments to exhibit the protection potential of those materials in terms of physical and mechanical properties. The concepts of functionally graded material inspire us with a new idea for energy redirecting in a constrained space: multilayer plate structure.

1.2.3 *Wave propagation in solids and multilayer medium*

In general, the dynamic response of a multilayer plate structure under a blast load is of great complexity because of numerous possible combinations of physical and material properties, as well as wave scattering at interfaces between two layers and wave reflecting at boundaries. In

the case of high damping sublayers or non-perfect bonding interfaces, i.e. fracture happens at interfaces, the situations are even more complicated that most of theories in mechanics of materials are no longer applicable. However, the problem becomes less difficult if it is seen from the perspective of wave propagation. Therefore, understanding how waves generated from a blast source perform and propagate in solids is of great importance before we start studying energy redirection characteristics of multilayer plate structures.

In fact, wave propagation in solids was one of the oldest subjects of elasticity. It began with Navier's theory and most of the early researches were on theoretical seismology. It was until 1940s that the propagation of elastic waves, plastic waves, and viscoelastic waves were studied, related to dynamic loading on engineering materials and structures. Since then, the research activity on wave propagation has grown rapidly within the community of engineering. Thomson (1950) investigated transmission of elastic waves through a stratified solid medium. Synge (1957) investigated transmission of elastic wave in an anisotropic solid medium. Abramson, Plass, and Ripperger (1958) first studied the wave propagation in simple structures including rods and beams. Mindlin (1959) studied the vibrations and wave propagation in simple plate structures and their corresponding response under dynamic loadings. Mindlin (1960) also studied transmission of axially symmetric waves in elastic rods structures. Chao (1960) studied dynamic response of an elastic half-space subjected to tangential surface loadings. Pao and Mow (1962) expanded the general dynamic problems of wave propagation in plates into the study of dynamic stress concentration in plates. Kraut (1963) developed advanced theories of wave propagation in anisotropic solids along with experimental results. Meeker and Meitzler (1964) investigated waveguides in elongated cylindrical and plate structures. Gekenheimer and Miklowitz (1969) investigated wave propagation in an elastic half-space solid caused by

transient excitations and travelling point loads on the surface. Zemenek (1972) performed theoretical and experimental investigation of elastic wave propagation in a cylinder. Two great textbooks were published in 1970s: "Wave propagation in solids" by Achenbach (1973) and "Wave motion in elastic solids" by Graff (1975). They systematically represented theories of wave propagation in solids and became great references over the past 40 years.

After that, the research of wave propagation in solids became a popular topic, from which many branches were spawned. The wave propagation in multilayer materials is one of the most important branches and of great interest to researchers in the field of aerospace engineering, naval architecture, and automotive engineering. Liu, Han, and Lam (1998) investigated elastic waves propagating in multilayer plates excited by plane pressure wavelets, and derived a general solution for obtaining displacement and stress in frequency domain by using linearly inhomogeneous elements. Abdelkarim, Vrouwenvelder, and Verweij (1999) developed a method to calculate the three-dimensional response of multilayer elastic half-space solids subjected to a surface loading in space-frequency domain by using Fourier transform techniques. Xi, Liu, Lam, and Shang (2000) investigated dispersion behaviors and characteristic surfaces of waves in a multilayer circular cylindrical shell by using a semi-analytical method based on the theory of three-dimensional elasticity, and studied the influence of inner radius and thickness of the shell. Liu and Ma (2002) studied the transition from transient response to steady-state response for a multilayer material subjected to anti-plane loadings, from near field to far field as well as from low frequency to high frequency. Kobayashi, Biwa, and Ohno (2004) theoretically and numerically examined wave transmission characteristics in multilayer elastic solids with periodic microstructure and fiber arrays. Shorter (2004) developed a spectral finite element method to analyze the properties of wave propagation and wave dispersion in linear viscoelastic multilayer

materials in wavenumber-frequency domain. Sun and Luo (2008) extended the three dimensional wave propagation problems in elastic multilayer solids to ones in viscoelastic multilayer solids, by using both analytical transformation approaches and finite element methods. Abid, Abbes, Chazot, Hammemi, Hamdi, and Haddar (2011) studied sound wave propagation and acoustic response of an elastic-viscoelastic multilayer panel by using transfer matrix method, and performed parametric studies to maximize its sound energy insulation capability. Based on the wave finite element methods, Chronopoulos, Troclet, Bareille, and Ichchou (2012) developed a dynamic stiffness approach for studying wave propagation and predicting the vibratory response of thick multilayer plate structures and sandwich panels.

The multilayer plates have been applied extensively in design of energy absorbing structures and blast resistance structures. Gupta and Ding (2001) developed multilayer plate structures with high wave speed layers to rapidly spread local impact loads laterally instead of penetrating through thickness in order to enhance structural blast resistance. Robbins, Ding, Gupta (2003) also performed various numerical studies to examine the effects of layer damage and imperfect interfaces on load spreading and blast resistance capabilities of the multiplayer plate structures. Xue and Hutchinson (2003) investigated performance of multilayer plates with different cores under impulsive blast loads and studied the structural topology for increasing blast resistance and reducing structural weight simultaneously. The RKU equations developed by Ross, Kerwin, and Ungar were widely used in constrained damping layer treatment for increasing energy absorbing capabilities in a multilayer plate structure. Gallimore, Kochersberger, and DeVita (2009) designed a thin multilayer plate structures with constrained damping sublayers for an aircraft landing gear system and optimized the structures to meet weight, strength and reliability requirements simultaneously. Dewangan (2009) extended the

studies of multilayer plate structures with constrained damping sublayers in three different approaches, including analytical solutions of the RKU equation, numerical analysis by using finite element methods, and experimental tests. Langdon, Chi, Nurick, and Haupt (2009) experimentally studied the dynamic response of multilayer panels subjected to blast loadings, and analyzed the influence of fracture at interfaces to dynamic characteristics of such panels. Fatt and Surabhi (2012) studied through-thickness stress wave response of a multilayer cylindrical shell with a foam core under external blast and optimized its blast resistance by tuning material properties of the core. Liu, Tian, Lu, Zhou, and Liang (2012) used finite element simulations to investigate the dynamic response and blast resistance improvement of all-metallic hollow multilayer cylinders with graded aluminum foam cores. Hassan, Guan, Cantwell, Langdon, Nurick (2012) investigated the influence of varying core density on the blast resistance of multilayer plates based on crosslinked PVC cores and aluminum alloy skins.

1.2.4 *Reverberation-ray matrix method and its application*

In the past, the two main approaches for analyzing wave propagation in multilayer plate structures are classic analytical solution obtained from stiffness matrix method, and numerical analysis by using finite element methods. However, both approaches have their drawbacks. The analytical stiffness matrix method is not able to correctly capture the response of the structures in either low frequency domain or high wavenumber domain. Although the finite element methods can calculate the response in the entire frequency-wavenumber domain accurately, the computational costs by using finite element methods are usually extremely expensive. It is necessary to develop a reduced-order model for the multilayer plate structures that is able to fast

evaluate a number of alternative configurations, and suitable for entire frequency and wavenumber domain.

The reverberation-ray matrix method, which is a combination of generalized ray theory and reverberation matrix method, has been developed and can be employed as a suitable reduced-order model for multilayer media problems. It benefits from both of its parents: the fast computational speed from generalized ray theory, and the all frequency-wavenumber domain suitability from the reverberation matrix method. The early form of the reverberation-ray matrix method was first developed by Pao and Gajewski (1977). They elaborated the generalized ray theory and constructed a reverberation matrix to capture the wave propagation and scattering in entire frequency-wavenumber domain for multilayer media. At that time, the reverberation-ray matrix method was mostly used in seismology for capturing the wave propagation in an earthquake and analyzing dynamic response of earth crust, which can be simplified as an infinite multilayer media. Along with rapid development of material science in late 1990s, the multilayer materials have gradually replaced homogeneous materials in many engineering fields, especially in lightweight structure design and blast resistance armor analysis. Because of its full-field suitability and computational efficiency, the reverberation-ray matrix method was brought to the forefront in extensive research and engineering applications of multilayer material and structure. Pao, Keh, and Howard (1999) renovated and fully described the reverberation-ray matrix method, and analyzed dynamic response of planar frames and trusses in terms of the propagation of longitudinal and flexural stress waves, which are multi-scattered at joints of the structural members. Lee and Ma (1999) theoretically reformed the reverberation-ray matrix method particularly for analyzing transient elastic waves propagating in a multilayer medium subjected to in-plane dynamic loading, and performed an acoustic emission experiments to verify the

theoretical solutions. Pao, Su, and Tian (2000) applied the reverberation-ray matrix method for wave propagation in stratified liquid, and numerically studied the response of the stratified liquid subjected to a shock load in underwater explosive events. Su, Tian, and Pao (2002) also extended the reverberation-ray matrix method in a two-dimensional multilayer solid by considering horizontal shear stresses, and performed numerical studies to analyze the wave propagation in a five-layer solid. Tian, Yang, and Su (2005) applied the reverberation-ray matrix method to investigate transient waves in a transversely isotropic laminate that is impacted by axisymmetric load, and parametrically studied the influence of thickness and elastic constant of each sublayer on the wave propagation in laminate. Chen, Wang, and Bao (2007) investigated the dispersion behavior of waves in an elastic plate with material properties varying along the thickness direction by using the reverberation-ray matrix method. They also compared the reverberation-ray matrix method with traditional stiffness matrix method and state-space method in numerical examples. Pao, Chen, and Su (2007) reviewed the reverberation-ray matrix method and compared it with transfer matrix method in unidirectional wave motion analyses to verify that the reverberation-ray matrix method is a viable alternative to the solutions of initial value and two-point boundary value problems of unidirectional wave motions. Guo and Chen (2007) applied the reverberation-ray matrix method to analyze the free vibration, frequency response, and transient response of space structures with multiple tuned mass dampers. Jiang and Chen (2008) extended the formulation of reverberation-ray matrix method to cases of continuously distributed loads and moving point loads on a non-uniform elastic bar, and validated the results by comparing with other existing analytical solutions. Guo, Chen, and Pao (2008) applied the reverberation-ray matrix method for modal analysis of complex three-dimensional framed structures. They also established orthogonal conditions for different natural model by integrating

Betti's reciprocity theorem with the reverberation-ray matrix method to performed transient response analysis based on the mode superposition. Based on the reverberation-ray matrix method, Tian and Xie (2009) developed a hybrid method that replaced the inverse Laplace transform and inverse fast Fourier transform in original reverberation-ray matrix method by Cagniard-De Hoop method, which had a capacity to analyze the transient wave propagation in a multilayer solid more accurately and efficiently. Cai, Nie, and Zhang (2009) applied the reverberation-ray matrix method for dynamic response of space structures that composed of bar elements with damping effect. They investigated axial, bending, and twisting wave motions numerically in beam structures and compared the results with those from finite element analysis. Tian (2010) developed a generalized reverberation-ray matrix formulation by combining classic reverberation-ray matrix method and stiffness matrix method. The generalized reverberation-ray formulation had higher calculation efficiency for analyzing the wave propagation in a complex multilayer-solid configuration, which composed of a large number of sublayers. Jiang, Chen, and Pao (2011) extended the reverberation-ray matrix method to investigate the transient response of a multi-span, continuous Timoshenko beam subjected to a moving load without discretization error. Zhu, Chen, and Ye (2011) extended the reverberation-ray matrix method to analyze the wave propagation and wave dispersion in multiferroic plates with imperfect interfacial bonding. Zhang and Nie (2015) applied the reverberation-ray matrix method for static analysis of planar framed structures composed of anisotropic Timoshenko beam members, and performed parametric analysis of geometrical and material properties of the frame structures.

1.3 Dissertation Contributions

In the area of vehicle structural dynamics, the proposed systematic design methodology and non-traditional simulation algorithm, which enables modeling of a lightweight vehicle structure with effective energy absorbing and redirecting mechanisms, are valuable for providing a design balance of two mutually exclusive objectives: occupant survivability enhancement and vehicle structural weight reduction.

The main contributions of this dissertation are:

- A spinal-lumbar injury metric used in underbody explosive events is developed based on the dynamic response index (DRI), which is a dimensionless number proportional to the maximum spinal-lumbar compression. A generic one-degree-of freedom model of human body is developed for fast evaluating the spinal-lumbar injury probability of occupants. After that, a more realistic three-degree-of-freedom model is developed, with the two intermediate degree-of-freedom representing seat and floor of the vehicle, which have highly non-linear dynamic characteristics. These two models have high compatibility with most of the numerical simulation algorithms, and are readily integrated with complex finite element models created in LS-DYNA and Nastran.

- A simplified TARDEV V-hull finite element model is developed for underbody blast analysis and blast mitigation technologies evaluation with LS-DYNA. The body surface of the vehicle structure and the inner floor of occupant compartment are connected by five bulkhead structures that perform as blast energy absorbers and insulators. Instead of using the traditional design of networks of connected structural elements, which absorb

destructive energy through their large plastic deformation and fracture at the time of blast occurrence, a novel design methodology is developed to absorb blast energy within a constrained design space by utilizing the damping properties of viscoelastic materials. In bulkhead design, the upper-bulkheads are made of high-strength steel to avoid the large local deformation and high local stress concentration, and the lower-bulkheads are made of viscoelastic material to absorb energy. Parametric studies for both single degree-of-freedom model and three-degree-of-freedom model are presented along with the final design configurations that simultaneously reduce both the structural weight and the spinal-lumbar injury probability of the occupant in underbody blast events. The investigation performed in this dissertation considers the total weight of the vehicle to remain constant when the weight of the structure is reduced. This provides an opportunity to increase the payload or the weights associated with other vehicle performance attributes, such as propulsion, mobility, radiated noise, etc.

- A reduced-order model for studying the non-linear dynamic response of multilayer plate structures subjected to an impulsive load is developed and implemented with MATLAB based on the reverberation-ray matrix method. In this model, the wave potential of each sublayer is transformed into the spectral domain by applying double Fourier Transforms. The waves generated by external loading are reflected and refracted at the interfaces of adjacent sublayers, and a scattering matrix S is built to represent the condition of continuity of stresses and displacements at each interface. The phase lag values of the traveling waves within each sublayer are represented by a phase matrix P. By inserting a permutation matrix U, a reverberation matrix R is generated as R=SPU to represent the

wave propagation and dynamic characteristics of the entire structure. By employing the generalized ray theory and inverse Fourier Transform, the dynamic response of the multilayer plate structure can be evaluated very quickly. Thus, the reduced-order dynamic model can be used to rapidly evaluate the performance of alternative multilayer plate designs and generate information for identifying the preferred directions and amounts of energy transfer. Then, by tuning material and physical properties in each sublayer, the information generated by the reduced-order model can be used as part of a design methodology that can be applied to a large number of candidate configurations of multilayer plates. The accuracy and efficiency of the method is validated for a numerical example of a three-layer plate. First, the free response results are compared with those from spectral finite element analysis. Then, the forced response results and CPU times are compared with those from classical finite element method using the commercial code Nastran.

- An effective screening metric of reduced-order model is developed for ranking a large number of candidate multilayer plate structures, which utilizes the one-degree-of-freedom DRI model as a foundation. A five-layer plate model is presented for validating the screening metric by randomly changing the stiffness of sublayers but keep the overall stiffness of the five-layer plate constant. An optimization frame work is developed by using DS Toolkit, for assessing the energy insulation capacity of multilayer plate structures that can minimize the screening metric subjected to a blast load at a structural weight reduction. An NSGA-II optimizer is used for identify the best multilayer plate structures configuration with varying number of sublayers, and a convergence analysis is

performed along with the optimization. The optimal configuration is validated by using finite element analysis in Nastran. Thus, a reliable and easy accessible package is successfully developed for fast evaluating the dynamic characteristics of multilayer plate structures with considerable number of sublayers and substantial candidate materials for each sublayer, from which the information generated can be used in a complex finite element analysis with a significant computational-cost reduction.

1.4 Dissertation Organization

In Chapter 1, a brief introduction of the motivation and background of this research is presented firstly. A general literature review of relevant technical approaches are provided and discussed in four subsections. After that, the main contribution of this research is also presented in this chapter.

In Chapter 2, the development of dynamic response index (DRI) is provided as a standard injury metric in underbody explosive events. In particular, a single degree-of-freedom model of human body, and an intermediate three degree-of-freedom model of human body integrating with an energy-absorbing seat and an energy-absorbing floor are presented respectively.

In Chapter 3, a numerical analysis in a generic V-hull vehicle structure is studied for the purpose of enhancing survivability and reducing structural weight simultaneously. The design of energy absorbing bulkhead structure is presented, and a brief introduction on viscoelastic materials is also provided. The process followed in the parametric study is discussed along with the final design configurations for both one degree-of-freedom DRI model and three degree-of-freedom DRI model.

In Chapter 4, the development of a reduced-order model for rapidly evaluating non-linear dynamic characteristics of multilayer plate structures is detailed in this chapter. The validation for the reduced-order model are also discussed respectively in a three-layer plate configuration by using spectral finite element analysis and classic finite element code in Nastran.

In Chapter 5, an effective screening metric is provided for ranking a large number of alternative configurations. The development of an optimization framework is presented, and its corresponding convergence analysis is studied. Four numerical examples are presented, and their optimal configurations are compared with the results obtained from Nastran.

In Chapter 6, the conclusion of this research is presented. The limitations for current approaches and the recommendations for future work are discussed in this final chapter as well.

CHAPTER 2

The Dynamic Response Index for Injury in Underbody Explosive Events

2.1 Introduction

In the last few decades, the appearance of regional militarization and worldwide terrorism has made blast events, especially underbody explosive events by IEDs and mines, a rising threat to the occupants in vehicles that may be exposed to them. The underbody explosive event is a very complex and highly non-linear transient phenomenon. The peak accelerations in underbody explosive events are larger in magnitude and shorter in duration than those in typical automotive crash events, as presented in Table 2.1, which may result in serious injuries to the occupant.

Catastrophic Events	Typical Peak Accelerations	Typical Time Duration
30 mph Frontal Automotive Crash	25g to 50g	70ms to 120 ms
Underbody Explosion	100g to 400g	3ms to 30ms

Table 2.1: The comparison between front crash and underbody explosion

In this chapter, The Dynamic Response Index (DRI), which is a standard occupant injury metric for underbody blast simulations and testing, is introduced as a measure of the structural

performance with respect to survivability. A simple single degree-of-freedom model of human body, and an intermediate three degree-of-freedom model of human body integrating with an energy-absorbing seat and an energy-absorbing floor are presented respectively.

2.2 Spinal-Lumbar Injury and the Dynamic Response Index

To evaluate the safety of vehicle designs, various injury metrics have been considered based on the prediction of dynamic response of occupants. Most of the occupant injury risk assessment tools and injury metrics are based on regular automotive crash standards that focuses on head and body acceleration in the direction paralleled to ground. For underbody explosive events, the blast loading imposed on the vehicle structure mainly concentrates in the upright direction, which leads the lower legs, lumbar, and spinal injuries to be the most likely threats to the occupant in the vehicle. In fact, the injuries in lower legs usually occur due to fast local structural effects in the first 10-15 millisecond of a blast event. They can be effectively mitigated by local structural reinforcement and basically may not lead to extreme damages to the occupant. While the core spinal and lumbar injuries caused by global vehicle dynamic effects in the next 50 millisecond are proved to be the most threat to the occupant in an underbody explosive event. Therefore, it's crucial to have a standard spinal-lumbar injury metric in the research of underbody blast mitigation technologies development.

The DRI, which is a dimensionless number proportional to maximum vertical spinal-lumbar compression, is developed and applied as a standard occupant injury metric for underbody simulations and testing. In the absence of an anthropomorphic test device in numerical models to measure the loading condition on occupants, which is usually highly non-

linear and highly dynamic in reality, the DRI provides an alternative linear indicator of occupant injury assessment in an underbody explosive event. The DRI is used throughout our research for determining the effectiveness of each blast mitigation configuration.

2.3 The Development of Single Degree-of-Freedom Model

A spinal system of human body is shown in Figure 2.1, and the upper body and pelvis are connected by the lumbar. For the occupant seating in a vehicle subjected to an underbody explosive load, most of the blast energy is delivered to the lumbar in a short time period along with a significant lumbar compression, and only small amount of the blast energy is transmitted to the upper body of the occupant so that the deformation of the upper body can be negligible.

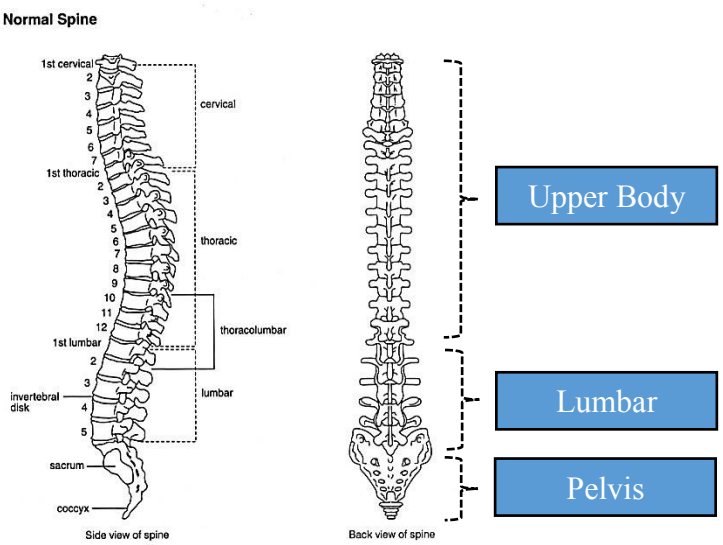

Figure 2.1: The structure of the human spine system

Then it is suitable to simplify the entire upper body as a rigid-body lumped mass and the lumbar as a mechanism that links the upper body and the pelvis by a spring and a damper

connected in parallel. As a result, a simple mass-spring-damper system is created to simulate the biomechanical response of the human spinal system, as illustrated in Figure 2.2.

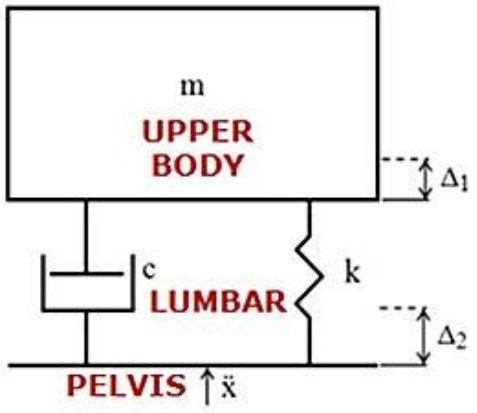

Figure 2.2: A mass-spring-damper system for modeling the human spine system

Because most of the blast energy is transferred upwards and unidirectional along the vertebrae of the occupant, the simple mass-spring-damper system only considers the motion in the vertical orientation thus it is also called single degree-of-freedom (SDOF) model in this dissertation. The parameter values of m, k, and c used here are derived by compressive strength of individual vertebrae and load-deflection curve from a representative population of Air Force pilots with a mean age of 28 years. The upper body lumped mass is approximated as 34.51 kg. A spring coefficient of 9.66×10^4 N/m and a damping coefficient of 818.1 N·sec/m are used to simulate the dynamic properties of the human lumbar. Therefore, the natural frequency ω_n and the damping ratio ζ of human lumbar are calculated as 52.9 rad/s and 0.224, respectively.

The biomechanical response is modeled as a linear second-order ordinary differential equation with lumbar compression as the variable. The time-dependent acceleration shown in Figure 2.2 is the shock load delivered to the pelvis location through the vehicle structure by the

blast event. Using this loading as the forcing function, the governing equation for the SDOF model is:

$$\frac{d^2\delta}{dt^2} + 2 \cdot \zeta \cdot \omega_n \frac{d\delta}{dt} + {\omega_n}^2 \cdot \delta = \frac{d^2x}{dt^2} \quad (2.1)$$

Where,

$\frac{d^2x}{dt^2}$**:** Time-dependent shock acceleration

ω_n**:** Natural frequency of human lumbar = $\sqrt{\frac{k}{m}}$ =52.9 rad/s

ζ**:** Damping ratio of human lumbar = $\frac{c}{2*\sqrt{m*k}}$ =0.224

δ**:** Lumbar Compression (relative displacement between pelvis and upper body) = $\Delta_2 - \Delta_1$

The DRI depends on the maximum lumbar force due to the maximum lumbar compression, $\delta_{max} = (\Delta_2 - \Delta_1)_{\max}$ which is the maximum relative displacement between pelvis and upper body. This stiffness portion of the force developed in the SDOF, $k\,\delta_{max}$, is normalized by the static lumbar force due to the weight of the upper body, *mg*, to yield the following definition of the DRI:

$$\textbf{DRI} = \frac{k\delta_{max}}{mg} = \frac{{\omega_n}^2}{g} \cdot \delta_{max} \quad (2.2)$$

The limiting DRI value is 17.7 with a 10% chance of serious injury which corresponds to a maximum lumbar compression of about 62 mm. The injury probability is based on the data of voluntary aviators subjected to the ejection seat mechanism, which has similar peak magnitude and loading duration to a blast load. The rate of compression might also be an important factor for injury, because it could lead to a significant force contribution in the representative SDOF

model through the viscous term. However, the traditional definition of the DRI is considered in this dissertation, which does not include a viscous term. In this research, it is assumed that reducing the DRI by absorbing or redirecting the destructive energy in vehicle structure would help keep the occupants safe in a blast event.

2.4 The Development of Three Degree-of-Freedom Model

In the SDOF model, the occupant is seating directly on the hull structure of the vehicle which can hardly happen in reality, and it makes the SDOF model a low-fidelity configuration. In a high-fidelity configuration, an inner floor structure and a generic seat system should be added between the occupant and the hull structure of the vehicle.

Therefore, a second three degree-of-freedom lumped parameter configuration is considered and implemented, with the two intermediate degree-of-freedom representing the seat and the inner floor of the vehicle. In this three degree-of-freedom model, an energy-absorbing seat and an energy-absorbing floor are mounted on the hull structure which is under the occupant's lumbar (SDOF model) and these two components can also be simplified and modeled as mass-spring-damper systems. Thus, two mass-spring-damper systems need to be included in the model as additional energy absorbers so as to simulate the environment in a more realistic way, as shown in Figure 2.3 on next page. In this case, the DRI is determined by the relative compression in the spring-damper system connecting the top and middle masses.

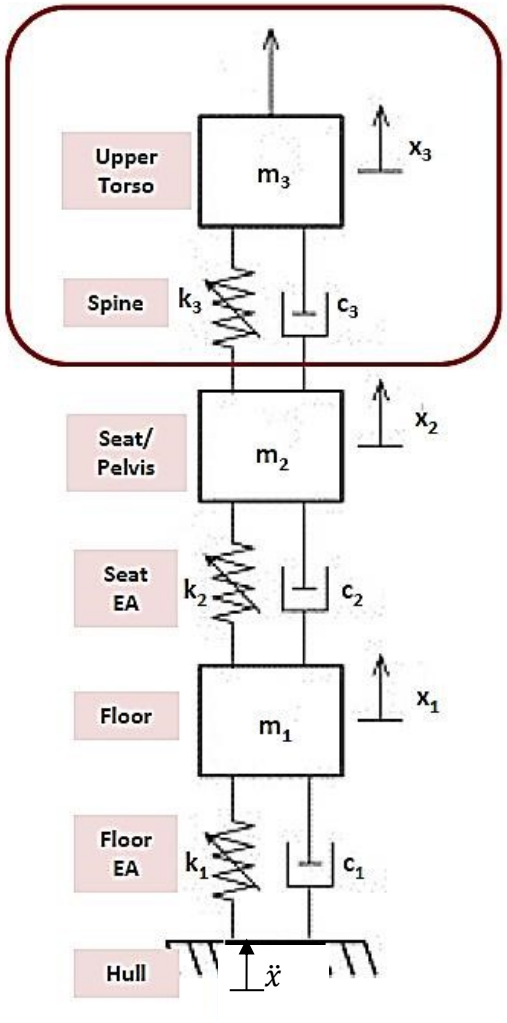

Assume: $z_3 = x_3 - x_2$;
$z_2 = x_2 - x_1$;
$z_1 = x_2 - x$

$$m_3\ddot{x}_3(t) = F_{spring3} + F_{damper3}$$

$$m_3\ddot{x}_3(t) = -k_3(x_3 - x_2) - c_3(\dot{x}_3 - \dot{x}_2)$$

$$m_3(\ddot{z}_3 + \ddot{x}_2) = -k_3 z_3 - c_3\dot{z}_3$$

$$\boldsymbol{m_3\ddot{z}_3(t) = -m_3\ddot{x}_2 - k_3 z_3 - c_3\dot{z}_3}$$

$$m_2\ddot{x}_2(t) = -F_{spring3} - F_{damper3} + F_{spring2} + F_{spring2}$$

$$m_2\ddot{x}_2(t) = k_3(x_3 - x_2) + c_3(\dot{x}_3 - \dot{x}_2) - k_2(x_2 - x_1) - c_2(\dot{x}_2 - \dot{x}_1)$$

$$m_2(\ddot{z}_2 + \ddot{x}_1) = k_3 z_3 + c_3\dot{z}_3 - k_2 z_2 - c_2\dot{z}_2$$

$$\boldsymbol{m_2\ddot{z}_2(t) = -m_2\ddot{x}_1 + k_3 z_3 + c_3\dot{z}_3 - k_2 z_2 - c_2\dot{z}_2}$$

$$m_1\ddot{x}_1(t) = -F_{spring2} - F_{damper2} + F_{spring1} + F_{spring1}$$

$$m_1\ddot{x}_1(t) = k_2(x_2 - x_1) + c_2(\dot{x}_2 - \dot{x}_1) - k_1(x_1 - x) - c_1(\dot{x}_1 - \dot{x})$$

$$m_1(\ddot{z}_1 + \ddot{x}) = k_2 z_2 + c_2\dot{z}_2 - k_1 z_1 - c_1\dot{z}_1$$

$$\boldsymbol{m_1\ddot{z}_1(t) = -m_1\ddot{x} + k_2 z_2 + c_2\dot{z}_2 - k_1 z_1 - c_1\dot{z}_1}$$

Figure 2.3: Three-DOF spring-mass-damper system simulating human lumbar, energy-absorbing seat, and energy-absorbing floor

The mass of the floor m_1 is 34 kg and the mass of the seat m_2 is 95 kg. The damping coefficient c_1 and c_2 are set to a constant value of 9220 N*sec/m for both the seat and the floor. However, the spring is now piecewise-linear, with the spring stiffness values shown in Figure 2.4 for the floor and Figure 2.5 for the seat. Three regimes are defined for the spring stiffness: an

initial stiffness regime, a low stiffness regime after yield, and a high stiffness regime after bottoming out.

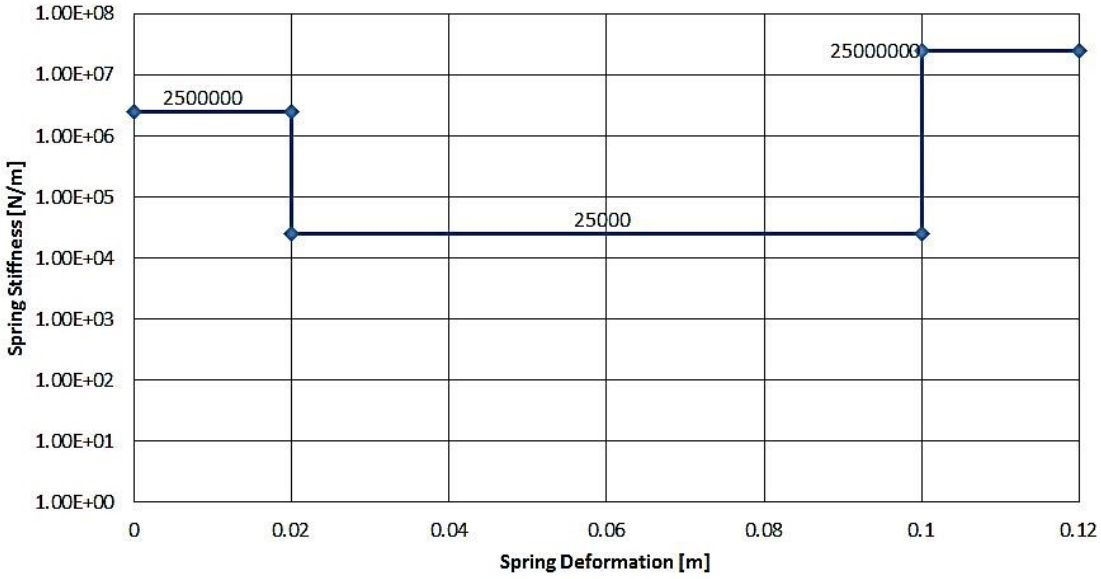

Figure 2.4: Spring stiffness curves for the energy absorbing floor (k_1)

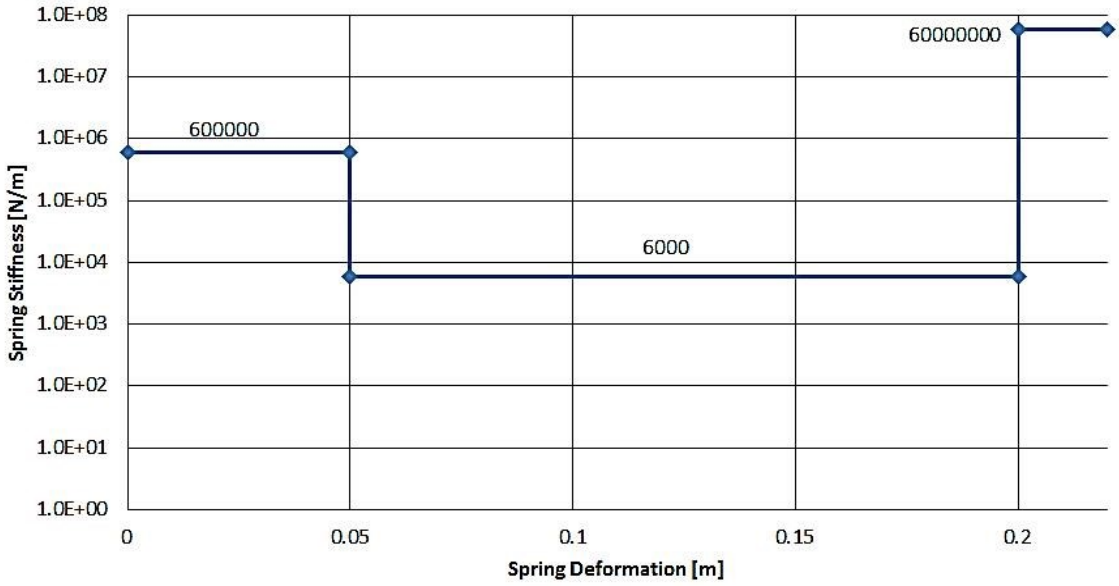

Figure 2.5: Spring stiffness curves for the energy absorbing seat (k_2)

CHAPTER 3

Numerical Analysis in a Notional V-Hull Structure to Reduce Structural Weight and Increase Blastworthiness

3.1 Introduction

One of the main thrusts in current automotive research is the development of occupant-centric vehicle structures that make the operation of the vehicle both comfortable and safe for the occupant. However, increased occupant protection often comes at a cost of increased weight of the vehicle. Ideally, a new vehicle design would feature a lighter-weight structure, because this enables faster transport, higher mobility, greater fuel conservation, and higher payload capacity. Therefore, a key design challenge for the vehicle is to develop occupant-centric ground vehicle structures that can provide high levels of protection while maintaining or reducing the weight of the vehicle structure.

In this research, a computational investigation is presented that examines whether the properties of the materials and/or components used in the construction of a ground vehicle structure can be effectively used as design variables to significantly improve the dynamic characteristics of the vehicle in an underbody explosive events. More specifically, the goal of this chapter is to explore the possibility of tuning the material and component properties to

improve the underbody blastworthiness (as characterized by the DRI metric from Chapter 2) while simultaneously lowering the weight of vehicle structure. A finite element model of a notional V-Hull structure is used as a numerical example in this study. The material properties and the configuration of the inner bulkheads that connect the V-shaped outer surface with the inner floor are used as design parameters for reducing the DRI at a typical occupant location. In this particular example, it is demonstrated that both the weight of the structure and the DRI can be reduced simultaneously. This is achieved by creating a new structural design that features energy absorbing and decoupling mechanisms among the bulkheads, floor, seat, and the occupant. The investigation performed in this research considers the total weight of the vehicle to remain constant when the weight of the structure itself is reduced. This provides an opportunity to increase the payload or the weights associated with other vehicle performance attributes (i.e. propulsion, mobility, radiated noise, etc.). Reducing the overall weight of the vehicle is not part of this study since it will increase the overall rigid body acceleration of the vehicle and therefore the forces experienced by the occupant.

In this chapter, the concept of using properties of "softer" structural materials i.e. viscoelastic materials is investigated. This allows for higher deformation levels in the structure, which—in combination with a damping mechanism—can result in a reduced base excitation, leading to lower DRI values that indicate a decreased risk of occupant injuries. Specifically, the properties of the inner bulkheads that connect the outer V-Hull bottom to the inner floor are tuned in this manner, thereby offering an isolation mechanism that reduces the DRI metric. The two main contributions of the work in this chapter are:

(1) The implementation of this structural design strategy;

(2) The demonstration of its effectiveness in terms of simultaneously reducing structure weight and increasing blastworthiness for a numerical example of a notional, generic V-hull structure.

In the following sections of this chapter, information is first presented about the numerical models employed in this study, namely the V-Hull finite element model subjected to an underbody explosive load, and the DRI lumped parameter models. The commercial software LS-DYNA is used in the blast simulations, and the LS-DYNA viscoelastic material definition is used for setting the various properties of the internal bulkheads in a parametric study. Therefore, a brief discussion on the linear viscoelastic material definition in LS-DYNA is presented. In the first setup, a mass-spring-damper model with a single degree-of-freedom representing the upper body of the occupant (as described in Chapter 2) is mounted directly in the middle of the inner floor. In the second setup, a three- degree-of-freedom model representing the upper body of the occupant, an energy-absorbing seat, and an energy-absorbing floor is mounted to the hull. Finally, the process followed in the parametric study is discussed along with the final design configurations that reduce both the structural weight and the DRI metric simultaneously.

3.2 The Development of Notional V-Hull Model

A generic finite element V-Hull structure model developed by the U.S. Army TARDEC (Tank Automotive Research Development and Engineering Center), referred to as the TARDEC Generic V-Hull, which is shown in Figure 3.1, is used for underbody blast analysis and blast mitigation technologies evaluation.

Figure 3.1: Finite element models for the TARDEC Generic V-Hull structure

This is a representative but notional ground vehicle structure that can be used in survivability research studies. In fact, this model is developed to be sufficiently generic that it can be used to evaluate the effectiveness of underbody blast analysis methods and blast mitigation technologies in a collaborative manner. Historically, the Army has had difficulty collaborating with industry and academia on research related to underbody blast events due to the sensitive nature of the work. Data generated from testing military vehicles typically cannot be shared with external research partners. To alleviate this issue, TARDEC has developed this generic vehicle hull model with the intent to share it with academia and industry in the hope of spurring innovation in blast analysis methods and blast mitigation technologies.

However, more than 220,000 elements in the TARDEC Generic V-Hull model result in an excessive consumption of computational source, and it is practically impossible to use such a

model to perform meaningful parametric study for academic research without sufficient high-performance computers (HPC). In this research, the main dimensions and the geometry of the TARDEC Generic V-Hull are used as a basis for creating a simplified V-hull model in Hypermesh that is shown in Figure 3.2.

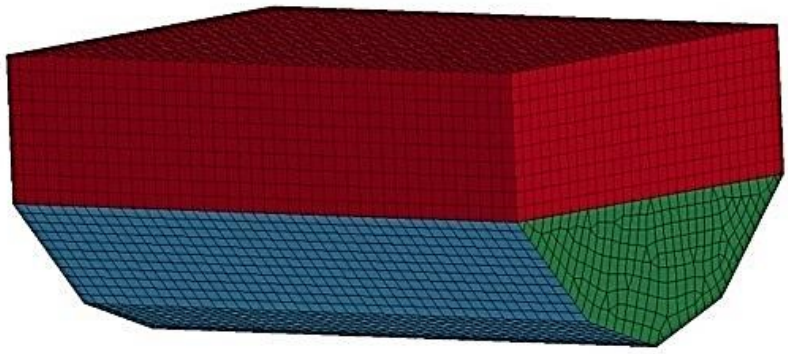

Figure 3.2: Simplified finite element V-Hull structure model that is used for the numerical results in this research

This simplified V-hull model is used for all of the numerical results shown in this dissertation. The baseline model for the simplified V-hull model has the same material properties and section properties for the main structural components as the TARDEC Generic V-Hull model. Figure 3.3 on next page shows the single degree-of-freedom lumped parameter model connected directly to the vehicle structure to evaluate the DRI. The upper part of the structure and the inner floor are removed from the figure in order for the internal bulkheads to be visible. These and all other parts that are omitted from the figure for visualization purposes are included in the simulations.

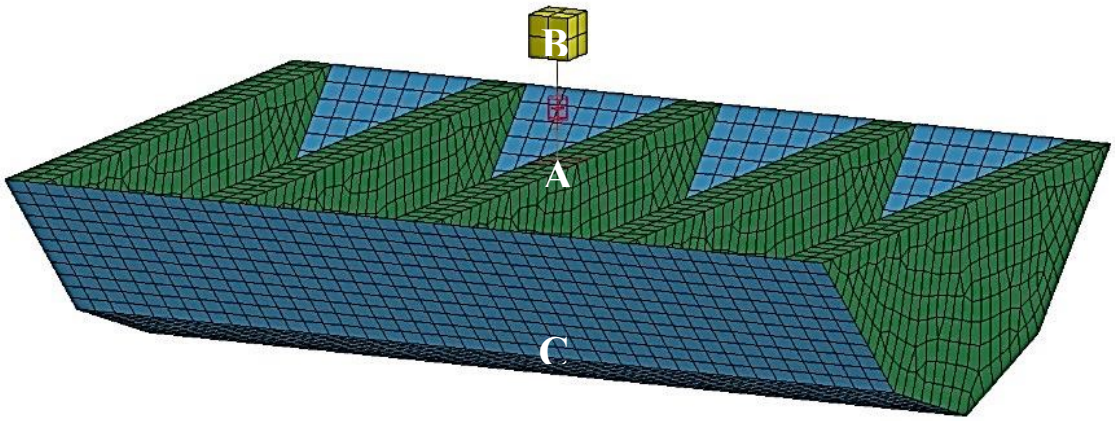

Figure 3.3: The single degree-of-freedom DRI model for evaluating blastworthiness of the V-hull structure

The V-hull model contains five inner bulkhead structures (solid elements) connecting the outer V-shaped surface with the inner floor (shell elements), as shown in Figure 3.3 and Figure 3.4. The material properties of the bulkheads are used as design parameters in the parametric study. The two DRI models are also integrated with the finite element V-hull structure model. In this research, it is assumed that reducing the DRI by absorbing or guiding the destructive energy in the hull structure would help keep the occupants safe in a blast event.

As mentioned earlier, a second three degree-of-freedom lumped parameter configuration is also considered, with the two intermediate degree-of-freedom representing the seat and the floor. This second configuration is shown in Figure 3.4. In this case, the DRI is determined by the relative compression in the spring connecting the top and middle masses. The nonlinear spring constants and linear damping coefficients for the lowest (floor) degree-of-freedom and for the middle (seat) degree-of-freedom are described in Chapter 2.

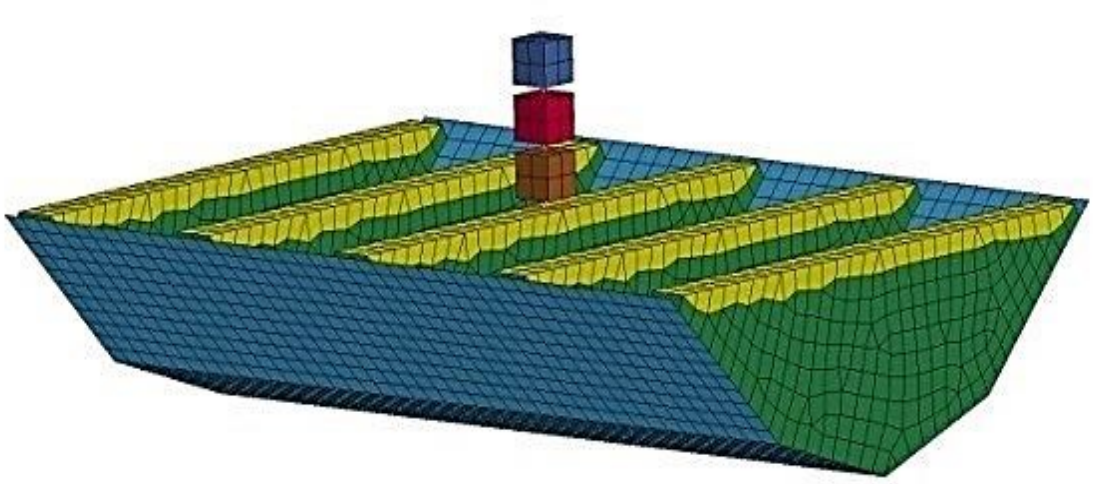

Figure 3.4: The three degree-of-freedom DRI model for evaluating blastworthiness of the V-hull structure

By including these single degree-of-freedom and three degree-of-freedom models directly in the LS-DYNA models, the calculations of the DRI are automatically performed when running the LS-DYNA simulations.

3.3 Viscoelastic Materials and Design of Energy-Absorbing Bulkheads

Viscoelastic materials, such as rubbers, foams, and most of the biological tissues, exhibit both viscous and elastic characteristics when they are undergoing mechanical deformation. For elastic materials, each stress state corresponds to an instantaneous strain state, which is independent of time history of the strain. While for viscoelastic materials, the stress state not only depends on the instantaneous strain, but also has a high dependence of strain rate. Therefore,

purely elastic materials can barely dissipate energy during loading and unloading while viscoelastic materials possess a capacity to dissipate energy through hysteresis effects during the loading cycle. The coexistence of an elastic component and a viscous component makes the spring-damper system an ideal mathematical model to represent viscoelastic materials. Two classical linear models, namely the Maxwell model and the Kelvin model, are shown in Figure 3.5, illustrating two elementary type of viscoelasticity. The strain-dependent elastic stress is associated with the spring element and the strain-rate-dependent viscous stress is associated with the damper element.

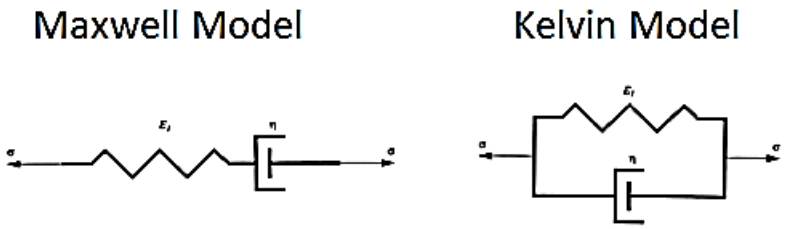

Figure 3.5: Linear viscoelastic material model - Maxwell model and Kelvin model

The only difference between these two models is the pattern of connection of the spring-damper system. The spring and damper are connected in series in the Maxwell model, and in parallel in the Kelvin model. As a result, the stresses are equal in both spring and damper element for the Maxwell model, while the total strain equals to the summation of the strain of the spring and the strain of the damper. In contrast, the strains are equal in both spring and damper element for the Kelvin model, while the total stress equals to the summation of the stress of the spring and the stress of the damper. However, the Maxwell model and the Kelvin model are valid for a limited set of viscoelastic materials.

For the materials with more typical viscoelastic properties, a more elaborate spring-damper model is used to simulate general material viscoelasticity. It is called a standard linear viscoelastic material model as shown in Figure 3.6.

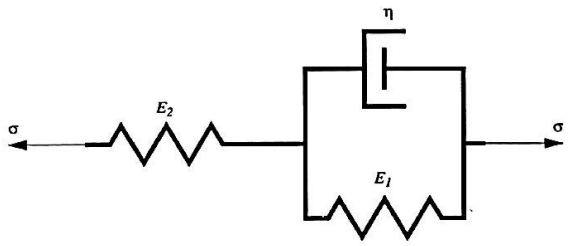

Figure 3.6: Standard linear viscoelastic material model

The standard linear model is a combination of the Maxwell and the Kelvin model. The damping constant is η, and the spring constant is assigned to be E_1 for the leftmost spring and E_2 for the spring connected in parallel with the damper (the Kelvin model). The stresses and strains yield the following constraints in Eq. (3.1) and Eq. (3.2), and the strain rate is shown in Eq. (3.3).

$$\sigma = \sigma_{E_2} = \sigma_{Kelvin} \tag{3.1}$$

$$\varepsilon = \varepsilon_{E_2} + \varepsilon_{Kelvin} \tag{3.2}$$

$$\dot{\varepsilon} = \dot{\varepsilon}_{E_2} + \dot{\varepsilon}_{Kelvin} \tag{3.3}$$

By applying Hooke's Law and taking the first derivative of the strain, the strain rate of the leftmost spring and the Kelvin model can be expressed as:

$$\dot{\varepsilon}_{E_2} = \dot{\sigma}/E_2 \tag{3.4}$$

$$\dot{\varepsilon}_{Kelvin} = (\sigma - E_1 * \varepsilon_{Kelvin})/\eta \tag{3.5}$$

By substituting Eq. (3.2), Eq. (3.4), and Eq. (3.5) into Eq. (3.3) and performing simple steps of algebra, the strain rate of the standard linear model can be obtained and shown in Eq. (3.6):

$$\dot{\varepsilon} = \frac{\sigma}{E_2} + \frac{\sigma}{\eta} * \left(1 + \frac{E_1}{E_2}\right) - \frac{E_1}{\eta} * \varepsilon \tag{3.6}$$

Assume initial stress $\sigma_0 = 0$ and a constant initial strain $\varepsilon = \varepsilon_0$ is applied instantaneously at time t = 0, then the strain rate $\dot{\varepsilon}$ would be zero when t > 0. Therefore, a linear first-order ordinary differential equation (ODE) can be obtained by substituting the initial conditions into Eq. (3.6):

$$\dot{\sigma} + \frac{(E_1+E_2)}{\eta} * \sigma - \frac{E_1*E_2*\varepsilon_0}{\eta} = 0 \tag{3.7}$$

Eq. (3.7) is a first-order differential equation and can be solved by using the initial stress $\sigma = 0$ and yield a solution:

$$\sigma(t) = \varepsilon_0 * \left[\frac{{E_2}^2}{E_1+E_2} * e^{-\frac{E_1+E_2}{\eta}*t} + \frac{E_1*E_2}{E_1+E_2}\right] = \varepsilon_0 * E(t) \tag{3.8}$$

It can be observed that the effective modulus of elasticity of the standard linear viscoelastic material model $E(t)$ is no longer constant but time-dependent now. As the strain assumed to be a time-independent constant $\varepsilon = \varepsilon_0$, the corresponding stress curve is illustrated in Figure 3.7 on next page.

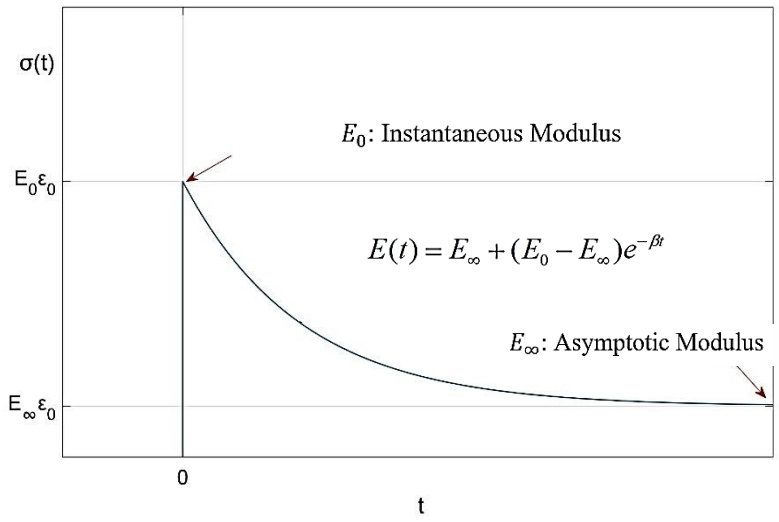

Figure 3.7: The stress curve for the standard linear viscoelastic material model under a constant strain

The effective modulus of elasticity of the standard linear viscoelastic material model $E(t)$ can be expressed in a compact form as:

$$E(t) = E_\infty + (E_0 - E_\infty) * e^{-\beta t} \tag{3.9}$$

Where,

The instantaneous modulus $E_0 = \frac{{E_2}^2}{E_1+E_2}$;

The asymptotic modulus $E_\infty = \frac{E_1*E_2}{E_1+E_2}$;

The decay constant $\beta = \frac{E_1+E_2}{\eta}$;

The viscoelastic material definition of LS-DYNA (MAT_061: *MAT_KELVIN-MAXWELL_VISCOELASTIC) is used for modeling this material in the finite element analysis. The parameters that are considered include: mass density ρ, bulk modulus $K = \frac{E_\infty}{3(1-2\nu)}$, short-

time shear modulus $G_0 = \frac{E_0}{2(1+v)}$, long-time shear modulus $G_\infty = \frac{E_\infty}{2(1+v)}$, and decay constant β. The bulk modulus, the short-time shear modulus, and the long-time shear modulus are determined by the instantaneous modulus of elasticity E_0 and the asymptotic modulus of elasticity E_∞. A linear relationship between the instantaneous modulus of elasticity E_0 and the asymptotic modulus of elasticity E_∞ is used in this research, with $E_0=1000\times E_\infty$. Therefore, the Poisson's ratio of the material v, the mass density ρ, the decay constant β, and the asymptotic modulus of elasticity E_∞ are sufficient for defining the viscoelastic material properties in LS-DYNA simulations.

As mentioned in the preceding section, the bulkhead structures connecting the outer surface and the inner floor of the V-hull are expected to perform as an energy absorber and/or insulator. The density, the modulus of elasticity, and the dissipation properties of the material comprising the bulkheads are used in the parametric study for simultaneously reducing the weight of the structure and the DRI. In this research, the bulkheads are designed to be softer and more compressible than regular steel bulkheads so that the damping property of viscoelastic material can become an active contributor in the energy absorption, similar to the energy dissipation mechanism in a dashpot. By tuning the viscoelastic material properties in a large numbers of parametric studies, an energy isolation mechanism is created to reduce the occupant DRI while also reducing the total structural weight. Providing an energy dissipation capability in the bulkheads and altering their dynamic characteristics results in an improvement of the DRI metric. The location where the DRI is evaluated will influence the outcome of the study. In this parametric study the location right above the explosive is selected as representative of a location where a severe loading is expected. It's also necessary to mention that the purpose of parametric

study is not selecting real engineering materials but rather to investigate how materials properties would affect the dynamic response of the structure.

3.4 Parametric Study Using SDOF DRI Model

Before starting the parametric study, it is necessary to define a proper loading condition that will be applied on the V-hull finite element model. The CONWEP load (*LOAD_BLAST) in LS-DYNA is used to simulated the underbody air blast loading caused by TNT explosive, with the origin located 0.2m beneath the midpoint of the keel of the V-hull. The air blast loading is described by the Friedlander waveform and its time history is shown in Figure 3.8, where P_s is the peak blast pressure, t^* is the positive phase duration and t_d is the negative phase duration. They all depend on the total mass of explosive.

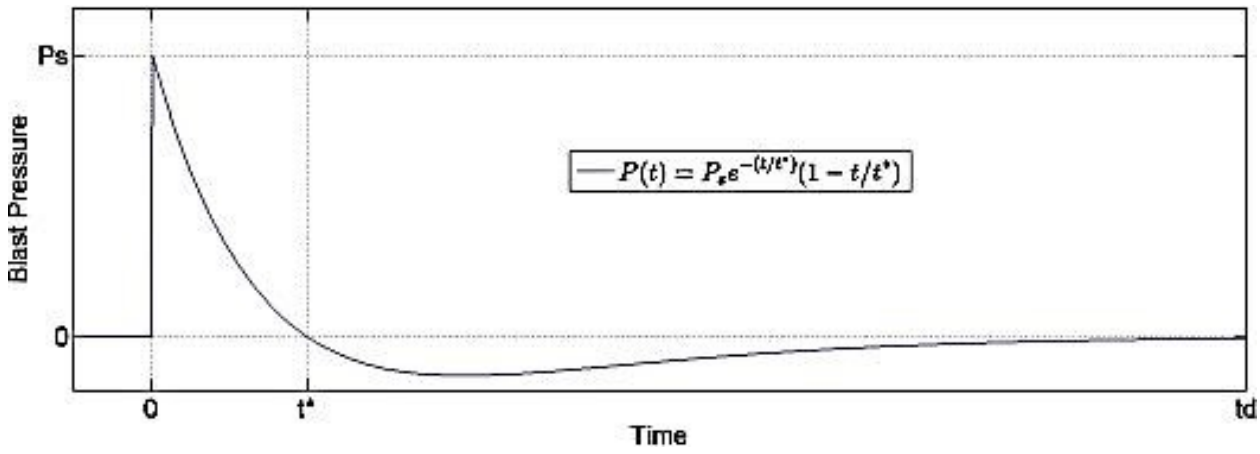

Figure 3.8: The CONWEP air blast loading

The configuration with the SDOF DRI model connected to the floor (Figure3.3) for evaluating the DRI was analyzed first. In an initial parametric study, the material properties

were changed for the entire volume of each bulkhead. In order to fast evaluate multiple configurations in the preliminary trial tests, a relative weak explosive source was used to economize the computational cost. First, an original configuration made of regular steel (density of 7,800 kg/m^3, Young's modulus of 200×10^9 N/m^2) was tested without having any damping properties. The vertical displacement for the pelvis (point A in Figure 3.3) and the upper torso (point B in Figure 3.3) were recorded and shown in Figure 3.9.

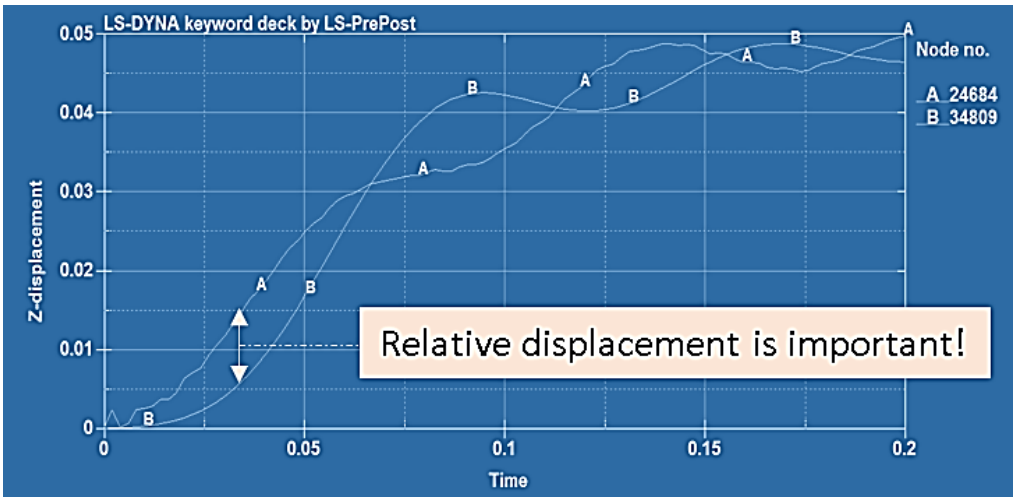

Figure 3.9: Time histories of vertical displacement for pelvis and upper body in baseline model under a weak explosive load

The difference between the line A and line B was the relative displacement of the human lumbar/spinal system. As discussed in Chapter 2, the purpose of the design was to minimize the maximum positive value of the relative displacement, i.e. the lumbar/spinal compression, in order to reduce the occupant's injury probability. Visually, it was desirable to have those two lines as close as possible by tuning the material properties in the parametric study. If the two lines were perfectly matched, then the occupant seating in the vehicle would be 100% safe. In this baseline configuration, the maximum lumbar/spinal compression was 9.39 mm.

It was also observed that the relative displacement/velocity of the bulkhead (between point A and C in Figure 3.3) was extremely small as the regular steel bulkheads were too stiff to deform and they performed as a rigid body. In order to utilize the properties of viscoelastic material, it was critical to make the bulkheads deformable so that they would have a chance to perform as a spring-damper system with relative displacement and relative velocity between point A and point C. After reducing the modulus of elasticity of the bulkheads to be 200×10^5 N/m^2, the resulting lumbar/spinal compression became larger but the bulkheads were deformable now, as shown in Figure 3.10. In this configuration, the maximum lumbar/spinal compression was 12.11mm. The corresponding DRI was 129% of that in the baseline configuration.

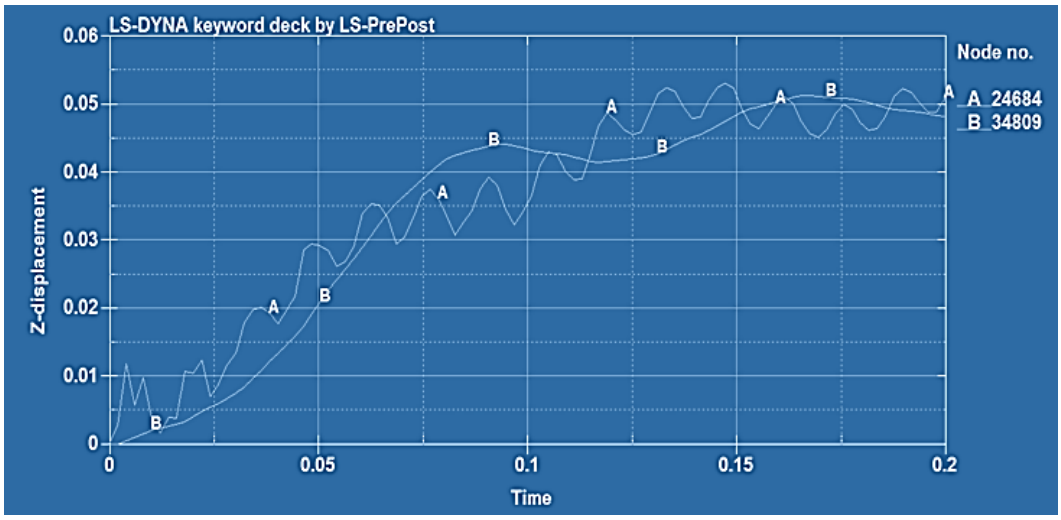

Figure 3.10: Time histories of vertical displacement for pelvis and upper body in the configuration of E= 200×10^5 N/m^2 under a weak explosive load

As the bulkheads became "softer", it was the time to add proper damping properties in the bulkheads to make it viscoelastic for the purpose of absorbing blast energy. By keeping the modulus of elasticity of the bulkheads 200×10^5 N/m^2 unchanged, the decay constant β was tuned. It was found that the decay constant should be constrained in a particular range for each

configuration with different modulus of elasticity. The excessive damping added in the bulkheads would make them lost their capability of energy absorption because the substantial phase lag resulted in a significantly large relative displacement, while the insufficient damping would have negligible influence on the energy absorption by the nearly elastic bulkheads. The proper decay constant for current configuration was found to be β=0.01 by trial and error, and similarly to Figure 3.9 and Figure 3.10, the corresponding vertical displacement time histories were plotted in Figure 3.11 below.

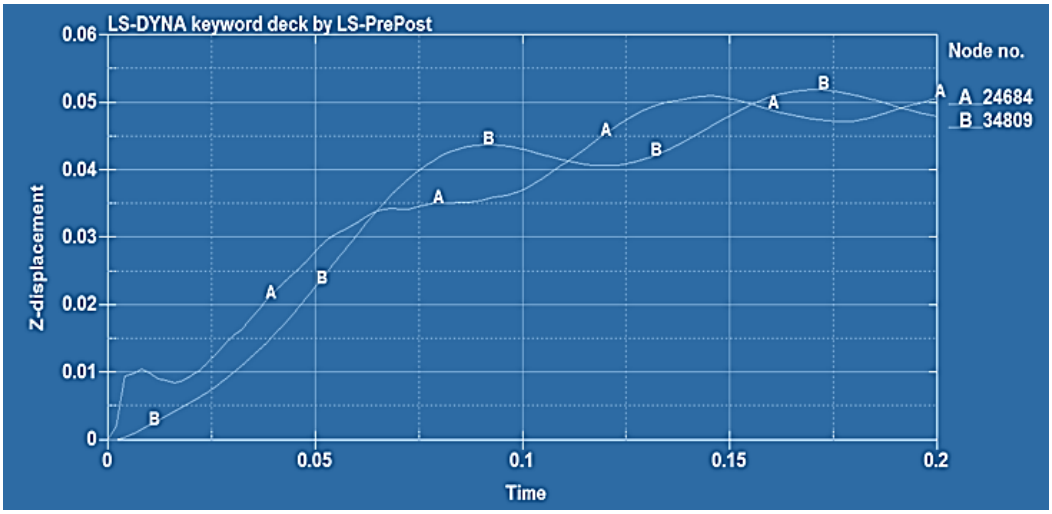

Figure 3.11: Time histories of vertical displacement for pelvis and upper body in the configuration of E= 200×10^5 N/m^2 and β=0.01 under a weak explosive load

The maximum lumbar/spinal compression was 9.07mm and the corresponding DRI was calculated to be 96.59% of that in the baseline configuration. It indicated that the viscoelastic bulkheads were capable to reduce the DRI by partially absorbing the blast energy from the underbody explosive loading. Nevertheless, the percentage of DRI reduction was not significant and several design drawbacks were found during the preliminary parametric study. In order to enlarge the energy absorbing capacity of the viscoelastic bulkheads, the original configuration

needed to be modified in a conservative manner meanwhile preserved its V-shaped geometry features.

Two main conclusions were drawn from this initial effort and a new vehicle structure configuration is presented accordingly in Figure 3.12.

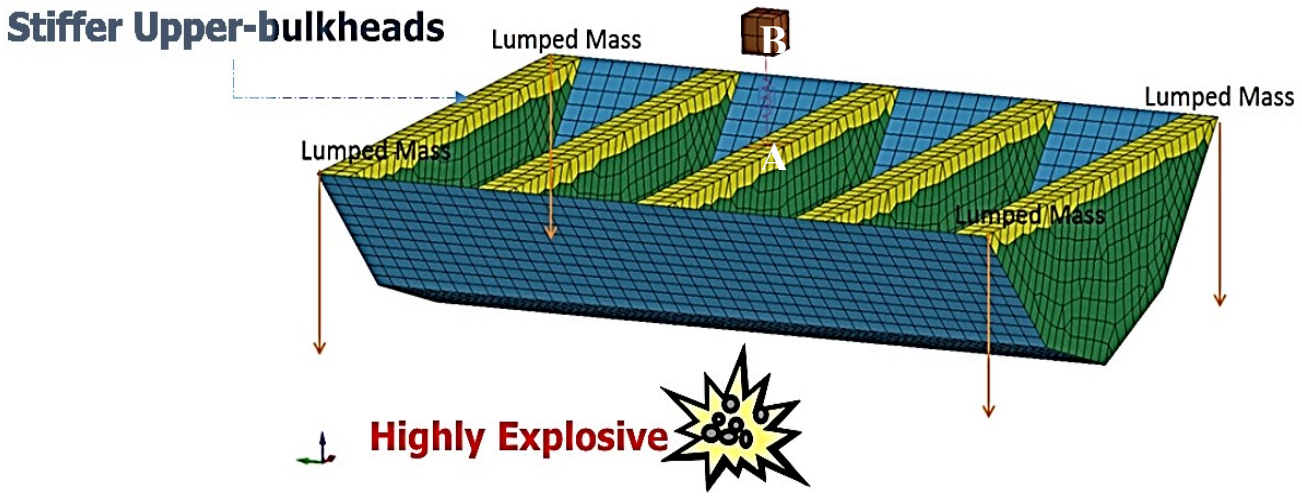

Figure 3.12: Partition of the bulkheads into two sections (yellow and green); and locations where lumped masses are attached for preserving the overall vehicle mass

First, it was decided to preserve the original steel properties for the upper part of each bulkhead (colored yellow in Figure 3.12) and alter the stiffness, the density, and the dissipation characteristics in the remaining portion of each bulkhead (colored green in Figure 3.12). The reason for this approach is to avoid excessive local flexibility at the location where the SDOF model is attached to the floor when the bulkhead has reduced stiffness properties. The local flexibility at the attachment point makes it difficult to control the spring compression that determines the DRI values.

The second observation was that the overall mass of the vehicle has an impact on the overall rigid body response of the vehicle and reducing the overall mass of the vehicle may increase the occupant injury probability and the DRI value. Therefore, four equal lumped masses were added at the four corners of the vehicle to keep the total weight constant at the typical representative weight of such a vehicle. For each configuration, the values of the lumped masses were selected in a manner that the overall mass of the vehicle remained constant. The locations where the lumped masses were attached are shown in Figure 3.12. This approach also reflects the ability to increase the payload of a vehicle even when the structure itself becomes lighter.

In the V-hull analysis, a similar testing procedure is applied. An original configuration with both of the upper bulkheads and lower bulkheads made of regular steel (density of 7,800 kg/m^3, Young's modulus of 200×10^9 N/m^2) was first tested. A high explosive load is used at this time so that the mass of the underbody explosive yields a DRI value that is slightly above the level that corresponds to a serious injury risk. The result obtained from this all steel configuration is set to be the baseline. Then, a viscoelastic material was used instead of regular steel in the lower bulkhead design. After tuning the asymptotic modulus of elasticity from 200×10^9 N/m^2 to 200×10^3 N/m^2 and decay constant from 0.0001 to 1000 in the lower bulkheads, based on 168 testing runs in LS-DYNA, the final configuration identified from the parametric study had the following values: density equal to 6,000 kg/m^3, asymptotic modulus of elasticity equal to 800×10^6 N/m^2, and a decay constant equal to 0.0015. The Poisson's ratio did not vary and was set equal to 0.3.

The time histories of vertical displacement for pelvis (red line) and upper torso (green line) are shown in Figure 3.13 and Figure 3.14 on the next page, for both the regular steel bulkheads configuration and the viscoelastic bulkheads configuration.

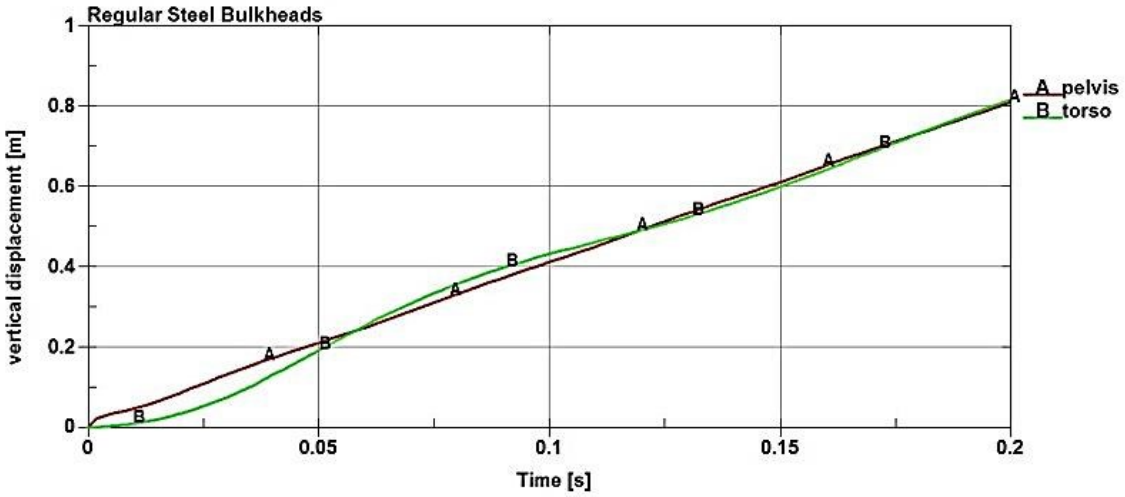

Figure 3.13: Time histories of vertical displacement for pelvis and upper body in baseline model under a high explosive load

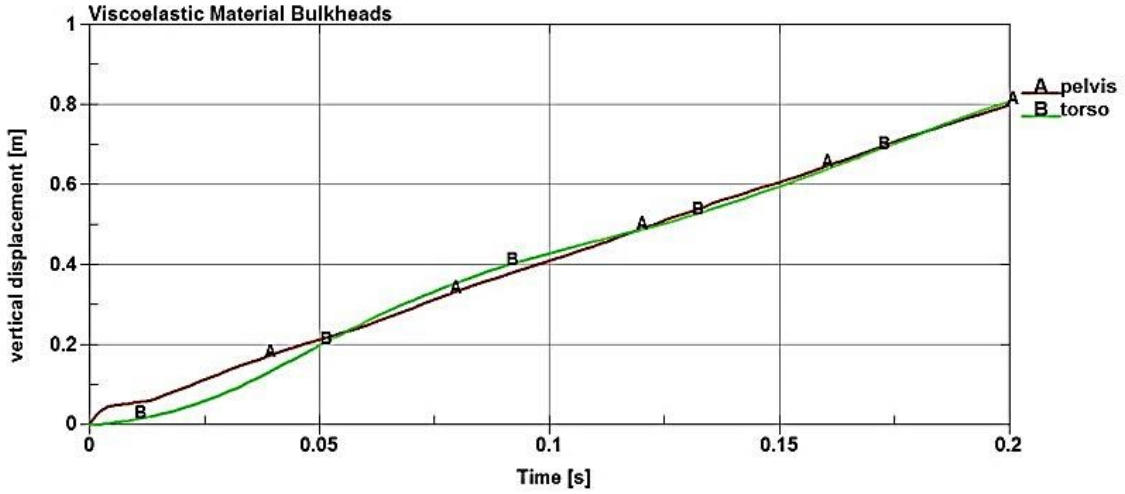

Figure 3.14: Time histories of vertical displacement for pelvis and upper body in the model with viscoelastic bulkheads under a high explosive load

The most important observation is that in the viscoelastic bulkhead configuration, the pelvis displacement has a “jump-up” around 0.004s and gradually stops increasing, and then it behaves similarly with the regular steel configuration. It is because the lower density makes the viscoelastic bulkheads lighter so they are easier to be lifted up compared to the regular steel bulkheads configuration. Meanwhile, this effect is also gradually balanced by the larger viscoelastic bulkhead deformation due to the lower stiffness in combination with the damping property. Therefore, the appearing and vanishing of the first “peak” in Figure 3.14 could be explained. After that, the rigid body motion of the vehicle becomes the dominant factor for the pelvis displacement.

The relative displacement, namely the deformation of the upper body relative to the pelvis can be easily calculated, and illustrated in Figure 3.15 on next page. The red line represents the results obtained from the baseline model (regular steel bulkheads), and the blue line represents the results of the parametric study (viscoelastic bulkheads). The amount of explosive is tuned to impose the DRI of the baseline configuration just reach the critical point of 10% serious injury in order to have a high fidelity simulation.

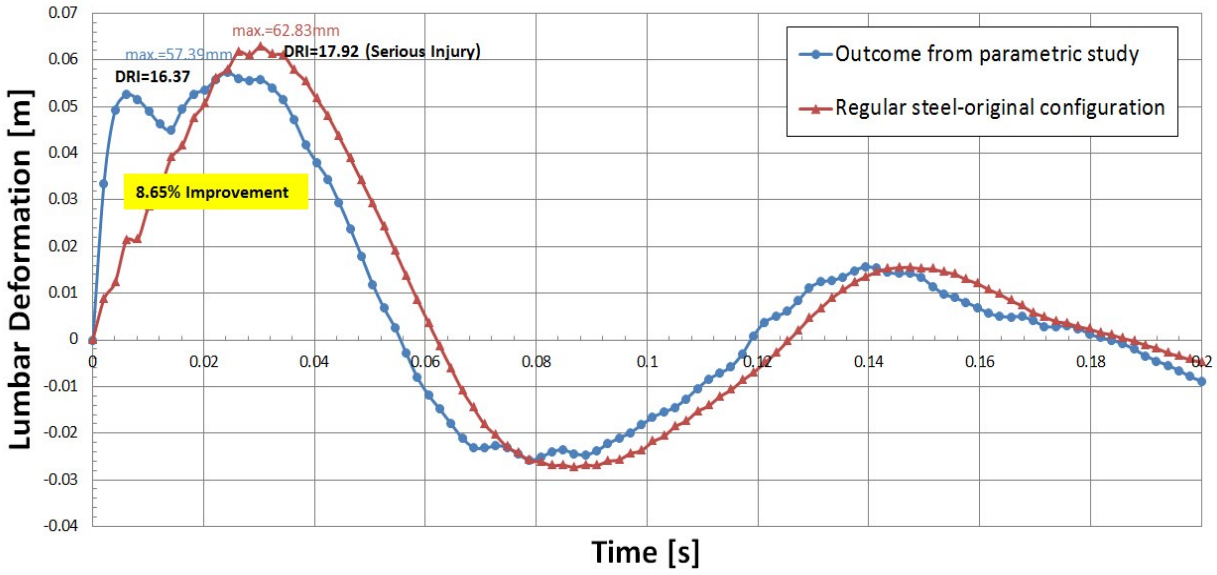

Figure 3.15: Time histories of lumbar deformation in the single degree-of-freedom lumped parameter DRI model

Figure 3.15 summarizes the time histories of deformation of the upper torso relative to the pelvis, for the original configuration (bulkheads made of regular steel) and the final configuration. The values for the maximum spring compression and the associated DRI are also included in the figure. An improvement of 8.65% is observed in the DRI while achieving a 12.5% reduction in the mass of the structure by designing lower density bulkheads without changing the structure geometry. Also, as mentioned earlier, the overall mass of the vehicle is kept at a constant value for all configurations.

The parametric study for various decay constants under asymptotic modulus of elasticity of 800×10^6 N/m^2 is also shown in Figure 3.16 on next page.

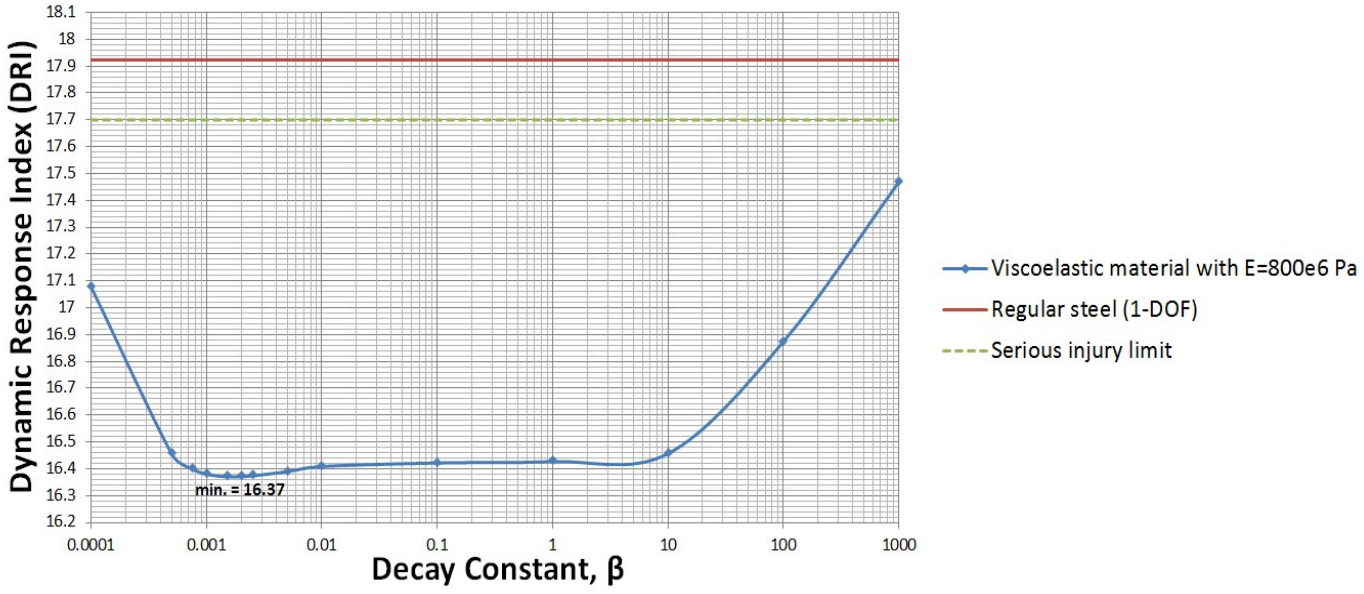

Figure 3.16: Parametric study for decay constant when asymptotic stiffness = 800×10^6 N/m^2

It shows that neither a low decay constant (below 0.001) nor an excessive decay constant (above 10) will yield significant improvement in the DRI. This is because low damping has negligible ability for absorbing energy, and excessive damping causes a large phase lag that also has negative effects on decreasing the relative displacement. Based on this analysis, a value of 0.0015 was selected for the decay constant, and this was used in the final configuration for which results are presented in Figure 3.15.

3.5 Parametric Study Using Three DOF DRI Model

In a similar manner, a parametric study was conducted involving multiple configurations with the three degree-of-freedom lumped parameter model, as shown in Figure 3.4, which is

used for evaluating the DRI. This parametric study retains the value of 6,000 kg/m^3 for the density of the lower section of each bulkhead, based on the configuration identified by the earlier work. The same blast load condition and same analysis process is applied to the three degree-of-freedom model. The asymptotic stiffness and the decay constant were varied as design parameters. Based on 72 testing runs in LS-DYNA, these two parameters were assigned values of 700×10^6 N/m^2 and 10, respectively in the final configuration.

Figure 3.17 summarizes the time histories of deformation of the upper body relative to the pelvis, for the original configuration and the final configuration. The values for the maximum spring compression and the associated value of DRI are also included in the figure. Actually, the DRI has already been improved significantly (a reduction of 41.2% corresponding to 10% chance of serious injury) by adding the energy-absorbing floor and seat. The energy-absorbing floor and seat perform as an energy isolator by absorbing a large amount of energy as well as significantly delaying the contact between the vehicle and its occupant during an explosion. The DRI improvement by the changes in the vehicle structure is 4.91% this time, however the reduction in the mass of the structure remains at 12.5%. The important aspect of this analysis is that the structural mass can be reduced while at the same time achieving a modest improvement in the DRI, which results a reduction of injury probability.

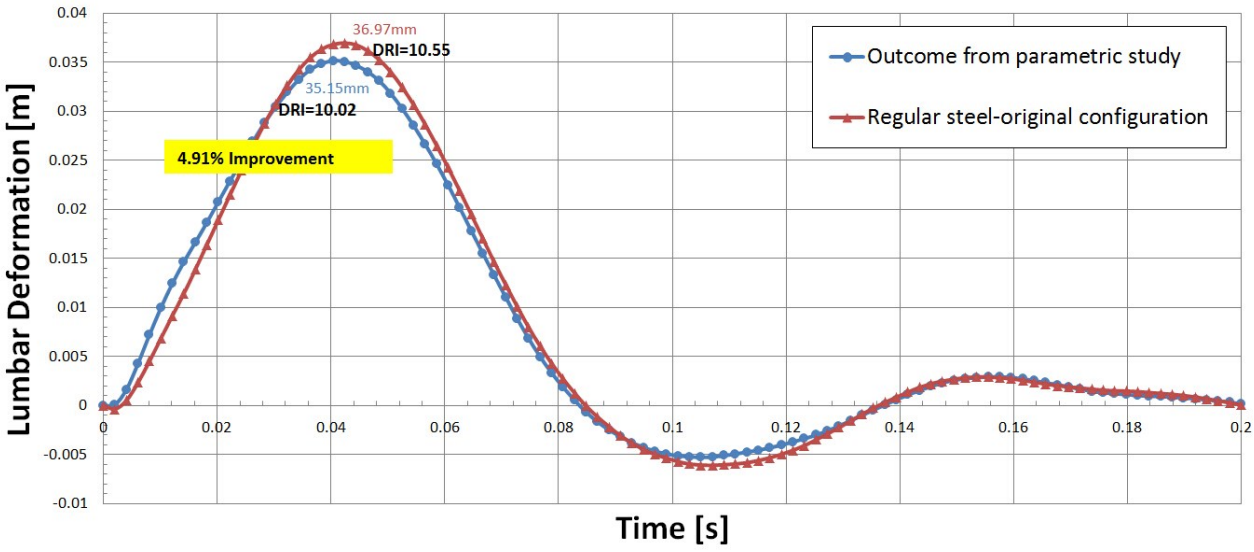

Figure 3.17: Time histories of lumbar deformation in the three degree-of-freedom lumped parameter DRI model

The parametric study for various decay constants under asymptotic modulus of elasticity of 700×10^6 N/m^2 is shown in Figure 3.18 on the next page. It shows the DRI is not sensitive to the decay constant when its value becomes greater than 0.001. This is because the energy-absorbing seat and energy absorbing floor play a more important role in the non-linear dynamic characteristics of the V-hull structure, and most of the destructive energy is absorbed by the energy-absorbing seat and the energy-absorbing floor instead of by the bulkhead structures. Based on this analysis, a value of 10 was selected for the decay constant, and this was used in the final configuration for which results are presented in Figure 3.17.

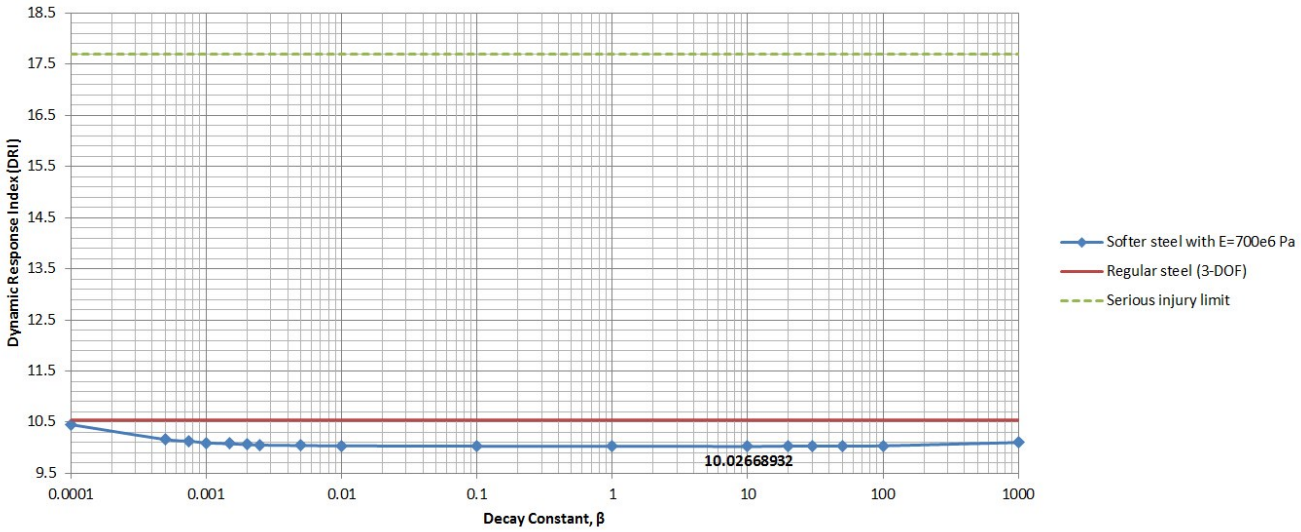

Figure 3.18: Parametric study for decay constant when asymptotic stiffness = 700×10^6 N/m^2

3.6 Conclusions

The results in this chapter indicate that material properties can be tuned for changing the structural dynamic behavior of a vehicle in order to reduce the DRI while simultaneously maintaining or reducing the total weight. The intent is not to identify a specific material or design, but rather to demonstrate a process for identifying suitable stiffness, inertia, and damping characteristics of the various components. In addition to the material properties, the results depend on how and where the seat is connected to the vehicle as well as the relative stiffness and energy absorption characteristics of the floors and the seats. The selection process is driven by controlling and minimizing the DRI created from a blast load. It is demonstrated that the weight of the tuned structure can be reduced while simultaneously creating various levels of improvement in blast protection as measured by the DRI.

While the results shown in this chapter are very promising, it should be noted that they are for a specific numerical example of a notional vehicle structure. Furthermore, the definition of the DRI from the literature, which is used as an injury metric in this research, considers only the maximum lumbar compression and ignores the rate of compression. It is possible that different results would be obtained with different injury metrics. In addition, the effects of design changes on other vehicle performance metrics beyond mass and DRI were not considered, even though these effects might be significant. For example, by reducing the density of bulkheads, the center of gravity of the vehicle is elevated, which increases the risk of rollover. Therefore, the dimensions of the lightweight vehicle under the proposed design philosophy might need to be modified in order to meet requirements for rollover resistance. Also, the reduction of stiffness of the bulkheads will change the overall stiffness and strength of the vehicle. Therefore, lighter and stiffer body structure elements might need to be considered in the design process as a way to compensate for this effect. Overall, the design process demonstrated in this chapter would need to be included as part of a larger, multidisciplinary design optimization process in order to properly account for and evaluate these types of tradeoffs.

CHAPTER 4

A Reduced-Order Model for Evaluating the Dynamic Response of Multilayer Plates to Impulsive Loads

4.1 Introduction

The concepts of energy absorption and re-direction are used in vehicle designs for improving vehicle survivability, as well as force protection by mitigating injury due to underbody blast and vehicle crash events. Full system, end-to-end modeling and simulation methodologies have been used extensively for the development of more blastworthy ground vehicles. However, due to space and packaging constraints, utilizing traditional connected structural elements to distribute energy is often infeasible for vehicle structures subjected to underbody blast loads.

Recently, the concept of using properties of softer structural materials in combination with a damping mechanism has been investigated for a V-hull structure. This was found to reduce the Dynamic Response Index (DRI), and hence the occupant injury risk, by absorbing destructive energy through higher deformation compared to isotropic high strength steel. Few monolithic materials appear likely to be able to meeting the conflicting demands of greater survivability and lighter structure weight, which is also an important factor in vehicle design.

Thus, innovative multilayer materials or structures have been developed, and the study of the dynamic performance of multilayer plates is of great interest as a mechanism to absorb and spread the energy from an impulsive load in the lateral direction instead of entering the occupant space. To reduce the expensive computational cost by using finite element analysis on a large number of alternative configurations, many reduced-order modeling approaches have been applied in preliminary design.

In this chapter, the reverberation-ray matrix method provides the foundation for developing a reduced-order model for studying the dynamic response of multilayer structures subjected to an impulsive load. In this method, the wave potential of each sublayer is transformed into the spectral domain by applying double Fourier Transforms. The waves generated by external loading are reflected and refracted at the interfaces of adjacent sublayers, and a scattering matrix **S** is built to represent the condition of continuity of stresses and displacements at each interface. The phase lag values of the traveling waves within each sublayer are represented by a phase matrix **P**. By inserting a permutation matrix **U**, a reverberation matrix **R** is generated as $\mathbf{R} = \mathbf{SPU}$ to represent the wave propagation and dynamic characteristics of the entire structure. By employing the generalized ray theory and inverse Fourier Transform, the dynamic response can be evaluated very quickly. Thus, the reduced-order dynamic model can be used to rapidly evaluate the performance of alternative multilayer plate designs and generate information for identifying the preferred directions and amounts of energy transfer. Then, by tuning material and physical properties in each sublayer, the information generated by the reduced-order model can be used as part of a design methodology that can be applied to a large number of candidate configurations of multilayer plates.

In the next section, the reduced-order modeling method is presented. In the following sections, the accuracy and efficiency of the method is validated for a numerical example of a three-layer plate. First, the free response results are compared with those from spectral FEA. Then, the forced response results and CPU times are compared with those from classical FEA using the commercial code Nastran.

4.2 The Reduced-Order Model of Multilayer Plate Structures

Based on the concept of functional graded materials (FGM), as illustrated in Figure 4.1, the concept of absorbing and spreading energy by using multilayer structures is investigated in this research.

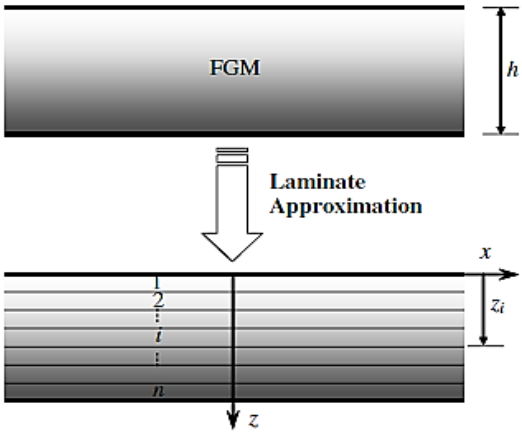

Figure 4.1: Functional graded materials and multilayer structure

The reverberation-ray matrix method, which is a combination of the reverberation matrix method and the generalized-ray method, is employed to develop a reduced-order model for analyzing the dynamic response of a multilayer medium under an excitation. The material

properties of each sublayer are pre-defined in this reduced-order model, including modulus of elasticity E_i, Poisson ratio ν_i, mass density ρ_i, loss factor η_i, and thickness of sublayer t_i.

In this section, the following five steps for developing the reduced-order model of a multilayer plate subjected to an external impulsive excitation are presented:

(1) Definition of local coordinate systems;

(2) Elastic wave propagation in spectral domain;

(3) Scattering phenomenon and boundary conditions;

(4) Phase matrix and reverberation matrix generation;

(5) Dynamic response calculation;

4.2.1 Definition of local coordinate systems

The reduced-order model is a two-dimensional model. To apply the reduced-order model, an infinite multilayer plate with N layers and N+1 interfaces $y=y^J$ (J=0, 1, 2… N), is considered and shown in Figure 4.2. A two-dimensional coordinate system (*x, y*) is constructed in which the wave normal of the p-wave (in-plane longitudinal wave) and s-wave (shear wave) lie. The double local coordinate system $(x^{IJ},\ y^{IJ})$ and $\left(x^{I(I-1)},\ y^{I(I-1)}\right)$ at each interface and a regular local coordinate system at the top surface boundary $(x^{01},\ y^{01})$ and the bottom surface boundary $\left(x^{N(N-1},\ y^{N(N-1)}\right)$ are defined respectively, as shown in Figure 4.2.

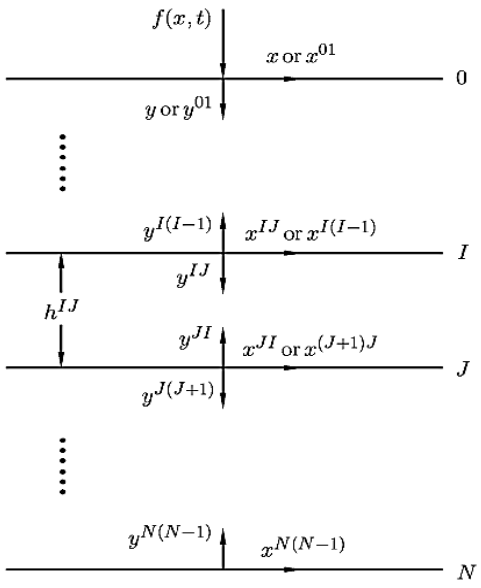

Figure 4.2: An infinite multilayer plate and its local coordinate systems at the boundaries and interfaces

The material properties, including mass density ρ^J, Lame's elasticity modulus λ^J and μ^J, and the thickness h^J, are isotropic in each sublayer but can be varying between different layers. It's worth noting that the Lame's elasticity moduli are derived as:

$$\lambda = \frac{E*\nu}{(1+\nu)(1-2\nu)} \tag{4.1}$$

$$\mu = \frac{E}{2(1+\nu)} \tag{4.2}$$

If the waves are not purely elastic but with energy dissipation properties, which is called evanescent waves, an additional term of loss factor needs to be considered and the modulus of elasticity of each sublayer will be modified accordingly as:

$$\tilde{E} = E * (1 - \eta) \tag{4.3}$$

Basically, in this research, all the loads are from external excitations and no loading sources exist at interfaces or within sublayers. The excitation applied at the interface and/or at the top and bottom boundaries is defined as a loading source vector $\mathbf{f}^J$.

4.2.2 Elastic Wave Propagation in Spectral Domain

In this chapter, only the propagation of elastic waves is investigated in this reduced-order model. The p-wave potential $\phi^{IJ}(x, y, t)$ with p-wave speed ${C_p}^{IJ}$ and s-wave potential $\psi^{IJ}(x, y, t)$ with s-wave speed ${C_s}^{IJ}$ are defined in each layer. Both wave potentials satisfy classical wave equation.

$$\nabla^2\phi = \frac{1}{{c_p}^2}\frac{\partial^2\phi}{\partial t^2} \tag{4.4}$$

$$\nabla^2\psi = \frac{1}{{c_s}^2}\frac{\partial^2\psi}{\partial t^2} \tag{4.5}$$

Where,

P-wave speed is $c_p = \sqrt{\frac{\lambda+2\mu}{\rho}}$; S-wave speed is $c_s = \sqrt{\frac{\mu}{\rho}}$;

By applying the double Fourier Transform on the fundamental wave equations in the space and time domains, the wave equations are represented in the wave number *k* and frequency ω domains:

$$\frac{d^2\tilde{\phi}}{dy^2} + \alpha^2\tilde{\phi} = 0 \tag{4.6}$$

$$\frac{d^2\tilde{\psi}}{dy^2} + \beta^2\tilde{\psi} = 0 \tag{4.7}$$

Where，

$\alpha = \sqrt{\frac{\omega^2}{{c_p}^2} - k^2}$: (p-wave number in y direction);

$\beta = \sqrt{\frac{\omega^2}{{c_s}^2} - k^2}$: (s-wave number in y direction);

The solutions for the wave equations can be expressed in terms of the arrival wave amplitude and departure wave amplitude as follows:

$$\tilde{\phi}(k, y, \omega) = \tilde{a}_p(k,\ \omega)e^{-i\alpha y} + \tilde{d}_p(k,\ \omega)e^{i\alpha y} \tag{4.8}$$

$$\tilde{\psi}(k, y, \omega) = \tilde{a}_s(k,\ \omega)e^{-i\beta y} + \tilde{d}_s(k,\ \omega)e^{i\beta y} \tag{4.9}$$

In Eq. (4.8) and Eq. (4.9), $\tilde{a}_p, \tilde{a}_s$ are the unknown arrival wave amplitudes and $\tilde{d}_p, \tilde{d}_s$ are the unknown departure wave amplitudes that need to be solved. Once the wave amplitudes vectors are obtained, the corresponding displacement field and the stress components can be solved as well.

The displacement fields $u = [u_x, u_y]$ and the stress components $\sigma = [\sigma_{xy}, \sigma_{yy}]$ can be calculated by applying fundamental elastodynamic solutions in each local coordinate system:

$$u_x = \frac{\partial \phi}{\partial x} - \frac{\partial \psi}{\partial y} \tag{4.10}$$

$$u_y = \frac{\partial \phi}{\partial y} + \frac{\partial \psi}{\partial x} \tag{4.11}$$

$$\sigma_{xy} = \mu[2\frac{\partial^2 \phi}{\partial x \partial y} + \frac{\partial^2 \psi}{\partial x^2} - \frac{\partial^2 \psi}{\partial y^2}] \tag{4.12}$$

$$\sigma_{yy} = \lambda \nabla^2 \phi + 2\mu[\frac{\partial^2 \phi}{\partial y^2} + \frac{\partial^2 \psi}{\partial x \partial y}] \tag{4.13}$$

4.2.3 Scattering Phenomenon and Boundary Condition

The scattering phenomenon at each interface is shown in Figure 4.3, where ***a*** represents the "arrival waves" and ***d*** represents the "departure waves". Also, the subscript ***p*** represents the "p-wave", which is also called the longitudinal wave, and the subscript ***s*** represents the "s-wave", which is also called the shear wave. Because the current reduced order model is a 2D model, the shear waves only exist in the xy-plane (sv-wave). If the model is expanded to be in 3D, the shear waves will exist in both of the xy-plane (sv-wave) and the xz-plane (sh-wave), and the scattering phenomenon will become more complicated.

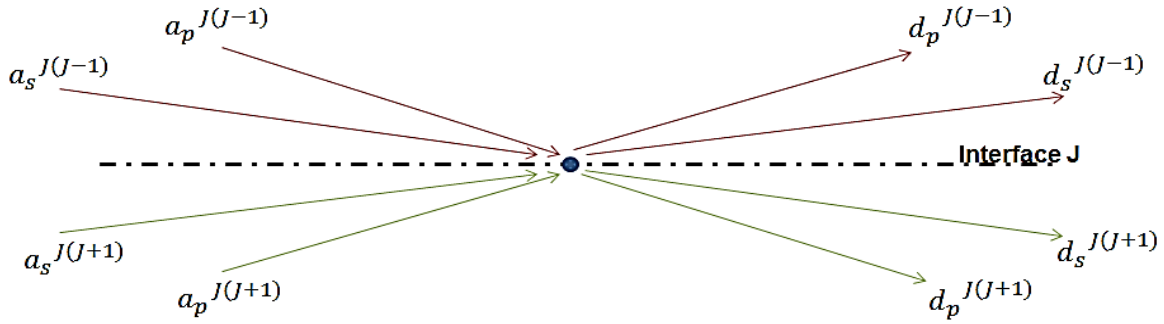

Figure 4.3: Scattering phenomenon at interface J

During the scattering, the incident waves will separate into reflected waves and refracted waves, and the wave types will interconvert during scattering. Therefore, a local scattering matrix is built to represent this complicated phenomenon by linking the incident waves (arrival) to the transmitted/reflected waves (departure).

Basically, if there are no wave sources inside the multilayer plate, and assume all of the adjacent layers share perfect interfaces without energy loss during the scattering, the

displacement and stress yield the continuity conditions at each interface, as shown in Eq. (4.14) – Eq. (4.17):

$$\tilde{u}_x{}^{J(J-1)}(k,\omega) - \tilde{u}_x{}^{J(J+1)}(k,\omega) = 0 \tag{4.14}$$

$$\tilde{u}_y{}^{J(J-1)}(k,\omega) + \tilde{u}_y{}^{J(J+1)}(k,\omega) = 0 \tag{4.15}$$

$$\tilde{\sigma}_{xy}{}^{J(J-1)}(k,\omega) + \tilde{\sigma}_{xy}{}^{J(J+1)}(k,\omega) = 0 \tag{4.16}$$

$$\tilde{\sigma}_{yy}{}^{J(J-1)}(k,\omega) - \tilde{\sigma}_{yy}{}^{J(J+1)}(k,\omega) = 0 \tag{4.17}$$

If two adjacent layers are not perfectly glued or bonded, dislocation and delamination will occur at the interface, which indicates that the continuity conditions in Eq. (4.14) – Eq. (4.17) are no longer convincing and need to be modified. The problem can be solved by inserting an additional intermediate layer of glue if the material properties of the glue, especially the viscos properties, are known. Another simpler modification is adding a complementary term in Eq. (4.14) – Eq. (4.17) to simulate the mechanism of glue, which performs as a linear spring for small deformation, when the material properties of the glue cannot be easily identified. In this case, for Eq. (4.14) and Eq. (4.15), a linear displacement term $\tilde{u}_{dis}$ will be added on the right-hand side replacing the zeros. In Eq. (4.16) and Eq. (4.17), a corresponding linear forcing term $k * \tilde{u}_{dis}$ will be added on the right-hand side to complement the new equations.

By substituting the elastodynamic solution Eq. (4.10) – Eq. (4.13) into the above equations, a linear system is built to describe the scattering phenomenon, where $\boldsymbol{A}^J$ and $\boldsymbol{D}^J$ are both 4×4 matrices.

$$\boldsymbol{A}^J \cdot \widetilde{\boldsymbol{a}}^J + \boldsymbol{D}^J \cdot \widetilde{\boldsymbol{d}}^J = \widetilde{\boldsymbol{g}}^J(k,\omega) = 0 \tag{4.18}$$

And the unknown arrival and departure wave amplitude vectors are:

$$\widetilde{\boldsymbol{a}}^{J} = \left(\tilde{a}_p{}^{J(J-1)}, \tilde{a}_s{}^{J(J-1)}, \tilde{a}_p{}^{J(J+1)}, \tilde{a}_s{}^{J(J+1)}\right) \tag{4.19}$$

$$\widetilde{\boldsymbol{d}}^{J} = \left(\tilde{d}_p{}^{J(J-1)}, \tilde{d}_s{}^{J(J-1)}, \tilde{d}_p{}^{J(J+1)}, \tilde{d}_s{}^{J(J+1)}\right) \tag{4.20}$$

The linear system can be also written in the form of Eq. (4.21), by multiplying $(\boldsymbol{D}^J)^{-1}$ to Eq. (4.18):

$$\widetilde{\boldsymbol{d}}^{J} = \boldsymbol{S}^J \cdot \widetilde{\boldsymbol{a}}^{J} + \boldsymbol{s}^J \tag{4.21}$$

Where,

$\boldsymbol{S}^J = -(\boldsymbol{D}^J)^{-1} \cdot \boldsymbol{A}^J$, is the local scattering matrix at interface J;

$\boldsymbol{s}^J = -(\boldsymbol{D}^J)^{-1} \cdot \widetilde{\boldsymbol{g}}^J$, is the local source vector at interface J;

In fact, all of the elements in the local source vector at the interfaces s^J are zero, because in our configuration there are no wave sources inside the multilayer plate itself and the transmission and reflection waves are merely from the incident wave source that is generated by the external excitation.

But the condition would be different at the top and bottom boundaries. First of all, the local scattering matrix will degenerate into 2×2 instead of 4×4, because there is only one local coordinate system and no continuous displacement relationships exist at the top and bottom boundary surface. Second, the external excitation is applied at the top surface of the plate, so the elements in the local source vector $\boldsymbol{s}^0$ of the top surface are nonzero. The boundary condition is illustrated in Figure 4.4.

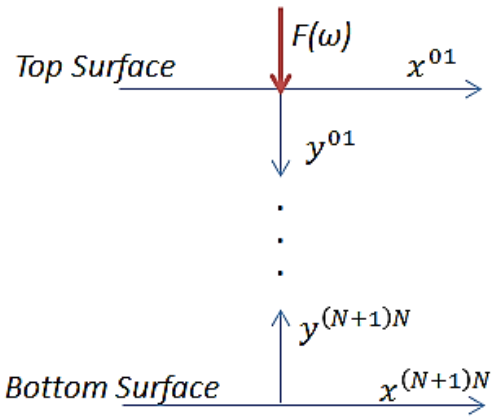

Figure 4.4: Boundary condition of top surface and bottom surface of a multilayer plate

The boundary conditions can be presented as:

$$\tilde{\sigma}_{xy}{}^{01}(k,\omega) = 0 \tag{4.22}$$

$$\tilde{\sigma}_{yy}{}^{01}(k,\omega) = F(\omega) \tag{4.23}$$

$$\tilde{\sigma}_{xy}{}^{N(N+1)}(k,\omega) = 0 \tag{4.24}$$

$$\tilde{\sigma}_{yy}{}^{N(N+1)}(k,\omega) = 0 \tag{4.25}$$

$\boldsymbol{S}^0$ and $\boldsymbol{S}^N$ now degenerate into 2×2 matrices and the source vector $\boldsymbol{s}^0 \neq 0$ if any loads apply on top surface of the multilayer plate.

By combining all the local scattering matrices at interfaces and the local scattering matrices at boundary, a 4N×4N global scattering matrix $\boldsymbol{S}$ is constructed and a global linear system for the entire multilayer plate is represented in the following compact form:

$$\tilde{\boldsymbol{d}} = \boldsymbol{S} \cdot \tilde{\boldsymbol{a}} + \tilde{\boldsymbol{s}} \tag{4.26}$$

This could also be shown in an expanded form as:

$$\begin{pmatrix} \tilde{d}^0 \\ \tilde{d}^1 \\ \tilde{d}^2 \\ \vdots \\ \tilde{d}^{N-2} \\ \tilde{d}^{N-1} \\ \tilde{d}^N \end{pmatrix} = \begin{pmatrix} \boldsymbol{S}^0 & 0 & 0 & & 0 & 0 & 0 \\ 0 & \boldsymbol{S}^1 & 0 & \cdots & 0 & 0 & 0 \\ 0 & 0 & \boldsymbol{S}^2 & & 0 & 0 & 0 \\ & \vdots & & \ddots & & \vdots & \\ 0 & 0 & 0 & & \boldsymbol{S}^{N-2} & 0 & 0 \\ 0 & 0 & 0 & \cdots & 0 & \boldsymbol{S}^{N-1} & 0 \\ 0 & 0 & 0 & & 0 & 0 & \boldsymbol{S}^N \end{pmatrix} \begin{pmatrix} \tilde{a}^0 \\ \tilde{a}^1 \\ a^2 \\ \vdots \\ \tilde{a}^{N-2} \\ \tilde{a}^{N-1} \\ \tilde{a}^N \end{pmatrix} + \begin{pmatrix} \tilde{s}^0 \\ \tilde{s}^1 \\ \tilde{s}^2 \\ \vdots \\ \tilde{s}^{N-2} \\ \tilde{s}^{N-1} \\ \tilde{s}^N \end{pmatrix}$$

Figure 4.5: The full expression of the scattering relation in a multilayer plate

4.2.4 Phase Matrix and Reverberation Matrix

In order to solve the two unknown wave amplitude vectors $\tilde{a}$ and $\tilde{d}$, another equation is necessary to be provided besides the Eq. (4.26). An additional equation is developed and supplemented by noting that a wave departing from one side of the layer becomes the wave arriving at another side of the same layer, with a phase lag, which is shown on next page in Eq. (4.27) - Eq. (4.30).

$$\tilde{a}_p{}^{J(J-1)} = e^{i\alpha_J h_J} \cdot \tilde{d}_p{}^{(J-1)J} \tag{4.27}$$

$$\tilde{a}_s{}^{J(J-1)} = -e^{i\beta_J h_J} \cdot \tilde{d}_s{}^{(J-1)J} \tag{4.28}$$

$$\tilde{d}_p{}^{J(J-1)} = e^{-i\alpha_J h_J} \cdot \tilde{a}_p{}^{(J-1)J} \tag{4.29}$$

$$\tilde{d}_s{}^{J(J-1)} = -e^{-i\beta_J h_J} \cdot \tilde{a}_s{}^{(J-1)J} \tag{4.30}$$

The phase relation is also illustrated in Figure 4.6 with a visual interpretation.

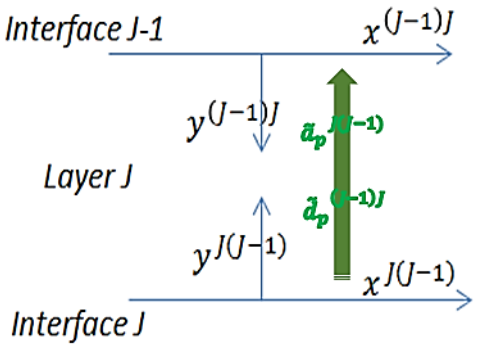

Figure 4.6: Phase relation in sublayer J

Then similarly, all the "arrival waves" could be linked to the "departure waves" by a 4N×4N global phase matrix $\boldsymbol{P}(h)$ as:

$$\tilde{\boldsymbol{a}} = \boldsymbol{P}(h) \cdot \tilde{\boldsymbol{d}}^{*} \tag{4.31}$$

The full expansion of global phase matrix $\boldsymbol{P}(h)$ is shown in Figure 4.7. Each submatrix $\boldsymbol{P_i}(h)$ in the global phase matrix is a 4×4 diagonal local phase matrix.

Local Phase Matrix:

$$\boldsymbol{P_J}(h_J) = \begin{pmatrix} e^{i\alpha_J h_J} & 0 \\ 0 & -e^{i\beta_J h_J} \end{pmatrix}$$

where the **4Nx4N Global Phase Matrix** is:

$$\boldsymbol{P}(h) = \begin{pmatrix} \boldsymbol{P_1}(h_1) & 0 & \cdots & 0 \\ 0 & \boldsymbol{P_1}(h_1) & & \\ \vdots & & \ddots & \vdots \\ 0 & & \cdots & \begin{matrix} \boldsymbol{P_N}(h_N) & 0 \\ 0 & \boldsymbol{P_N}(h_N) \end{matrix} \end{pmatrix}$$

Figure 4.7: Local phase matrix and global phase matrix

The departure waves vector $\widetilde{\boldsymbol{d}}^*$ and $\widetilde{\boldsymbol{d}}$ contain the same elements but in different order. They can be expressed in equivalence through a global permutation matrix $\boldsymbol{U}$ as shown in Eq. (4.32):

$$\widetilde{\boldsymbol{d}}^* = \boldsymbol{U} \cdot \widetilde{\boldsymbol{d}} \tag{4.32}$$

Where,

$\boldsymbol{U}$ is a 4N×4N block-diagonal matrix composed of N identical 4×4 sub-matrices $\boldsymbol{u}$:

$$\boldsymbol{U} = \begin{pmatrix} \boldsymbol{u} & 0 & 0 & 0 \\ 0 & \boldsymbol{u} & 0 & 0 \\ 0 & 0 & \boldsymbol{u} & 0 \\ 0 & 0 & 0 & \boldsymbol{u} \end{pmatrix} \tag{4.33}$$

Where,

$$\boldsymbol{u} = \begin{pmatrix} 0 & 0 & 1 & 0 \\ 0 & 0 & 0 & 1 \\ 1 & 0 & 0 & 0 \\ 0 & 1 & 0 & 0 \end{pmatrix} \tag{4.34}$$

By combining the global scattering matrix, $\boldsymbol{S}$, global phase matrix, $\boldsymbol{P}$, and global permutation matrix, $\boldsymbol{U}$, the 4N×4N reverberation matrix $\boldsymbol{R}$ is built as:

$$\boldsymbol{R}(k, \omega) = \boldsymbol{S} \cdot \boldsymbol{P} \cdot \boldsymbol{U} \tag{4.35}$$

The reverberation matrix captures both scattering phenomenon and phase lag phenomenon together and describes the complex wave propagation in an efficient format. It contains the information of physical and material properties in each sublayer, and it is sensitive to the wave number and the frequency. The reverberation matrix can also help to link the unknown arrival wave amplitudes and the unknown departure amplitudes to the external excitation in the frequency and wave number domains.

Therefore, the arrival wave amplitudes are:

$$\widetilde{\boldsymbol{a}} = \boldsymbol{P} \cdot \boldsymbol{U} \cdot [\boldsymbol{I} - \boldsymbol{R}]^{-1} \cdot \tilde{\boldsymbol{s}} \tag{4.36}$$

The departure wave amplitudes are:

$$\widetilde{\boldsymbol{d}} = [\boldsymbol{I} - \boldsymbol{R}]^{-1} \cdot \tilde{\boldsymbol{s}} \tag{4.37}$$

The matrix of $[I - R]^{-1}$ links the response of the multilayer medium to the excitation $\tilde{s}$ in the frequency-wave number domain. The wave dispersion relationship of the multilayer plate can also be obtained as:

$$\boldsymbol{det}[\boldsymbol{I} - \boldsymbol{R}(k, \omega)] = \boldsymbol{0} \tag{4.38}$$

Based on the dispersion relation, it is also possible to plot the wave dispersion curve and determine the travelling wave number under certain frequencies. Eq. (4.38) is important in the study of wave propagation characteristics and will be used in next section for validating the reduced-order model in a free-response problem i.e. eigenvalue problem, by comparing the results obtained from the spectral finite element method.

4.2.5 Dynamic Response Calculation

The dynamic response of multilayer plate in terms of the displacement field can be calculated by substituting $\tilde{a}$ and $\tilde{d}$ into the elastodynamic equations and expressed in a matrix form as shown in Eq. (4.39):

$$\begin{aligned} \boldsymbol{W}(k, y, \omega) &= \boldsymbol{A_u} \cdot \widetilde{\boldsymbol{a}} + \boldsymbol{D_u} \cdot \widetilde{\boldsymbol{d}} \\ &= (\boldsymbol{A_u} \cdot \boldsymbol{P} \cdot \boldsymbol{U} + \boldsymbol{D_u}) \cdot [\boldsymbol{I} - \boldsymbol{R}]^{-1} \cdot \tilde{\boldsymbol{s}} \end{aligned} \tag{4.39}$$

The matrix A_u and D_u are the global receiver matrices, in which the elements are the coefficients in elastodynamic solutions that contain the user-defined receiver location information. Eq. (4.39) can also be seen in a system engineering perspective, where the external excitation $\tilde{s}$ is the input to the system, the response of the multilayer plate $\boldsymbol{W}(k, y, \omega)$is the output of the system, and the combination of matrices $(A_u \cdot P \cdot U + D_u) \cdot [I - R]^{-1}$ is the transfer function that links the input and the output of the entire system.

Based on the generalized-ray theory, the matrix $[I - R]^{-1}$ can be decomposed in a form of Neumann series:

$$[\boldsymbol{I} - \boldsymbol{R}]^{-\mathbf{1}} = \boldsymbol{I} + \boldsymbol{R} + \boldsymbol{R^2} + \cdots + \boldsymbol{R^M} \tag{4.40}$$

Then the dynamic response can be evaluated in a summation form, where $\boldsymbol{I}$ represents the source waves travel to receiver directly without any scattering at interfaces and boundaries, and $\boldsymbol{R^M}$ represents the source waves travel to receiver after M times reflections and transmissions in the multilayer plate. The number of times of reflections and transmissions M is an important parameter which will be discussed in detail in Chapter 5.

By applying inverse Fourier Transform in wave number domain, the frequency response can be represented in space-frequency domain:

$$\boldsymbol{W}(x, y, \omega) = \frac{1}{2\pi} \int_{-\infty}^{\infty} \boldsymbol{W}(k, y, \omega)\, e^{ikx} dk \tag{4.41}$$

The frequency response at any locations in the multilayer plate, including the top and bottom surfaces and all the interfaces, can be calculated by using Eq. (4.41).

In the following sections, the accuracy and efficiency of the method is validated for a numerical example of a three-layer plate. First, the free response results are compared with those from spectral finite element analysis. Then, the forced response results and CPU times are

compared with those from classical finite element analysis using the commercial code Nastran. A briefing is shown in Figure 4.8 representing the main framework of these two different validations.

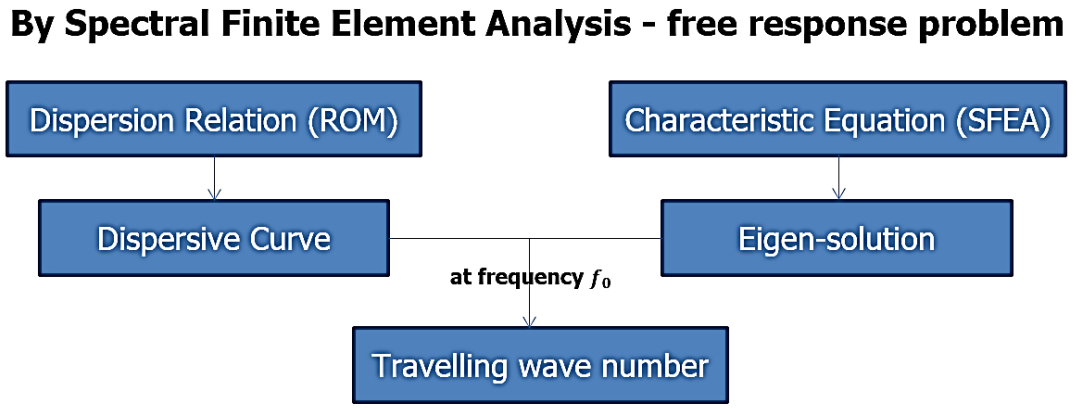

Figure 4.8: A framework of the validations for the reduced-order model

4.3 Validation of Free Response Predictions – By Spectral Finite Element Analysis

The spectral finite element analysis (SFEA) is a formulation of the finite element method that uses high-degree piecewise polynomials as the basis functions. The SFEA is applied on an infinite multilayered plate, as shown in Figure 4.9, to calculate the travelling wave numbers by conducting an eigenanalysis. The eigenvalues calculated from SFEA will be compared with the

results from the dispersion relationship of the reduced-order model in Eq. (4.38) to provide an effective validation.

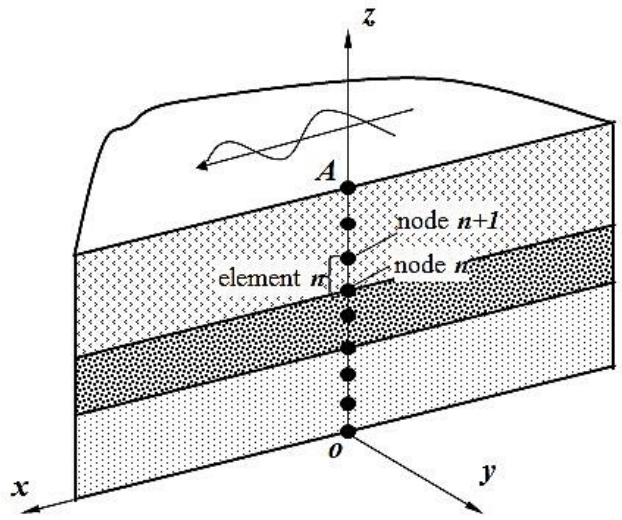

Figure 4.9: The spectral finite element analysis in an infinite multilayered plate

A full three-dimensional displacement field within a multilayered structure is approximated by a combination of one-dimensional finite element discretization in the thickness direction and plane harmonic wave propagating in the positive x direction with wavenumber k and frequency ω:

$$\boldsymbol{u}(x,y,z,t) = \boldsymbol{N}(z) * \boldsymbol{U} * e^{\mathrm{i}kx - \mathrm{i}\omega t} \tag{4.42}$$

Where,

$\boldsymbol{u} = [u \quad v \quad w]^{\mathrm{T}}$ is the displacement vector;

$\boldsymbol{N}(z)$ is the matrix of the element shape functions;

$\boldsymbol{U}$ is the nodal displacement vector;

For a linear finite element *n*, the displacements within the element can be expressed as:

$$\boldsymbol{u}(x,y,z,t) = \boldsymbol{N}_n(z) * \boldsymbol{U}_n(k,\omega) * e^{\mathrm{i}kx - \mathrm{i}\omega t} \tag{4.43}$$

Where,

$\boldsymbol{N}_n(z) = [(z_{n+1} - z)/h_n\mathbf{I} \quad (z - z_n)/h_n\mathbf{I}]$ is the shape function matrix;

$\boldsymbol{U}_n$=$[U_n \quad V_n \quad W_n \quad U_{n+1} \quad V_{n+1} \quad W_{n+1}]^{\mathrm{T}}$ is the amplitude vector;

I is a 3 by 3 identity matrix;

The governing differential equation for free vibration of multilayer structures can be expressed in matrix-vector form as:

$$\rho * \ddot{\boldsymbol{u}} - \boldsymbol{L}^{\mathrm{T}} * \boldsymbol{c} * \boldsymbol{L} * \boldsymbol{u} = \mathbf{0} \tag{4.44}$$

Where ρ is the mass density, $\boldsymbol{c}$ is the elasticity constants matrix, and $\boldsymbol{L}$ is the differential operator given by:

$$\boldsymbol{L}^{\mathrm{T}} = \begin{bmatrix} \partial/\partial x & 0 & 0 & 0 & \partial/\partial z & \partial/\partial y \\ 0 & \partial/\partial y & 0 & \partial/\partial z & 0 & \partial/\partial x \\ 0 & 0 & \partial/\partial z & \partial/\partial y & \partial/\partial x & 0 \end{bmatrix} \tag{4.45}$$

A standard one-dimensional finite element formulation with the assumed displacement field can be applied to derive the following form of algebraic eigenvalue equations, where k is the wave number and ω is the frequency.

$$[\boldsymbol{K}(k) - \omega^2\boldsymbol{M}]\boldsymbol{U} = \mathbf{0} \tag{4.46}$$

Where the global mass matrix **M** and the global stiffness matrix $\boldsymbol{K}(k)$ are, respectively, obtained by assembling the element mass matrix $\mathbf{M}_n = \int_0^{h_n} \rho_n \boldsymbol{N}_n^T \boldsymbol{N}_n dz$ and the element stiffness matrix $\mathbf{K}_n = \int_0^{h_n} \mathbf{D}^{\mathrm{T}} \boldsymbol{c} \mathbf{D} dz$.

Here,

$$\mathbf{D}^{\mathrm{T}} = \begin{bmatrix} \mathrm{i}k\mathbf{N}_n & 0 & 0 & 0 & \partial\mathbf{N}_n/\partial z & 0 \\ 0 & 0 & 0 & \partial\mathbf{N}_n/\partial z & 0 & \mathrm{i}k\mathbf{N}_n \\ 0 & 0 & \partial\mathbf{N}_n/\partial z & 0 & \mathrm{i}k\mathbf{N}_n & 0 \end{bmatrix} \tag{4.47}$$

Because the matrix $\boldsymbol{D}$ is linear in $\boldsymbol{k}$, it can be shown in the following form:

$$\boldsymbol{K}(k) = \boldsymbol{K}_2 k^2 + \boldsymbol{K}_1 k + \boldsymbol{K}_0 \tag{4.48}$$

Here, $\boldsymbol{K}_0$, $\boldsymbol{K}_1$, and $\boldsymbol{K}_2$ are independent of the wavenumber k. Because the eigenvalue equation for a given frequency, ω, is quadratic in k, it can be transformed to a linear eigenvalue problem of the form:

$$[\boldsymbol{A} - k\boldsymbol{B}]\boldsymbol{d} = \boldsymbol{0} \tag{4.49}$$

Where,

The matrix $\boldsymbol{A} = \begin{bmatrix} \boldsymbol{0} & \boldsymbol{I} \\ -\boldsymbol{K}_2^{-1}(\boldsymbol{K}_0 - \omega^2\boldsymbol{M}) & \boldsymbol{K}_2^{-1}\boldsymbol{K}_1 \end{bmatrix}$;

The matrix $\boldsymbol{B} = \begin{bmatrix} \boldsymbol{I} & \boldsymbol{0} \\ \boldsymbol{0} & \boldsymbol{I} \end{bmatrix}$;

The vector $\boldsymbol{d} = \begin{Bmatrix} \boldsymbol{U} \\ k\boldsymbol{U} \end{Bmatrix}$;

The above form of eigenvalue problem enables us to seek eigenvalues k at each frequency ω. In so doing, it can account for the frequency dependence of the material properties. The spectral finite element analysis is also implemented in MATLAB.

From this linear eigenvalue problem, the eigenvalues, i.e. the wavenumbers k can be calculated for a specific frequency ω. By setting a fixed frequency, it is possible to obtain the eigenvalues, which are the travelling wave numbers in both the reduced-order model and the

SFEA model. Three different testing cases of a three-layer plate configuration are built on the purpose of validating the reduced-order model, as illustrated in Figure 4.10.

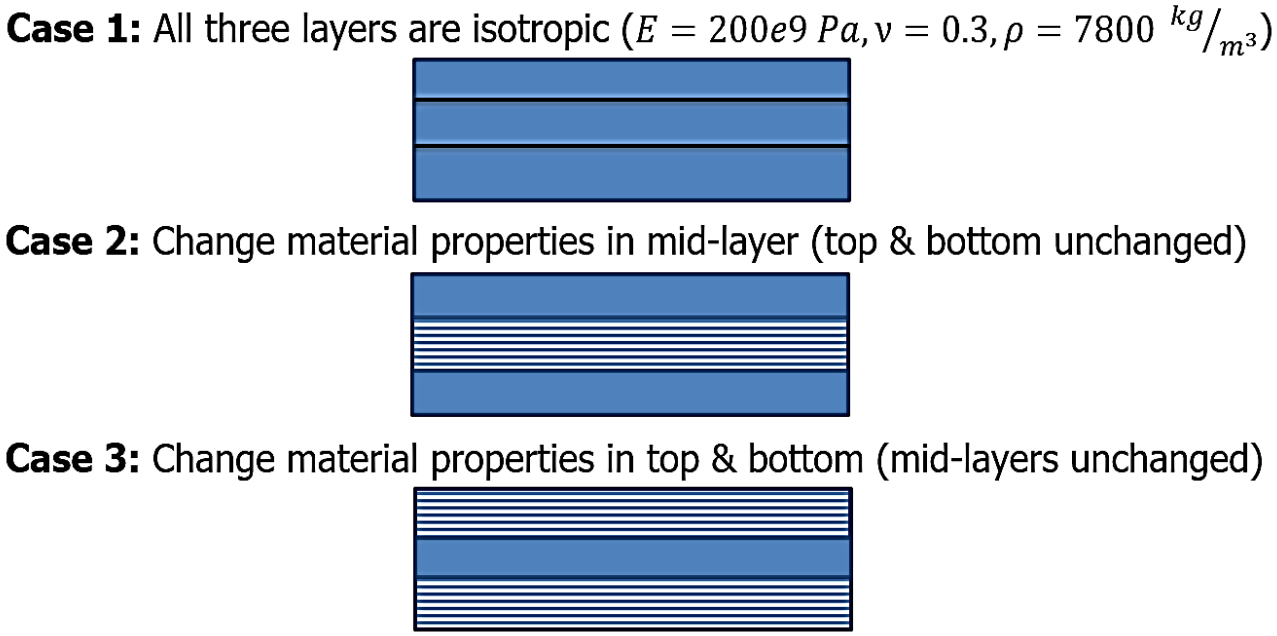

Figure 4.10: Three testing configurations for a three-layer plate

In case 1, a simple configuration is being tested by setting all three layers to have the same material properties, which actually represents an isotropic steel plate with the modulus of elasticity $E=200\times10^9$ Pa, the Poisson ratio $\nu=0.3$, and the mass density $\rho=7{,}800$ kg/m^3. It has also been called the baseline configuration. Then the material properties are being changed in the middle layer but keep unchanged in the top and bottom layers in case 2. At last, the material properties are being changed in the top and bottom layers but keep unchanged in the middle layer in case 3. In case 1, the modulus of elasticity E is doubled then halved simultaneously for all three sublayers. In case 2 and case 3, the investigation not only focuses on the modulus of elasticity but is also being extended to the Poisson ratio ν, and the mass density ρ.

The validations are performed under the frequency of 1,000 Hz, and the comparison results in a three-layered plate configuration are shown in Table 4.1below.

Change of Material Properties	**Case 1**		**Case 2**		**Case 3**	
	ROM	**SFEA**	**ROM**	**SFEA**	**ROM**	**SFEA**
Baseline (regular steel)	20.32	20.32				
Double E	17.07	17.07	19.99	19.99	17.23	17.23
Halve E	24.20	24.20	20.53	20.53	23.80	23.80
Double ρ			22.12	22.12	22.88	22.88
Halve ρ			19.22	19.22	18.58	18.58
Double ν			20.34	20.34	20.58	20.58
Halve ν			20.30	20.30	19.95	19.95

Table 4.1: Eigenvalues for the three-layer plate calculated by reduced-order model and spectral finite element analysis model

After changing the sublayer material properties in a multiple way, it is observed that the eigenvalues, i.e. travelling wave numbers k, calculated from both of the reduced-order model and the SFEA model are equivalent, with the precision up to six digits. This test of the free response predictions provides an effective numerical validation for the reduced-order model.

4.4 Validation of Forced Response Predictions – By Numerical Analysis in Nastran

For the forced response, a numerical validation is conducted by comparing the frequency response of a multilayer plate under an impulse load from the reduced-order model to the results from the commercial finite element analysis code Nastran (Solver 108). A 1m×1m three-layered plate model was created in Nastran, as shown in Figure 4.11. The thicknesses of the top and bottom layers were set to $h_1 = h_3 = 0.03$ m, while the thickness of middle layer were set to a slightly larger value of $h_2 = 0.04$ m. An impulse load was applied at the center of the top surface, and a simply support boundary condition was applied on the edges of the bottom surface.

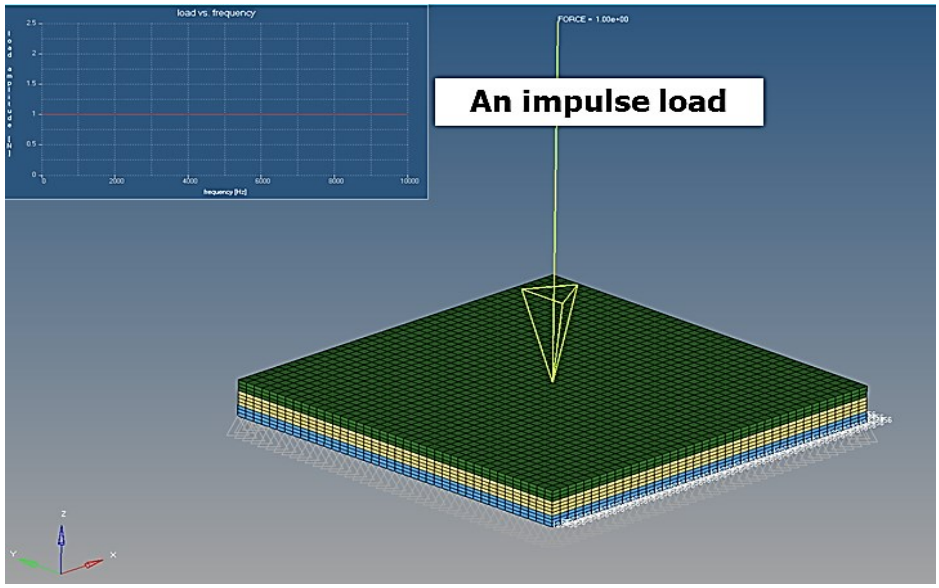

Figure 4.11: A three-layered finite plate model subjected to an impulse load in Nastran

The frequency response for the vertical displacement at the center node of the bottom surface was tracked. The results in frequency domain for the maximum vertical displacement from Nastran are compared with those from the reduced-order model approach for different

values of the modulus of elasticity for the middle layer. By changing the modulus of elasticity in the middle layer, the maximum vertical displacement values at the bottom center node of the plate from Nastran are shown as blue dots in Figure 4.12. It can be observed that when the modulus of elasticity in the middle layer increases, the maximum displacement of the plate decreases, as would be expected. Then the same loading condition and material properties were applied in the reduced-order model, and the numerical results are presented as red crosses in Figure 4.12. All the responses are normalized based on the material properties of the first layer and the magnitude of the force excitation using $u_z^* = \log(\frac{u_z * h_1 * E_1}{100 * F})$.

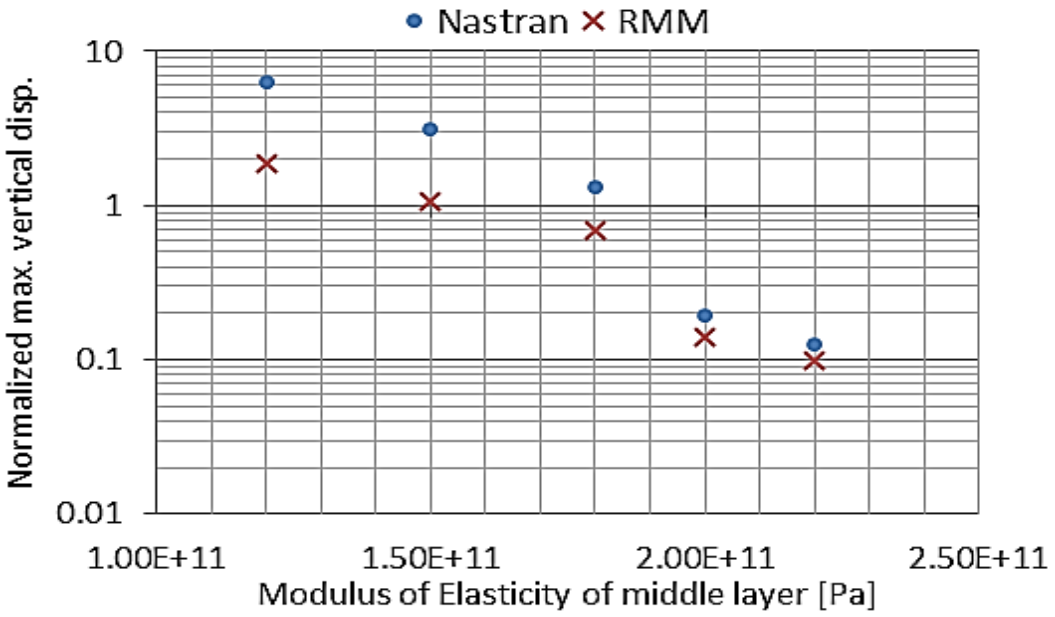

Figure 4.12: Maximum response of the three-layered plate that obtained from Nastran and the reduced-order model

It is observed that when the modulus of elasticity of the middle layer is changed, the forced response results from the reduced-order model show a similar trend with those from Nastran. It is important to note that the reduced-order model is much more efficient than the

finite element model: the average CPU time for running the reduced-order model is 9.4 seconds versus 1518 seconds for Nastran. If the pre-processing and post-processing time for the finite element analysis were included, the total time cost savings by using the reduced-order model would be even greater.

4.5 Conclusions

This chapter presented the reverberation-ray matrix method as a reduced-order dynamic modeling approach to rapidly evaluate a large number of alternative multilayer plate designs with respect to reducing the through-thickness response of the plate to an impulsive load. The accuracy and efficiency of this approach was validated for the free response by comparison with spectral finite element analysis results, and for the forced response by comparison with finite element analysis results using the commercial code Nastran. It was shown that the reduced-order model was able to predict the trend of the maximum response as design parameters were varied in a three-layer plate structure subjected to impulsive loading. In terms of computational efficiency, the CPU time required for predicting the forced response was reduced by two orders of magnitude using the reduced-order model compared to using classical finite element analysis.

Although this is just an initial study, the results indicate that this approach shows promise for future use in a two-part design exploration of multilayer plate structures. First, an efficient parametric study could be performed using the reduced-order model, which would identify the subset of the design space that is most promising for achieving the desired performance level. Second, using the information generated by the reduced-order model, a higher-fidelity (but much

more computationally expensive) structural analysis could be performed using a finite element code for relatively few configurations within this subset of the design space.

CHAPTER 5

An Optimization Framework and Case Studies for Design Lightweight Multilayer Plate Configurations with High Blastworthiness

5.1 Introduction

Assessing the dynamic performance of multilayer plates subjected to impulsive loading is of interest for identifying configurations that either absorb energy or transmit the energy in the transverse directions, thereby mitigating the through-thickness energy propagation. The development of a reduced-order modeling approach is presented in last chapter for rapidly evaluating the structural dynamic performance of multilayer plates. To identify the multilayer plate that has the highest levels of blastworthiness and lightest structural weight among a large number of alternative configurations, a design optimization process is also developed and integrated with the reduced-order model.

In this chapter, the framework of design optimization is introduced and a set of numerical case studies are provided for identifying the optimal configuration with different number of sublayers. First, an effective screening metric is developed based on the concepts of the DRI model as described in Chapter 2. This screening metric will help to rank candidate configurations

according to their capacity of blastworthiness. The screening metric is validated by using Nastran with a five-layer plate example. Then the framework of design optimization, including objective function, design constrains, and candidate material selection, is developed and presented. After that, a convergence study is performed along with the process of design optimization. Four case studies (a three-layer case, a four-layer case, a five-layer case, and a six-layer case) are presented and the optimal configurations are then identified with the smallest screening metric and a reduced structural weight. The selected configuration for each case is validated by using finite element analysis in Nastran. The information generated from the design optimization will help designers to select an optimal multilayer plate configuration as a proper armor in an early design stage, in order to reduce the occupant's injury probability and the structural weight simultaneously. Then the identified optimal configurations can be used in a more complex and computational consuming finite element analysis without performing tedious parametric studies.

5.2 A Screening Metric for Evaluating Multilayer Plate Configurations

The vertical displacement at the center of the bottom surface has been obtained from both reduced-order model and Nastran in Chapter 4. But the value of vertical displacement is not suitable to perform as an effective screening metric for determining which configuration has the best occupant protection capacity, because the occupant injury probability depends on the deformation of lumbar instead of the absolute value at the base of the structure. As described in Chapter 2, the expression of DRI is:

$$\text{DRI} = \frac{\omega^2}{g} \cdot \delta_{max} = \frac{\omega^2}{g} \cdot (\delta_{pelvis} - \delta_{upper\ body})_{max} \tag{5.1}$$

Therefore, before performing design optimization, it is necessary to first develop a DRI-based screening metric for effectively evaluating the occupant protection level of the multilayer plate.

The screening metric is obtained from a new DRI-based reduced-order model, which is a combination of a reduced-order multilayer plate model and a single degree-of-freedom mass-spring-damper system, as shown in Figure 5.1. The new DRI-based reduced-order model is implemented in MATLAB.

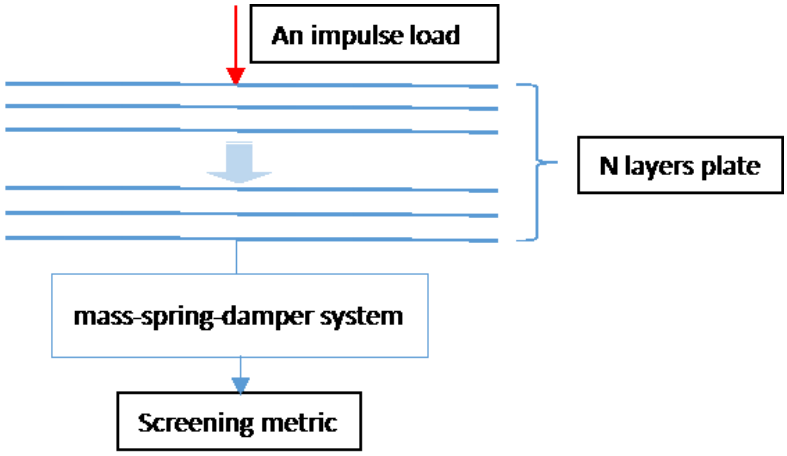

Figure 5.1: A reduced-order model for obtaining the screening metric

A numerical case of a five-layer plate is studied in this section. The mass density of each sublayer keeps the same, and the thickness of each sublayer is designated as: h_1=h_5=0.01 m, h_2=h_4=0.02 m, and h_3=0.04 m. Different from the numerical example in section 4.4, the overall stiffness E_{eff} of the multilayer plate keeps a constant instead of intuitively changing the stiffness of one certain layer to change dynamic response of the plate. Hence, the overall stiffness of the multilayer plate yields a constraint:

$$\sum_{i=1}^{n} E_i * h_i = E_{eff} * h_{total} \tag{5.2}$$

The screening metric is validated by comparing the results obtained from the reduced-order model to those obtained from a finite element model in Nastran. The Nastran model is shown in Figure 5.2, with the same sublayer thickness, material properties, and loading condition to the reduced-order model. It is also worth noting that the Nastran model is a finite plate with simply-supported boundary conditions at four edges of the bottom surface, which is different from the reduced-order model which is an infinite plate model. The length and width of the Nastran plate model are 1m. Similar to the model shown in Figure 4.11, the solver 108 in Nastran is set to be default to calculate the frequency response. The degrees of freedom of the lumped mass are constrained in the directions that are parallel to the plate in order to ensure the lumped mass is only capable of vertical movement.

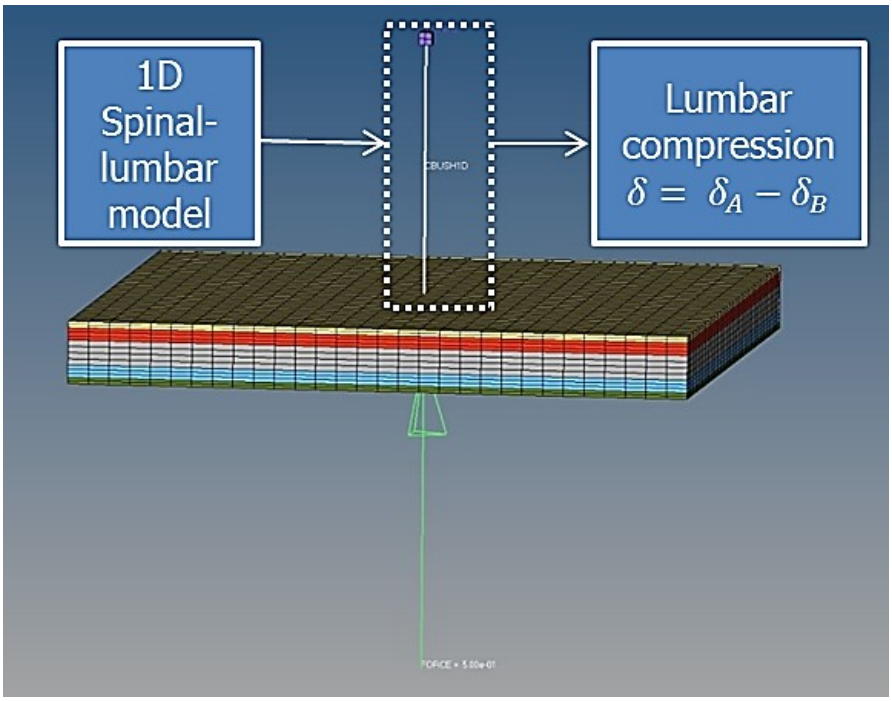

Figure 5.2: A finite element model in Nastran for obtaining the screening metric

Three different sets of modulus of elasticity of sublayers are presented in Table 5.1. First, a baseline model made of regular isotropic steel for each sublayer is tested. Then the modulus of elasticity of each sublayer is changed and randomly designated, but still yields to the overall stiffness constraint of Eq. (5.2). Though it has been known that the energy will transfer faster in a stiffer medium, the overall performance of the multilayer medium with respect to the energy absorption and redirection is still uncertain. At the current design stage, the outer layers (layer 1 and layer 5) are designated to be relative stiffer in order to minimize the local effect caused by the concentrated point loading condition.

Modulus of Elasticity	**Baseline**	**Case 1**	**Case 2**	**Case 3**
E of layer 1 (Pa)	220×10^9	300×10^9	250×10^9	250×10^9
E of layer 2 (Pa)	220×10^9	250×10^9	200×10^9	220×10^9
E of layer 3 (Pa)	220×10^9	150×10^9	225×10^9	205×10^9
E of layer 4 (Pa)	220×10^9	250×10^9	200×10^9	220×10^9
E of layer 5 (Pa)	220×10^9	300×10^9	250×10^9	250×10^9
$\boldsymbol{E_{eff}}$	$\mathbf{220\times10^9}$	$\mathbf{220\times10^9}$	$\mathbf{220\times10^9}$	$\mathbf{220\times10^9}$

Table 5.1: Modulus of elasticity of each sublayer for the five-layer plate configuration

The results obtained from the reduced-order model are presented in Table 5.2, and the results obtained from the Nastran model are presented in Table 5.3. The screening metric calculated from the regular steel baseline model are set to be 100%, which indicates that no benefits will be gained from the baseline model.

The screening metric obtained from the other three testing cases are expressed as a percentage of the baseline result, and ranked accordingly. Less percentage indicates more

improvement to the levels of blastworthiness of the multilayer plate. The computational time is also provided in the tables for a comparison.

ROM	Screening Metric	Ranking	Computational Time
Baseline	100%	4	10.2s
Case 1	81.36%	1	10.5s
Case 2	94.53%	3	10.4s
Case 3	94.09%	2	10.8s

Table 5.2: Results obtained from the reduced-order model

Nastran Model	Screening Metric	Ranking	Computational Time
Baseline	100%	4	2,025s
Case 1	87.96%	1	2,320s
Case 2	97.18%	3	2,298s
Case 3	95.33%	2	2,344s

Table 5.3: Results obtained from the Nastran model

The screening metric, which is expressed in a sequence of percentage, properly matches between the reduced-order model and the Nastran model. Accordingly, the ranking order is also captured correctly, which indicates the fact that the screening metric is reliable and can be fully used in a design optimization. In this five-layer plate example, the advantage on computational efficiency is more evident by using the reduced-order model, comparing to the Nastran model. In fact, the reduced-order model computers about 220 times faster than the classic finite element

code in Nastran. If considering the labor of pre-processing and post-processing, the Nastran model will be much more time-consuming.

5.3 A Framework of Design Optimization

Having the screening metric for evaluating the energy insulation performance of the multilayer plate, a design optimization framework is developed to identify the optimal configuration. The configuration that needs to be optimized and a baseline configuration are shown in Figure 5.3.

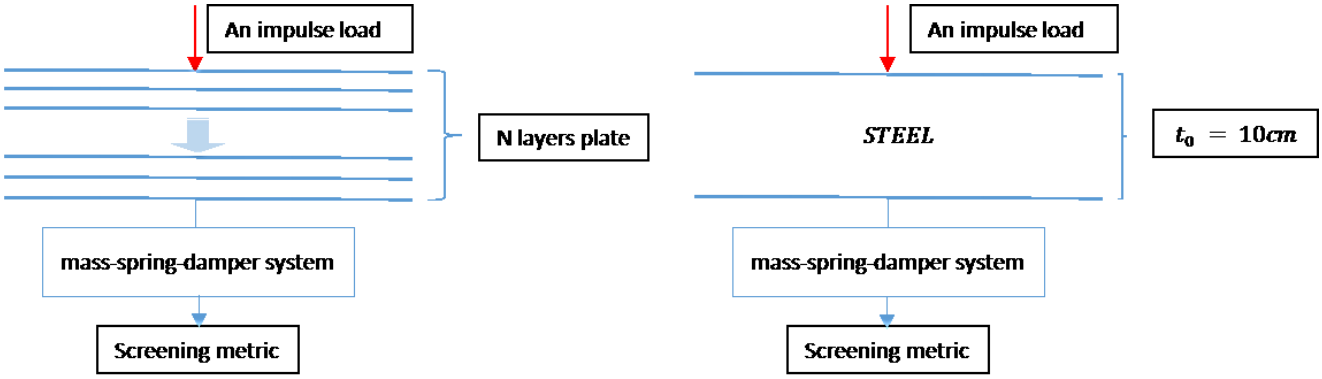

Figure 5.3: Optimization configuration baseline configuration

The optimization configuration has N sublayers with varying sublayer thickness. As discussed in preceding section, an impulse load is applied on the top surface of the multilayer plate and a single degree-of-freedom mass-spring-damper system is attached at the center of bottom surface of the plate to capture the screening metric. The baseline model is a particular multilayer plate configuration with only one layer (N=1), i.e. an isotropic plate, which is made of regular steel. The total thickness of the baseline plate model is set to be 10cm.

In the optimization, the total number of sublayers *N*, and the material selection for each sublayer s_j , are designated to be the two discrete design variables. The thickness of each sublayer t_i is designated to be a continuous design variable.

The objective function of the optimization is to minimize the screening metric, which is calculated based on the largest relative displacement experienced by the mass-spring-damper system, as presented in Eq. (5.3):

$$\boldsymbol{Objective\ Fucntion}\ f = min\ (Screening\ Metric) \tag{5.3}$$

Four design constraints are also provided:

(1) To avoid the thickness of each sublayers being either excessive thick or extreme thin, a fixed upper bound of 4.8cm and a lower bound of 1cm are set on the thickness of each sublayer:

$$1\ \text{cm} < t_i < 4.8\ \text{cm} \tag{5.4}$$

(2) The natural frequency and its corresponding mode shape not only depend on the material properties of each sublayer, but also highly depend on the total thickness of the multilayer plate. In order to investigate how component and material properties of each sublayer will improve the blastworthiness of multilayer plate, the total thickness of the multilayer plate is set to be unchanged to the total thickness of baseline model, with a 2% floating clearance:

$$9.8\ \text{cm} < \sum_i^N t_i < 10.2\ \text{cm} \tag{5.5}$$

(3) Another predominant factor to the dynamic response of the multilayer plate is its effective rigidity. Despite the fact that softer materials with relative low effective rigidity

may have potential to absorb energy as described in Chapter3, it's also important to keep the effective rigidity of the multilayer plate, which usually works as armor, within an acceptable range to avoid dramatic deformation. Thus, the effective sectional stiffness is set to be greater than the one of the isotropic steel baseline configuration:

$$\sum_i^N E_i * t_i > 0.7 * (E_{steel} * t_0) \tag{5.6}$$

(4) Equally important to reducing the DRI-based screening metric, reducing the overall structural weight is another crucial purpose of multilayer plate design. The control of the structural weight is designated as an additional constraint instead of a mutual objective function for not increasing the framework complexity of the optimization. Therefore, the total sectional density is set to be less than the one of the baseline in order to achieve the purpose of structural weight reduction:

$$\sum_i^N \rho_i * t_i < (\rho_{steel} * t_0) \tag{5.7}$$

The optimization is set up by using DS Toolkit, which is developed by Michigan Engineering Service (MES). The algorithm for reduced-order modeling, which is developed in MATLAB, is compiled and integrated with the DS Toolkit. The solver selected in the optimization is NSGA-II. The generation size is set to be 10 in order to ensure a numerical stable convergence for different configurations with varying number of sublayer in the following case study. The population size of each generation is set to be as large as 200, so that enough testing points are provided for identifying the feasible solutions. A group of five alternative materials are selected as candidates for each sublayer, including RHA high strength steel, 6061 Aluminum

Alloy, Silicon-Carbon (SiC), OFHC copper, and Ti-6AI-4V-Alloy. The corresponding material properties are presented in Table 5.4 below.

# (s_j)	Materials Selection	Modulus of Elasticity (GPa)	Density (kg/m^3)	Poisson Ratio
s_1	RHA Steel	200	7,823	0.30
s_2	6061 Aluminum Alloy	74	2,704	0.34
s_3	SiC	445	3,200	0.16
s_4	OFHC Copper	129	8,940	0.35
s_5	Ti-6AI-4V Alloy	114	4,430	0.34

Table 5.4: Candidate materials for each sublayer and their corresponding material properties

5.4 Convergence Analysis and the Optimal Design in Case Studies

A convergence analysis is performed along with the design optimization. Both of convergence and computational time increase when the number of generation increases. In our case studies, four numerical testing configurations are prepared with different number of sublayers (N=3, N=4, N=5, and N=6). Under the current available computational capacity (CPU: 4 cores i7-5600U processor, up to 3.20GHz; Memory: 8GB), the minimum computational time which is for the case of N=3 and generation=1 is about 0.25 hour, and the maximum computational time which is for the case of N=6 and generation=10 is about 52 hours. The convergence analysis of a six-layer plate (N=6) is used as an example, illustrated in Figure 5.4 on following pages.

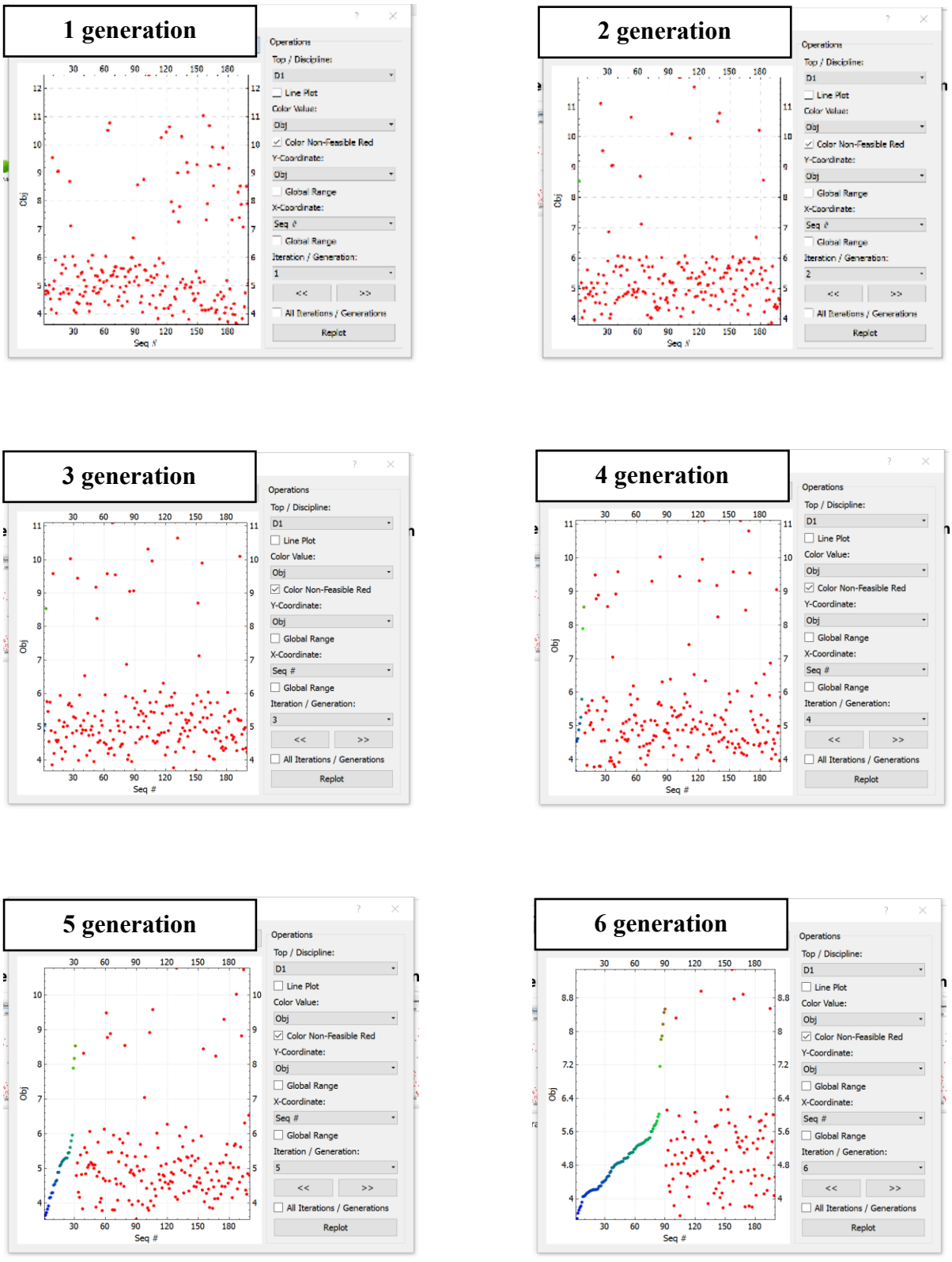

Figure 5.4: Convergence analysis of a six-layer plate

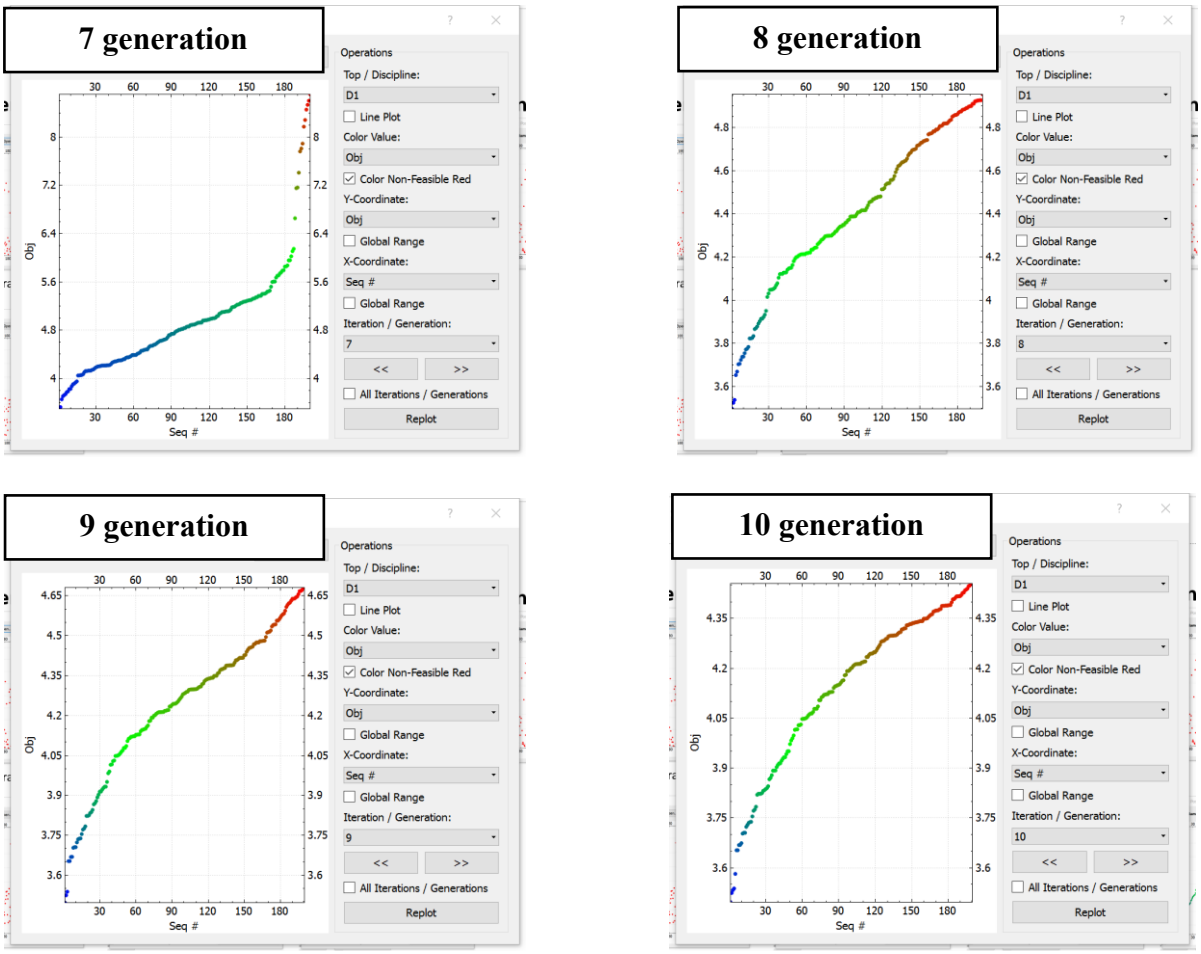

Figure 5.4: Convergence analysis of a six-layer plate (Continued)

In Figure 5.4, the red points are infeasible solutions and the non-red points are feasible solutions. In first four plots (from 1 generation to 4 generations), almost all points are infeasible and no convergence appears. This is because the small numbers of generation are not able to provide sufficient sampling points for the optimization solver to find an optimal direction within the constraints. As the number of generation increases, in the plots of 5-generation and 6-generation, more feasible solutions turn up and a vague convergence curve appears. By keeping increasing the number of generation, the randomly distributed non-feasible solutions are gradually eliminated from the plots as the optimization solver has already found the optimal

direction. As a result, clear convergence curves can be observed in the plot of large numbers of generation (from 8 generations to 10 generations). In fact, the difference between 9-generation plot and 10-generation plot is small, and the optimal solutions obtained from both cases are almost the same. Therefore, 10 generations are sufficient for the optimization of a six-layer plate to reach an optimal configuration. Because the six-layer plate is the most complex one among all the testing configurations, which has the most possible combination of sublayers with different materials, 10 generation will also be a applicable standard for other three testing configurations to stably converge to an optimal solution. It is also worth noticing that the number of transmission and reflection M, which is discussed in Eq. (4.40), will play an important role in the optimization process. As the value of M increases, the number of waves arriving to the bottom of the multilayer plate will increase and be able to be captured accumulatively. In order to have the response of each of the configuration at a consistent level, the value of M needs to be tuned and specified before the optimization. To achieve this purpose, a simple trial and error step is applied for each of the four configuration (N=3, 4, 5, 6). First, we divide the thickness of the plate by the number of N to have equally thick sublayers and apply regular steel as the default material for all sublayers. Then we tune the value of M in each configuration to ensure the resulting screening metric are equal, which indicate the total amount of the waves reaching the bottom surface of the plate are the same for all four configurations. The different M values are recorded and will be used in the optimization to avoid inconsistence. Finally, the optimal configurations of each testing case are shown in Figure 5.5 – Figure 5.8. The selection of material is labeled for each sublayer. The sublayer thickness, total thickness, and the sectional density are also provided from Figure 5.5 to Figure 5.8. It is observed that a variety of material combination is selected for each of the optimal configuration rather than having isotropic material for all of the sublayers.

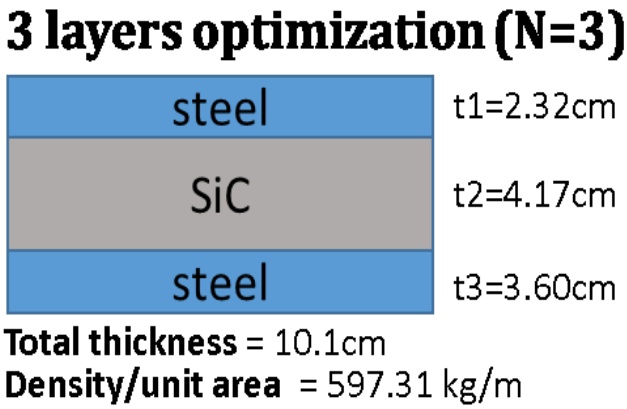

Figure 5.5: The optimal configuration of a three-layer plate

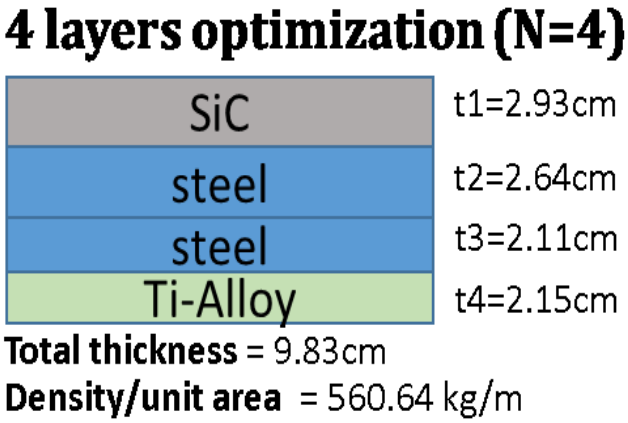

Figure 5.6: The optimal configuration of a four-layer plate

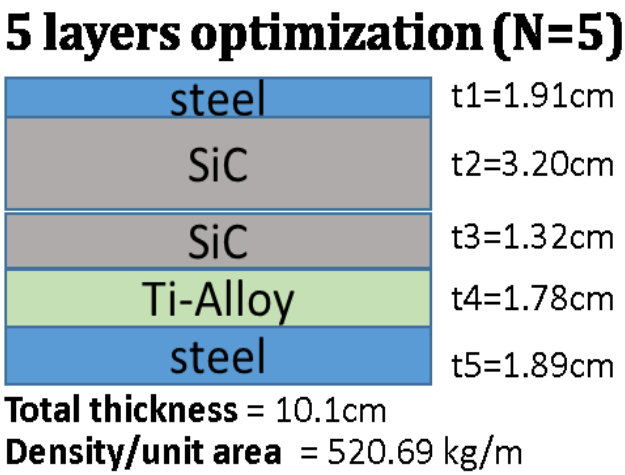

Figure 5.7: The optimal configuration of a five-layer plate

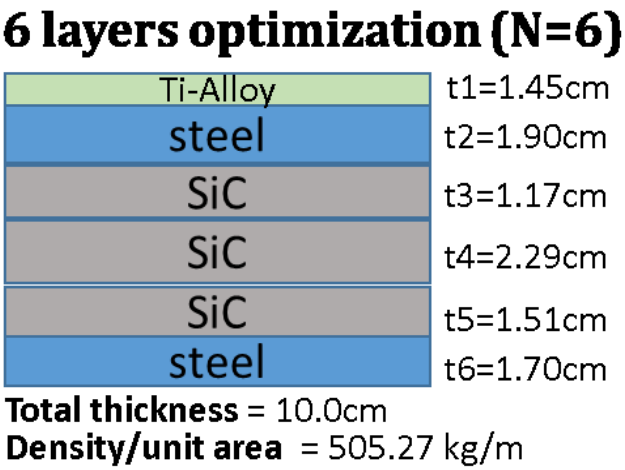

Figure 5.8: The optimal configuration of a six-layer plate

It is observed that only three materials, including RHA high strength steel, SiC, and Ti-6AI-4V Alloy are selected from the five candidate material of Table 5.4 to compose the optimal configuration, and some of the adjacent layers are made of same material. There are two possible reasons to explain this manner of material combination: One is that the five chosen candidate materials may not be sufficient to shape a promising feasible zone. The narrow design space is also further limited by merely considering the elastic material properties rather than including engineering viscosity and engineering plasticity. The other reason is that the results may indicate the presence of local minimum zones within the limited range of number of transmission/reflection M, the population size, and the generation size. While for all of the current four optimal configurations, the screening metric and the structural weight have been reduced simultaneously. The results from this reduced-order model optimization will be shown and discussed in detail in the following section, along with the validation results obtained by using Nastran.

5.5 Validation of the Optimization Framework

Again, the classic finite element code in NASTRAN is used to analyze the optimal configuration that is identified when different numbers of sublayers are considered. The relative ranking of the optimal configurations that correspond to the different number of layers are evaluated and compared with the results obtained from the reduced-order model optimization. The Nastran model is shown in Figure 5.9 on the next page.

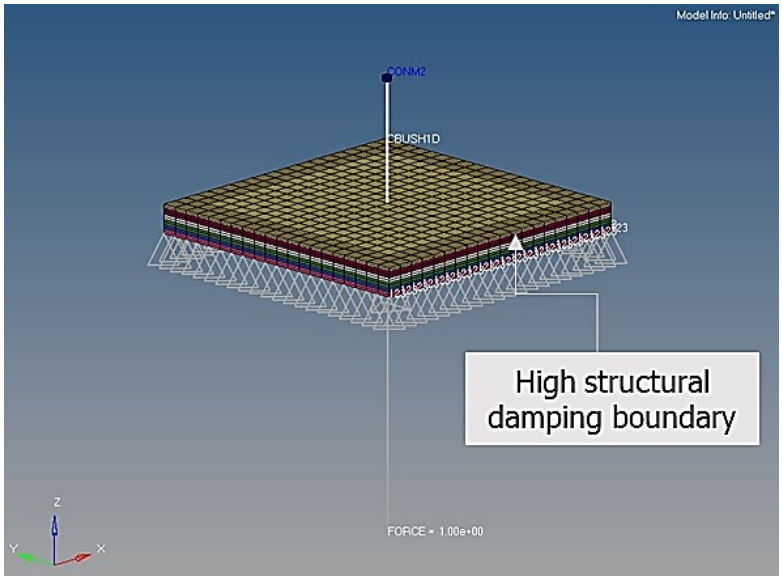

Figure 5.9: A finite element model in Nastran for validating the optimal configuration that is obtained from the reduced-order model optimization

In this Nastran model, a 1m×1m finite multilayer plate is created. An impulse load is applied at the center of bottom surface of the plate, and a single degree-of-freedom mass-spring-damper system is attached at the center of top surface of the plate. A simply-supported boundary condition is applied at four edges of the lower surface of the plate to prevent the mode of rigid body motion. Because in the optimization by utilizing the reduced-order model, the multilayer plate is infinite, which indicates that, in lateral direction all of the waves will travel to infinity without any reflection from the boundary. However, the Nastran model is a finite plate and the waves travelling in the plate will be multi-reflected by the lateral boundary and result a greater dynamic response, which is a superposition of the response of direct wave and the response of reflected waves. To eliminate the difference from two unmatched modeling, an additional boundary is applied in the Nastran model by changing the outer elements (shown in darker color) with a 40% structural damping. The high structural damping boundary will work as an effective

wave absorber to prevent the incoming waves reflecting back when they hit the boundary. Therefore, the modified Nastran model is able to simulate an infinite multilayer plate to match the reduced-order model.

The screening metric of the optimal configurations that are calculated from both reduced-order model and Nastran, are compared and shown in Figure 5.10. Similar to the comparison in section 5.2, the results from the baseline configuration is set to be 100%, and the results from optimal configurations are expressed accordingly in a percentage form.

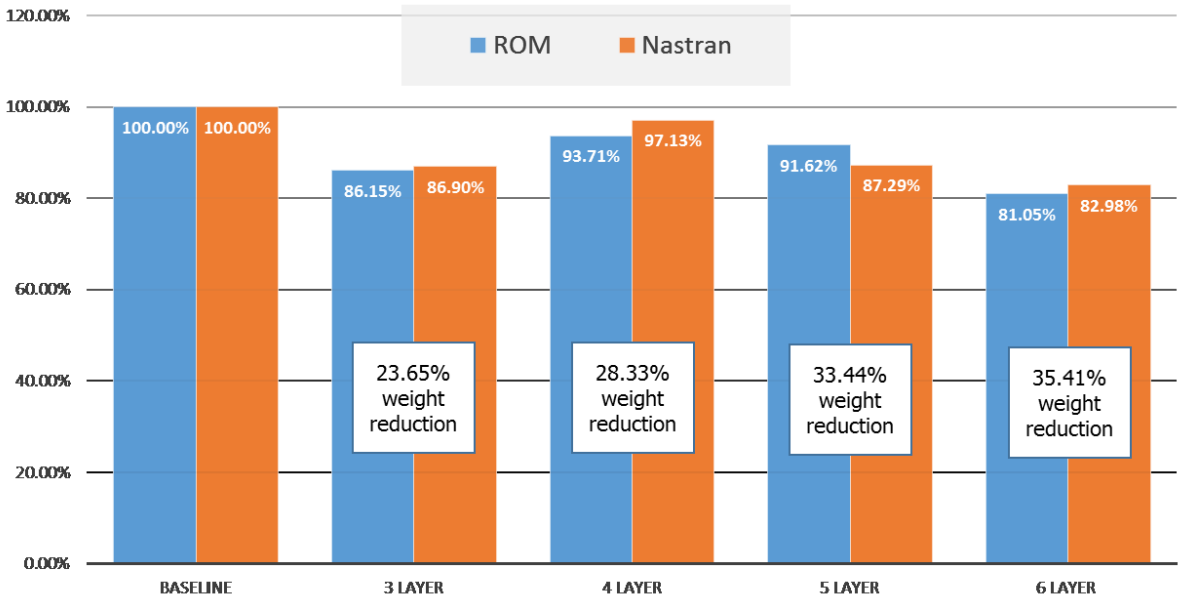

Figure 5.10: The Comparison between the results from reduced-order model optimization and Nastran

It is observed that the screening metric calculated from the reduced-order model optimization is similar to the results calculated from the Nastran model, which validates that the framework of optimization is reliable for design lightweight multilayer plate configurations with high blastworthiness. It is also found that by using the optimal six-layer plate configuration, both

the DRI-based screening metric and the weight of the structure have the greatest reduction. Based on current five candidate material, the optimal six-layer plate configuration shown in Figure 5.8 will be the best choice for a blastworthiness structure design to replace the isotropic steel plate.

5.6 Conclusion

This chapter presents an optimization framework for design lightweight multilayer plate configurations with high blastworthiness. A DRI-based screening metric is developed to correctly capture the levels occupant protection of the multilayer plate. The availability of the screening metric is validated by using classic finite element analysis in Nastran with a numerical study of a five-layer plate configuration. It is also shown that the computational time by using reduced-order model is 220 times faster than using Nastran. The design optimization framework of a multilayer plate subjected to an impulse load is configured, for improving the screening matric while pursuing a structural weight reduction. The number of layers, the material selection, and the thickness of the layers comprise the design variables. A convergence analysis is performed along with the optimization and the selected optimal configurations are also validated by using finite element analysis in Nastran.

This efficient optimization process, which is based on the reduced-order model developed in Chapter 4, provides a fast and reliable routine to identify the optimal multilayer plate among a large number of alternative configurations. It will help designers to select proper materials and determine the thickness of each sublayer in an early design stage of a multilayer plate armor design, which has a capacity to reduce the occupant injury probability and structural weight

simultaneously. Moreover, by using the information generated from the ROM-based optimization, a higher-fidelity structural analysis can be performed in a more complex finite element model for relatively few configurations without performing a tedious parametric study.

CHAPTER 6

Conclusions and Recommendations

6.1 Conclusion

In this dissertation, non-traditional methodologies of design lightweight occupant-centric vehicle structures that absorb and redirect energy away from the occupant in underbody explosive events are developed, which satisfy the mutually exclusive objectives of improving vehicle blastworthiness and reducing structural weight. The development of dynamic response index (DRI) is presented as a standard occupant injury metric to capture the occupant's lumbar compression in underbody explosive events. A V-hull structure with energy-absorbing bullheads and a reduced-order model of multilayer plate are developed in order to achieve the purpose of energy absorbing and energy redirecting. An optimization framework is developed to significantly reduce the computational time and rapidly identify the optimal design from a large number of alternative configurations

The major work and main contribution of this dissertation are:

1. A notional finite element V-hull structure model with energy absorbing bulkheads is developed. The material properties and the configuration of the bulkheads that connect

the V-shaped outer surface with the inner floor are used as design parameters for reducing the serious spinal-lumbar injury probability at a typical occupant location. The human spine system is simplified and modeled as a single degree-of-freedom mass-spring-damper system. Another three degree-of-freedom lumped parameter configuration is also developed, with the two intermediate degree-of-freedom representing the seat and the inner floor of the vehicle. In this three degree-of-freedom model, an energy-absorbing seat and an energy-absorbing floor are mounted on the hull under the occupant's lumbar. The lower bulkheads are designed to be made of softer viscoelastic material to absorb underbody blast energy and the upper-bulkheads are designed to be made of regular high strength steel to avoid excessive local deformation. The material properties of the lower bulkheads, including modulus of elasticity, Poisson ratio, mass density, and decay constant, are studied and tuned for changing the structural dynamic behavior of a vehicle in order to reduce the DRI while simultaneously maintaining the total vehicle weight but reducing the weight of the structure. This provides an opportunity to increase the payload or the weights associated with other vehicle performance attributes, such as propulsion, mobility, radiated noise, etc. This is achieved by creating a new structural design that features energy absorbing and decoupling mechanisms among the bulkheads, floor, seat, and the occupant. In addition to the material properties, the results depend on how and where the seat is connected to the vehicle as well as the relative stiffness and energy absorption characteristics of the floors and the seats. The selection process is driven by controlling and minimizing the DRI created from a blast load. It is demonstrated that the weight of the tuned structure can be reduced while

simultaneously creating various levels of improvement in blast protection as measured by the DRI.

2. A reduced-order dynamic modeling approach, which is based on the reverberation-ray matrix method, is developed to rapidly evaluate a large number of alternative multilayer plate designs with respect to reducing the through-thickness response of the plate to an impulsive load. In this reduced-order model, the wave potential of each sublayer is transformed into the spectral domain by applying double Fourier Transforms. The waves generated by external loading are reflected and refracted at the interfaces of adjacent sublayers, and a scattering matrix **S** is built to represent the condition of continuity of stresses and displacements at each interface. The phase lag values of the traveling waves within each sublayer are represented by a phase matrix **P**. By inserting a permutation matrix **U**, a reverberation matrix **R** is generated as **R** = **SPU** to represent the wave propagation and dynamic characteristics of the entire structure. By employing the generalized ray theory and inverse Fourier Transform, the dynamic response can be evaluated very quickly. Thus, the reduced-order dynamic model are used to rapidly evaluate the performance of alternative multilayer plate designs and generate information for identifying the preferred directions and amounts of energy transfer. The accuracy and efficiency of this approach are validated for the free response by comparison with spectral finite element analysis results, and for the forced response by comparison with finite element analysis results using the commercial code Nastran. It is shown that the reduced-order model is able to predict the trend of the maximum response as design parameters are varied in a three-layer plate structure subjected to impulsive loading. In

terms of computational efficiency, the CPU time required for predicting the forced response is reduced by two orders of magnitude using the reduced-order model compared to using classical finite element analysis.

3. An optimization framework is developed for designing lightweight multilayer plate configurations with high blastworthiness, and a set of numerical case studies are provided for identifying the optimal configuration with different number of sublayers. A DRI-based screening metric is developed to rank candidate configurations according to their capacity of blastworthiness. The availability of the screening metric is validated by using classic finite element analysis in Nastran with a numerical study of a five-layer plate configuration. It is also found that the computational time by using reduced-order model is 220 times faster than using Nastran. The design optimization framework of a multilayer plate subjected to an impulse load is configured, for improving the screening matric while pursuing a structural weight reduction. The number of layers, the material selection, and the thickness of the layers comprise the design variables. A convergence analysis is performed along with the optimization and the selected optimal configurations are also validated by using finite element analysis in Nastran. By utilizing this reduced-order model optimization, it is possible to fast identify and evaluate the best configuration among a large number of alternatives so that the purpose of increasing the structural protection level meanwhile reducing the structural weight becomes achievable and relative efficient. The optimal multilayer plate is capable to be considered and applied as an effective exterior armor in the lightweight vehicle structure design.

6.2 Recommendations for Future Work

This dissertation summarized the work regarding to the design of lightweight vehicle structures that absorb and redirect underbody blast energy, and the results showed the feasibility of the proposed non-traditional design methodologies for high levels of occupant protection and structural weight reduction. To extend the capability of current achievements and utilized those to their full advantage, the following work are recommended for future work:

1. The definition of the DRI, which is used as an injury metric in this dissertation, considers only the maximum lumbar compression and ignores the rate of compression. However, the lumbar injuries also relate to the rate of compression and pelvis acceleration. It is possible that different results would be obtained with different injury metrics. In fact, the DRI model is developed for unconstrained motion of a single degree-of-freedom lumped mass-spring-damper system. Restraint systems reduce the vertical motion, especially for energy-absorbing seats which extend the dynamic contact duration between vehicle structure and occupant. Because the model treats the whole body as a lumped mass-spring-damper system, the geometry and restraints of the seats, which are used in the test data, are critical to achieve the same results. Moreover, the data used to calculate fundamental coefficients of the DRI model lack fidelity in regards to gender, weight, anthropometrics and age. Therefore, a more direct injury metric is preferred to capture the lumbar load from detailed anthropomorphic test devices (ATD).
2. As described in section 3.6, the effects of design changes on other vehicle performance metrics beyond mass and DRI were not considered, even though these effects might be significant. For example, by reducing the density of bulkheads, the center of gravity of the vehicle is elevated, which increases the risk of rollover. Therefore, the dimensions of

the lightweight vehicle under the proposed design philosophy might need to be modified in order to meet requirements for rollover resistance. Also, the reduction of stiffness of the bulkheads will change the overall stiffness and strength of the vehicle. Therefore, lighter and stiffer body structure elements might need to be considered in the design process as a way to compensate for this effect. Overall, the design process demonstrated in this dissertation would need to be included as part of a larger, multidisciplinary design optimization process in order to properly account for and evaluate these types of tradeoffs.

3. The reduced-order model developed in this dissertation is only used for basic research of rapidly evaluating a large number of alternative configurations. It's a simple two-dimensional model, which only considers pure elastic waves and perfect bonding at each interface. However, the situation is much more complicated in reality and several modifications are required for the reduced-order modeling. First, extending the two-dimensional model to a three-dimensional model is necessary. It can be achieved by considering both "SV" shear stress and "SH" shear stress simultaneously and modifying S and P matrices into tensors. Despite the increase of computation cost by bringing in an additional dimensionality (but still much faster than using finite element analysis), the simulation results obtained from the three-dimensional reduced-order model will be closer to the real situation. Second, the damping properties can be added by defining the loss factor in each sublayer. The pure elastic waves become viscoelastic waves, which will leads to more energy dissipation in each sublayer.

4. The dislocation and delamination occurring at the interface need to be considered. These situations can be modeled by inserting an additional intermediate layer of glue if the

material properties of the glue are known, or adding a complementary term to simulate the mechanism of glue, which performs as a linear spring for small deformation, when the material properties of the glue cannot be easily identified. In this case, a linear displacement term $\tilde{u}_{dis}$ and a corresponding linear forcing term $k * \tilde{u}_{dis}$ will be added to build a new continuity relation at the interface.

BIBLIOGRAPHY

BIBLIOGRAPHY

1. D. E. Malen, *Fundamentals of Automobile Body Structure Design*, SAE International, (2011), pp. 209-368.

2. S. Reddy, M. Abbasi, M. Fard, *Multi-cornered thin-walled sheet metal members for enhanced crashworthiness and occupant protection*, Journal of Thin-Walled Structures, Volume 94, September 2015, pp. 56–66.

3. G. Nilakantan, A, Tabiei, *Computational Assessment of Occupant Injury Caused by Mine Blasts underneath Infantry Vehicles*, Journal of Vehicle Structures & Systems, (2009), pp. 50-58.

4. A. Cherkaev, E. Cherkaev, S. Leelavanichkul, *Principles of optimization of structures against an impact*, 8th World Congress on Structural and Multidisciplinary Optimization, June 2009.

5. G. Zhang, N. Vlahopoulos, R. Goetz, R. Van De Velde, "Blast event simulations for a vehicle structure subjected to an explosion," XXVI International Modal Analysis Conference, IMAC-Paper No. 200, February 2007.

6. N. Vlahopoulos, G. Zhang, Utilizing Simulation Technology for Improving Occupant Survivability for a Vehicle Subjected to Loads from Explosions, 2011 NDIA Ground Vehicle Systems Engineering and Technology Symposium, August 2011.

7. R. Thyagarajan, *End-to-end System level M&S tool for Underbody Blast Events*, 27th Army Science Conference, DTIC Report # ADA550921, TARDEC Registration # 21365, December 2010.

8. N. Vlahopoulos, G. Zhang, *Validation of a Simulation Process for Assessing the Response of a Vehicle and Its Occupants to an Explosive Threat*, 27th Army Science Conference, December 2010.

9. J. Sun, N. Vlahopoulos, T. Stabryla, R.Goetz, *Blast Event Simulation for a Structure Subjected to a Landmine Explosion*, SAE Technical Paper 2006-01-0931.

10. K. Ahn, K. Osaki, *A network model for predicting the shear thickening behavior of a poly (vinyl alcohol)—sodium borate aqueous solution*, Journal of Non-Newtonian Fluid Mechanics, Volume 55, Issue 3, December 1994, pp. 215-227.

11. Y. Lee, E. D. Wetzel, N. J. Wagner, *The ballistic impact characteristics of Kevlar® woven fabrics impregnated with a colloidal shear thickening fluid, Journal of Materials Science*, July 2003, Volume 38, Issue 13, pp. 2825–2833.

12. X. Z. Zhang, W. H. Li, X. L. Gong, *The rheology of shear thickening fluid (STF) and the dynamic performance of an STF-filled damper, Smart Materials and Structures*, Volume 17, Number 3, (2008).

13. B. D. Agarwal, L. J. Broutman, K. Chandrashekhara, *Analysis and Performance of Fiber Composites, 3rd Edition*, July 2006.

14. I. M. Daniel, O. Ishai, *Engineering Mechanics of Composite Materials*, Oxford University Press, (1994).

15. C. T. Herakovich, *Mechanics of Fibrous Composites*, John Wiley & Sons, (1997).

16. S. Kyriakides, R. Arseculeratne, E. J. Perry, K. M. Liechti, *On the compressive failure of fiber reinforced composites. International Journal of Solids and Structures*, 32(6-7), (1995), pp. 689-738.

17. A. Mouritz, *The effect of underwater explosion shock loading on the fatigue behavior of GRP laminates*, International Journal of Impact Engineering, Volume 18, Issue 2, March 1996, pp. 129-139.

18. A. Mouritz, *The damage to stitched GRP laminates by underwater explosion shock loading*, Composites Science and Technology, Volume 55, Issue 4, (1995), pp. 365-374.

19. H. S. Türkmen, Z. Mecitoglu, *Nonlinear Structural Response of Laminated Composite Plates Subjected to Blast Loading*, AIAA Journal, Vol. 37, issue 12, (1999), pp. 1639-1647.

20. J. L. R. Comtois, M. R. Edwards, M. C. Oakes, *The effect of explosives on polymer matrix composite laminates*, Composites Part A: Applied Science and Manufacturing, Volume 30, Issue 3, March 1999, pp. 181–190.

21. R. C. Batra, N. M. Hassan, *Response of fiber reinforced composites to underwater explosive loads*, Composites Part B: Engineering, Volume 38, Issue 4, June 2007, pp. 448–468.

22. R. C. Batra, N. M. Hassan, *Blast resistance of unidirectional fiber reinforced composites*, Composites Part B: Engineering, Volume 39, Issue 3, April 2008, pp. 513–536.

23. P. A. Buchan, J. F. Chen, *Blast resistance of FRP composites and polymer strengthened concrete and masonry structures - A state-of-the-art review*, Composites Part B Engineering, Vol. 38, No. 5-6, (2007), pp. 509-522.

24. C. J. Yungwirtha, D. D. Radfordа, M. Aronsona, H.N.G. Wadleya, *Experiment assessment of the ballistic response of composite pyramidal lattice truss structures*, Composites Part B: Engineering, Volume 39, Issue 3, April 2008, pp. 556–569.

25. P. Qiao, M. Yang, F. Bobaru, *Impact Mechanics and High-Energy Absorbing Materials: Review*, Journal of Aerospace Engineering, (2008), pp. 235-248.

26. M. J. Mullin, B. J. O'Toole, *Simulation of Energy Absorbing Materials in Blast Loaded Structures*, 8th International LS-DYNA Conference.

27. J. Carcione, D. Kosloff, R. Kosloff, *Wave propagation simulation in a linear viscoelastic medium*, John Willey & Sons, (1988).

28. I. Bartoli, A. Marzani, H. Matt, F. Lanza di Scalea, E. Viola, *Modeling Guided Wave Propagation for Structural Health Monitoring Applications*, IMAC-XXIV: Conference & Exposition on Structural Dynamics, (2006).

29. A. Hanyga, *Wave propagation in media with singular memory, Mathematical and Computer Modelling*, Volume 34, Issues 12–13, December 2001, pp. 1399-1421.

30. B. R. DeweyL. AdlerR. T. KingK. V. Cook, *Measurements of anisotropic elastic constants of type 308 stainless-steel electroslag welds*, Experimental Mechanics, Volume 17, Issue 11, November 1977, pp 420–426.

31. A. N. Norris, *A theory of pulse propagation in anisotropic elastic solids*, Wave Motion, Volume 9, Issue 6, November 1987, pp. 509-532.

32. J. M. Carcione, *Wave propagation in anisotropic linear viscoelastic media: theory and simulated wavefields*, Geophysical Journal International, Volume 101, Issue 3, June 1990, pp. 739-750.

33. P. Fellinger, R. Marklein, K. J. Langenberg, S. Klaholz, *Numerical modeling of elastic wave propagation and scattering with EFIT — elastodynamic finite integration technique*, Wave Motion, Volume 21, Issue 1, February 1995, pp. 47-66.

34. A. N. Norris, G. R. Wickham, Elastic waves in inhomogeneously oriented anisotropic materials, Wave Motion, Volume 33, (2001), pp. 97-107.

35. A. R. Ebrahimi, A. Abyazi, S. M. Abbasi, *Anisotropy in Microalloyed S355N Steel*, International Journal of Iron & Steel Society of Iran, Volume 5, Issue 2, (2008), pp. 14-20.

36. A. V. Amirkhizi, A. Tehranian, S. Nemat-Nasser, *Stress-wave energy management through material anisotropy*, Wave Motion, Volume 47, Issue 8, December 2010, pp. 519–536.

37. A. S. Phani, J. Woodhouse, N. A. Fleck, *Wave propagation in two-dimensional periodic lattices*, J Acoust Soc Am, April 2006, pp.1995-2005.

38. S. Gonella, M. Ruzzene, *Analysis of in-plane wave propagation in hexagonal and re-entrant lattices*, Journal of Sound and Vibration, (2008), pp. 125–139.

39. D. J. Colquitt, I. S. Jones, N. V. Movchan, A. B. Movchan, *Dispersion and localization of elastic waves in materials with microstructure*, Proceedings of the Royal Society A, May 2011.

40. G. G. Osharovicha, M. V. Ayzenberg-Stepanenko, *Wave localization in stratified square-cell lattices: The antiplane problem*, Journal of Sound and Vibration, Volume 331, Issue 6, March 2012, pp. 1378–1397.

41. M. Charlottea, L. Truskinovsky, *Lattice dynamics from a continuum viewpoint,* Journal of the Mechanics and Physics of Solids, Volume 60, Issue 8, August 2012, pp. 1508–1544.

42. F. Casadei, J. J. Rimoli, *Anisotropy-induced broadband stress wave steering in periodic lattices*, International Journal of Solids and Structures, Volume 50, Issue 9, 1 May 2013, pp. 1402–1414.

43. N. Bertolino, M. Monagheddu, A. Tacca, P. Giuliani, C. Zanotti, U. Anselmi Tamburini, *Ignition mechanism in combustion synthesis of Ti–Al and Ti–Ni systems*, Intermetallics, Volume 11, Issue 1, January 2003, pp. 41–49.

44. E. K. Sioh, *Functional graded material with nano-structured coating for protection*, International Journal of Materials and Product Technology, Vol. 39, No. 1/2, (2010).

45. W. T. Thomson, *Transmission of Elastic Waves through a Stratified Solid Medium*, Journal of Applied Physics, Volume 21, (1950).

46. J. L. Synge, *Elastic Waves in Anisotropic Media*, Studies in Applied Mathematics, Volume 35, Issue 1-4, April 1956, pp. 323–334.

47. H. N. Abramson, H. J. Plass und E. A. Ripperger, *Stress wave propagation in rods and beams*, Journal of Applied Mathematics and Mechanics, Volume 38, Issue 11-12, (1958).

48. M. A. Medick, R. D. Mindlin, *Extensional vibrations of elastic plates*, Journal of Applied Mechanics, Volume 26, (1959), pp. 561-569.

49. D. C. Gazis, R. D. Mindlin, *Extensional Vibrations and Waves in a Circular Disk and a Semi-Infinite Plate*, Journal of Applied Mechanics, Volume 27, September 1960, pp. 541-547.

50. H. D. McNiven, R. D. Mindlin, *Axially symmetric waves in elastic rods*, Journal of Applied Mechanics, Volume 27, (1960), pp. 145-151.

51. C. C. Chao, *Dynamical Response of an Elastic Half-Space to Tangential Surface Loadings*, Journal of Applied Mechanics, Volume 27(3), September 1960, pp. 559-567.

52. Y.H. Pao, *Dynamical Stress Concentration in An Elastic Plate*, Transactions of the ASME Journal of Applied Mechanics, Volume 29, (1962), pp. 299–305.

53. E. A. Kraut, *Advances in the theory of anisotropic elastic wave propagation*, Reviews of Geophysics, Volume 1, Issue 3, August 1963, pp. 401–448.

54. T.R. Meeker, A.H. Meitzler, *Guided Wave Propagation in Elongated Cylinders and Plates*, Physical Acoustics - Principles and Methods, (1964), pp. 111–167.

55. J. Zemanek. Jr., *An Experimental and Theoretical Investigation of Elastic Wave Propagation in a Cylinder*, The Journal of the Acoustical Society of America, (1972).

56. J. D. Achenbach, *Wave Propagation in Elastic Solids*, A volume in North-Holland Series in Applied Mathematics and Mechanics, (1973).

57. K. F. Graff, *Wave Motion in Elastic Solids*, Dover Books on Physics, (1975).

58. G. Liu, X. Han, K. Lam, *Stress waves in functionally gradient materials and its use for material characterization*, Composite Part B: Engineering, Volume 30, (1999), pp. 383–394.

59. A.M.A.M. Abdelkarim, A.C.W.M. Vrouwenvelder, M.D. Verweij, *Analysis of the dynamic response of layered, elastic media by means of the Fast Fourier Transform*, HERON, Vol. 44. No.2, (1999), ISSN 0046-7316.

60. Z. C. Xi, G. R. Liu, K. Y. Lam, H. M. Shang, *Dispersion and characteristic surfaces of waves in laminated composite circular cylindrical shells*, The Journal of the Acoustic Society of America, Volume 108, (2000).

61. F. Kobayashi, S. Biwa, N. Ohno, *Wave transmission characteristics in periodic media of finite length: multilayers and fiber arrays*, International Journal of Solids and Structures, 41 (2004), pp. 7361–7375.

62. P.J. Shorter, *Wave propagation and damping in linear viscoelastic laminates*, The Journal of the Acoustical Society of America, Volume 115, (2004).

63. M. Abid, M.S. Abbes, J.D. Chazot, L. Hammemi, M.A. Hamdi, M. Haddar, *Acoustic Response of a Multilayer Panel with Viscoelastic Material*, International Journal of Acoustics and Vibration, Vol. 17, No. 2, (2012).

64. D. Chronopoulos, B. Troclet, O. Bareille, M. Ichchou, *Modeling the response of composite panels by a dynamic stiffness approach*, Composite Structures, Volume 96, February 2013, pp. 111–120.

65. Y.M. Gupta, J.L. Ding, *Impact load spreading in layered materials and structures: concept and quantitative measure*, International Journal of Impact Engineering 27, (2002).

66. J.R. Robbins, J.L. Ding, Y.M. Gupta, *Load spreading and penetration resistance of layered structures – a numerical study*, International Journal of Impact Engineering 30 (2004).

67. Z.Y. Xue, J.W. Hutchinson, *Preliminary assessment of sandwich plates subject to blast loads*, International Journal of Mechanical Sciences, Volume 45, Issue 4, April 2003, pp. 687–705.

68. C. Gallimore, K. Kochersberger, R. DeVita, *Constrained Layer Damping Treatment Design for Aircraft Landing Gear*, IMAC-XXVII: Conference & Exposition on Structural Dynamics, 2009.

69. P. Dewangan, *Passive Viscoelastic Constrained Layer Damping for Structural Application*, Master Thesis, 2009.

70. G.S. Langdon, Y. Chi, G.N. Nurick, P. Haupt, *Response of GLARE© panels to blast loading*, pp. 3116-3120.

71. X.R. Liu, X.G. Tian, T.J. Lu, D.Q. Zhou, B. Liang, *Blast resistance of sandwich-walled hollow cylinders with graded metallic foam cores*, Composite Structures, Volume 94, Issue 8, July 2012, pp. 2485–2493.

72. M. Z. Hassan, Z. W. Guan, W. J. Cantwell, G. S. Langdon, G. N. Nurick, *The influence of core density on the blast resistance of foam-based sandwich structures*, International Journal of Impact Engineering, Volume 50, December 2012.

73. K. Kulkarni, J. Ramalingam, R. Thyagarajan, *Assessment of the Accuracy of Certain Reduced Order Models used in the Prediction of Occupant Injury during Under-Body Blast Events*, SAE Int. J. Trans. Safety 2(2), 2014.

74. K.B. Kulkarni, J. Ramalingam, R. Thyagarajan, *Evaluating the Effectiveness of Various Blast Loading Descriptors as Occupant Injury Predictors for Underbody Blast Events*, NDIA Ground Vehicle Systems Engineering and Technology Symposium (GVSETS), August 2013.

75. L. Li, N. Stowe, N. Vlahopoulos, S. Mohammad, C. Barker, R. Thyagarajan, *Utilization of Fast Running Models in Buried Blast Simulations of Ground Vehicles for Significant Computational Efficiency*, NDIA Ground Vehicle Systems Engineering and Technology Symposium (GVSETS), August 2013.

76. J. Ramalingam, S. Chandra, R. Thyagarajan, *Reduced Order Modeling for Rapid Simulations of Blast and Rollover Events of a Ground Vehicle and its Occupants Using Rigid Body Dynamic Models*, DTIC Report # ADA 585048, 2013.

77. R. Thyagarajan, J. Ramalingam, K.B. Kulkarni, *Comparing the Use of Dynamic Response Index (DRI) and Lumbar Load as Relevant Spinal Injury Metrics*, ARL Workshop on Numerical Analysis of Human and Surrogate Response to Accelerative Loading, Aberdeen, MD, 7-9 January 2014.

78. Y.H. Pao, R. Gajewski, *The generalized ray theory and transient response of layered elastic solids*, In: Mason, W.P. (Ed.), Physical Acoustics, vol. X. Academic Press, New York (Chapter 6), 1977.

79. Y.H. Pao, X.Y. Su, J.Y. Tian, *Reverberation Matrix Method for propagation of sound in a multilayered liquid*, Journal of Sound and Vibration 230(4):743-760, 2000.

80. W.Q. Chen, H.M. Wang, R.H. Bao, *On calculating dispersion curves of waves in a functionally graded elastic plate*, Composite Structures, Volume 81, Issue 2, 2007.

81. X.H. Su, J.Y. Tian, Y.H. Pao, *Application of the reverberation-ray matrix to the propagation of elastic waves in a layered solid. International Journal of Solids and Structures*, Volume 39, Issues 21–22, 2002.

82. J.Y. Tian, W.X. Yang, X.Y. Su, *Transient elastic waves in a transversely isotropic laminate impacted by axisymmetric load*, Journal of Sound and Vibration 289(1):94-108, 2006.

83. J.Y. Tian, Z.M. Xie, *A Hybrid Method for Transient Wave Propagation in a Multilayered Solid*, Journal of Sound and Vibration 325(1):161-173, 2009.

84. G.S. Lee, C.C. Ma, *Transient elastic waves propagating in a multi-layered medium subjected to in-plane dynamic loadings*. I. Theory, Proceedings of the Royal Society A 456(1998):1355-1374, 2000.

85. C.C. Ma, G.S. Lee, *Transient elastic waves propagating in a multi-layered medium subjected to in-plane dynamic loadings II*. Numerical calculation and experimental measurement, Proceedings of the Royal Society A 456(1998):1375-1396, 2000.

86. N. Vlahopoulos, N. Schiller, S. Lee, *Energy Finite Element Analysis Developments for Vibration Analysis of Composite Aircraft Structures*, SAE Int. J. Aerosp. 4(2):593-601, 2011.

87. D. Manion, *Computation and Validation of the Dynamic Response Index (DRI)*, DTIC Report # ADA 591869, 6 August 2013.

88. E.L. Stech, P.R. Payne, *Dynamic Models of the Human Body*, Aerospace Medical Research Laboratory (AMRL Technical Report 66-157), November 1969.

89. J.W. Brinkley, J.T. Shaffer, *Dynamic Simulation Techniques for the Design of Escape Systems: Current Applications and Future Air Force Requirements*, Aerospace Medical Research Laboratory (AMRL Technical Report 71-292), December 1971.

90. R.E. Zimmermann, N.A. Merritt, *Aircraft Crash Survival Design Guide*, U.S. Army Aviation Research and Technology Activity (USAAVSCOM TR 89-D-22A), December 1989.

91. *LS-DYNA Theory Manual*, (R5514), Livermore Software Technology Corporation, CA, 25 June 2014.